p-79

NASA Technical Memorandum 4189

(NASA-TM-4189) HIGH REYNOLDS NUMBER TEST OF THE BOEING TR77 AIRFOIL IN THE LANGLEY 0.3-METER TRANSONIC CRYOGENIC TUNNEL (NASA) 79 p

N92-31246

Unclas

H1/02 0116855

NASA Technical Memorandum 4189

High Reynolds Number Test of the Boeing TR77 Airfoil in the Langley 0.3-Meter Transonic Cryogenic Tunnel

Julio Chu, Stuart G. Flechner,
and Acquilla S. Hill
Langley Research Center
Hampton, Virginia

Roger A. Rozendaal
Boeing Commercial Airplanes
Seattle, Washington

NASA
National Aeronautics and
Space Administration
Office of Management
Scientific and Technical
Information Division

1990

Summary

In a cooperative effort with the U.S. manufacturers of large transport aircraft, NASA has undertaken an extensive experimental program to systematically study advanced-technology airfoils over a wide range of Reynolds numbers. This program, referred to as the Advanced Technology Airfoil Tests (ATAT) program, was conducted in the Langley 0.3-Meter Transonic Cryogenic Tunnel. As part of the program, Boeing had constructed a 12-percent-thick airfoil model with a nominal design lift coefficient of 0.65. The test Mach number was varied from about 0.50 to 0.78, and the Reynolds number (based on airfoil chord) was varied from 4.4×10^6 to 42.0×10^6. As was expected from pre-test analysis, increasing Mach number while maintaining constant Reynolds number yielded an increase in normal-force slopes and nose-down pitching-moment and a decrease in maximum normal-force coefficient. However, increasing Reynolds number while maintaining constant Mach number resulted in increased normal-force and nose-down pitching-moment coefficient and generally decreased drag coefficient.

Introduction

Interest in energy-efficient transport aircraft for the subsonic-transonic flight regime has stimulated the research of advanced-technology airfoils. Theoretical and experimental studies have shown that significant performance gains and increased fuel efficiency can be realized by the application of such airfoils (ref. 1). The National Aeronautics and Space Administration (NASA), Langley Research Center, undertook an airfoil test program over a wide range of Reynolds numbers in the Langley 0.3-Meter Transonic Cryogenic Tunnel (0.3-m TCT). This program, referred to as the Advanced Technology Airfoil Tests (ATAT) program (ref. 2), was initiated by the Aircraft Energy Efficiency Project Office (ACEE) at Langley.

A significant portion of the ATAT program was conducted in cooperation with three major U.S. manufacturers of large commercial transport aircraft; these manufacturers supplied technical personnel and airfoil models. The overall objectives of the ATAT program were: (1) to provide the U.S. transport aircraft companies the opportunity to test their advanced airfoils at flight Reynolds numbers and compare the performance of their advanced airfoils with the performance of the latest NASA designs; (2) to provide industry with experience in cryogenic wind-tunnel model design and testing techniques; (3) to expand the high Reynolds number airfoil data base; and (4) to evaluate advanced airfoil technology in general. Consistent with these overall objectives, the industry participants were encouraged to explore innovative airfoil designs which might not produce an optimum level of performance; therefore, care should be exercised in drawing conclusions regarding the overall levels of technology of the various participants from direct comparisons of their aerodynamic data.

The data presented in this report are from the second of two airfoil studies conducted with Boeing Commercial Airplanes (Boeing). The results from the first study, for a 10-percent-thick airfoil, were documented in reference 3. The present airfoil, designated as TR77, was designed with 12-percent maximum thickness and a nominal design section lift coefficient of 0.65. The test Mach number was varied from 0.50 to 0.78, and the Reynolds number (based on airfoil chord) was varied from 4.4×10^6 to 42.0×10^6. The selected test conditions encompassed the flight conditions envisioned for this particular airfoil design. The aerodynamic results presented include sectional normal-force and pitching-moment data obtained by integrating airfoil surface pressures and drag data obtained by integrating wake measurements. Details regarding model design, fabrication techniques, and operational experience are included herein.

Symbols

AOA	angle of attack
b	span, in.
C_p	pressure coefficient, $\frac{p_l - p_\infty}{q_\infty}$
c	chord, in.
c_d	section drag coefficient
c_l	section lift coefficient
c_m	section pitching-moment coefficient about quarter chord
$\partial c_m/\partial c_n$	stability parameter at constant section normal-force coefficient
c_n	section normal-force coefficient
$c_{n,\alpha}$	slope of section normal-force coefficient versus angle of attack
LN_2	liquid nitrogen
M	Mach number
M_p	tunnel Mach number when airfoil pressures measured at first rake step
$\overline{M}_r$	average tunnel Mach number for a full rake traverse

n/d	performance factor (ratio of section normal force to drag)
O_2	gaseous oxygen
Pt.	data point number
p	static pressure, psi
p_t	tunnel stagnation pressure, atm
R_c	Reynolds number, based on airfoil chord length
q	dynamic pressure, psi
T_t	tunnel stagnation temperature, K
X, Y	tunnel coordinate axes; X positive downstream, Y positive toward right side
x	chordwise distance from leading edge of airfoil, in.
y	spanwise distance from model centerline, in.
z	vertical distance, in.
α	angle of attack, deg
Δ	deviation from design airfoil dimensions, in.
σ	estimate of standard deviation

Subscripts:

amb	ambient
atm	atmosphere
d	design
dd	conditions at drag divergence, $\partial c_d/\partial M_\infty = 0.10$
l	local
max	maximum
min	minimum
te	trailing edge
∞	free-stream condition

Test Facility

Wind Tunnel

The test was conducted in the Langley 0.3-m TCT with a (8- by 24-in.) two-dimensional insert. A photograph of the tunnel is shown in figure 1(a) and a schematic showing some physical characteristics of the tunnel is shown in figure 1(b). A photograph of the two-dimensional insert installed in the tunnel is shown in figure 2. In the photograph, the plenum lid and test-section ceiling have been removed, and the removable turntable-support module is shown in the test position.

The tunnel is a continuous-flow transonic tunnel which uses nitrogen gas as the test medium. It is capable of operating at temperatures varying from about −316°F to about 129°F and stagnation pressures ranging from slightly greater than 1.0 atm to 6.0 atm. The ability to operate at 6-atm pressure and cryogenic temperatures provides an extremely high Reynolds number test capability at relatively low model loadings. The 0.3-m TCT operating envelope, shown in figure 3, indicates the tunnel capability for simulating flight conditions of aircrafts ranging from general aviation to transport-cargo. In addition to the high Reynolds number capability, the ability to vary pressure and temperature over a wide range independent of Mach number permits individual control and assessment of Reynolds number and aeroelastic effects of the test model. Additional features regarding the cryogenic wind-tunnel testing in general and the 0.3-m TCT in particular are presented in references 4 and 5, respectively.

Instrumentation

A brief discussion of the primary instrumentation and a typical data-point measurement procedure are presented in this section. A more detailed discussion of the instrumentation and measurement procedures of the 0.3-m TCT is documented in reference 6.

Airfoil pressure measurements. Static pressures over the airfoil surface were measured by individual pressure transducers with an accuracy of ±0.25 percent of the reading from −25 percent to 100 percent of full scale. The transducers, located outside the test section, were mounted on thermostatically controlled heater bases to maintain a constant temperature and on "shock" mounts to reduce vibrational effects. The electrical outputs from the transducers were connected to individual signal conditioners located in the tunnel control room. These signal conditioners had autoranging capability and had seven ranges available. As a result of this capability, the analog electrical output to the data-acquisition system was kept at a high level, even when a pressure transducer was operating at the low end of its range.

Airfoil wake-pressure measurements. A vertically traversing probe system (wake rake), located just downstream of the airfoil model (figs. 2 and 4), provided six total-pressure measurements across the span of the tunnel ranging from $y/b/2 = 0.25$ to -0.75. The spanwise measurements provided a means of evaluating the uniformity of the flow across the model span. This probe system moved through the model wake in steps and had a maximum vertical traversing range of 10 in. It can be either computer-driven or manually operated to map model wake size. The maximum number of steps in one traverse is 99. The vertical centerline of the probe support can be located either at tunnel station 10.2 in. or at tunnel station 12.2 in. (fig. 4). For this test, the probe support was located at the 10.2-in. station, which was about 1.2 chord lengths downstream of the model trailing edge. Total-pressure measurements at the probe and static-pressure measurements on the sidewall of the test section in the plane of the probes were used to calculate the airfoil drag coefficients based on the method outlined in reference 7.

Angle-of-attack system. The two-dimensional insert with its computer-controlled angle-of-attack system is shown in schematic form in figure 4. The system has a traversing range of ±20° that can be offset from 0° in either direction at model installation. Angle of attack is driven by an electric stepper motor that is connected through a yoke to the perimeter of the mounting turntables on both sides of the model. This arrangement provides parallel driving of the two ends of the model through the angle-of-attack range without model twisting. This system can also be operated manually.

Typical data-point measurement procedure. At the beginning of a data-taking cycle, the airfoil surface pressure measurements, tunnel free-stream conditions, wall pressures, and wake-rake total-pressure measurements with the rake in its first position were sampled 10 times over 1 sec and averaged. The remainder of the wake profile was defined by stepping the probe through a specified distance, pausing 0.25 sec for pressure to stabilize, sampling 10 pressures in 1 sec, averaging these measurements, and stepping the rake again. Each time the rake was stepped, the tunnel conditions were also measured. Because the width of the airfoil wake changes with angle of attack, the number of steps of rake traverse was varied to ensure accurate wake definition. For example, figure 5 illustrates the number of steps of rake traverse associated for the $M_\infty = 0.76$ test condition.

Model Description

The test model was a 12-percent-thick advanced-technology airfoil (designated by Boeing as TR77) with a chord of 6.0 in. The nominal design point was at $c_l = 0.65$ and $M \approx 0.76$. The model was designed and fabricated (in accordance with Langley Research Center's Wind-Tunnel Model System Criteria (LHB 1710.15)) by Boeing. Aerodynamic considerations required contour accuracies of ±0.001 in., surface finishes of 10×10^6 in. rms or better, and good experimental practices that required detailed definition of the pressure distribution over the model. Tunnel operating requirements included model chord and span dimensional tolerance, a selection of material suitable for use at cryogenic temperatures, safety factors of at least 3 at all operating conditions, Charpy impact strengths of at least 20.34 J at −321°F, and compatibility with the existing 0.3-m TCT sidewall turntables. A photograph of the TR77 airfoil installed between the sidewall turntables is shown in figure 6(a). In this view, the plenum lid and test-section ceiling have been removed, and the model with the sidewall turntables has been raised and set on the top of the test section. Figure 6(b) shows a sketch of the airfoil model with the location of the surface pressure orifices. The model was instrumented with 53 static pressure orifices, each having a diameter of 0.010 in.

The structural design of this model was basically the same as for the first Boeing model (ref. 3), but several enhancements were incorporated into the manufacturing of this model. Maraging 200 steel was chosen for the construction of the TR77 model instead of the A-286 stainless steel used for the first model because of superior dimensional stability during machining, ease of machining and handworking, and superior weldability. The Eutectic Eutec Rod 157 solder previously used was replaced with a solder especially formulated for cryogenic strain-gage installation. This solder has a melting point of 580°F, almost 280°F higher than Eutectic 157; therefore, the solder joints were less susceptible to melting during the electron-beam welding operation.

The primary enhancement in the manufacturing of this model was the innovative use of a numerically controlled traveling wire electron discharge machine (wire EDM) for the contouring of the airfoil shape. The EDM was originally used for cutting and checking templates, but it was found that with minor cutting-rate and power-setting modifications, material as deep as 12 in. could be cut with contour accuracies of ±0.00075 in. The cuts produced were smooth and not ridged, as are those from a milling operation. The wire EDM process resulted in a simplified contouring procedure that involved making a single cut of only 0.002 in. over target contour, removing the heat-affected zone, and polishing the surface. The net result was a satisfactory contour at a lower cost than the first Boeing airfoil.

Section beam properties were determined with a computer-aided design (CAD) system using a mathematical model of a segmented beam that was simply supported at the ends. A worst-case load stress analysis showed this model to be stiffer than the previous one with ample factors of safety.

The final contour (except near the leading edge) and pressure orifice locations were checked at Boeing with a validator probe. The leading-edge contours were checked separately at Boeing with templates. The model contour was also measured at Langley before testing, between tunnel entries, and after the test. Figure 7 shows the results of the three Langley contour measurements. The required contour accuracy of ± 0.001 in. was generally achieved, except on the aft two-thirds of the lower surface, and model contours remained stable after many cryogenic cycles. Surface finish was checked at Boeing with a profilometer and was shown to be 3.9×10^{-6} in., well within the specified tolerance.

Boundary-Layer Transition

Boundary-layer transition was fixed using aluminum disks, 0.06 in. in diameter and 0.001 in. in thickness, that were applied along the span on 0.15-in. centers. The disks were bonded onto both the upper and lower model surfaces along the 10-percent chord line with a two-part glue. The thickness of the glue bond added approximately 0.001 in. to the disk thickness. This thickness was taken into account for boundary-layer transition.

Test Program

Test conditions were selected to determine the effects of Reynolds number, Mach number, and transition on the airfoil, as well as to determine its general performance. Figure 8 shows the Reynolds number and free-stream Mach number conditions tested; these tests were conducted in two entries because of tunnel operational problems. The fixed-transition and free-transition data are presented as solid and open symbols, respectively. There were no fixed-transition data obtained during the second entry.

Data Reduction, Quality, and Repeatability

Data Reduction

Final aerodynamic coefficients were calculated at Boeing and are presented in table I. The normal-force and pitching-moment coefficients were computed by numerical integration of the pressures over the model surfaces. Runs 1 to 14 (fixed transition) and 15 to 24 (free transition) are associated with the first entry, and those numbered greater than 100 are associated with the second entry. For runs 15 to 19, incorrect pressures were measured on the lower surface at $x/c = 0.48$, and the normal-force and pitching-moment values for these runs were computed assuming a straight-line interpolation of the adjacent pressures. The pressure data from the first tunnel entry included a trailing-edge pressure, but similar data were not measured during the second entry because the orifice located there became plugged. The trailing-edge pressures for these runs were calculated by straight-line extrapolation of the last two upper surface pressure values.

The drag coefficient for each data point was obtained as an integration of wake total-pressure decrement (momentum loss), as measured by the rake, corrected for a "threshold" decrement. This threshold decrement is identified as that level associated with the noise band of the tunnel and instrumentation. For some data points, a small part of the wake was missed because of improper rake travel specification. In each of these cases, the wake profile was manually extrapolated. The error associated with this manual extrapolation was very small, since this process generally added less than one drag count (0.0001) to the drag coefficient.

In the 0.3-m TCT data-reduction process, the thermodynamic properties of the nitrogen gas were calculated using the Beattie-Bridgeman equation of state. This equation of state has been shown to give essentially the same thermodynamic properties and flow-calculation results in the temperature-pressure regime of the 0.3-m TCT as the more complicated Jacobsen equation of state (ref. 8). Detailed discussions of real-gas effects when testing in cryogenic nitrogen are contained in references 9 and 10.

The test Mach number M_∞ reflects the average local Mach number distribution (from static pressure orifices on each turntable) as a function of Reynolds number in the calibration of the "empty" test section. No attempt has been made to correct the data for wall interference effects due to either the top or bottom slotted walls or due to the sidewall boundary-layer growth effects. However, the techniques applicable for correcting this airfoil data set are documented in references 11 and 12.

Data Quality

Mach number fluctuations. In all wind-tunnel testing, and especially in transonic testing, the stability of the tunnel flow conditions, such as Mach number, has a direct bearing on the quality of the final aerodynamic data. In table I, values of Mach number and Reynolds number are shown as average values for each data point. Two Mach numbers are listed: $M_{\infty,p}$ is the tunnel free-stream Mach number when the airfoil pressures were measured at the first rake step; $\overline{M}_{\infty,r}$ is the average tunnel Mach number for a full rake traverse in acquiring data for calculation of c_d. The $M_{\infty,p}$ value from point to point indicates the precision in setting tunnel test conditions. Figure 9 shows, for several runs, samples of the tunnel free-stream Mach number at each probe position during a wake probe sweep. For some angles of attack, a distinct periodicity was apparent in the tunnel Mach number. Table II gives the standard deviation of $\overline{M}_{\infty,r}$ during the time required to survey the wake for several runs. This estimate is generally between 0.001 and 0.003, which is acceptable at Mach numbers below drag divergence.

Airfoil spanwise variation of drag. In two-dimensional airfoil testing, the uniformity of the flow across the test section is also critical to the quality of the final aerodynamic data. The interactions of tunnel sidewall boundary layer with the airfoil pressure field and with separated flow are potential sources of three-dimensional flow effects in a two-dimensional test section. The variation of section drag coefficient across the span provides a general indication of the uniformity of the flow.

A review of the section drag coefficients for $R_c = 30.0 \times 10^6$ (free transition) in figure 10, a typical flight condition, indicates that there is acceptable spanwise uniformity. At high section normal coefficients, however, beyond the onset of trailing-edge boundary-layer separation, this uniformity deteriorates. The lower value of section drag coefficient near the wind-tunnel wall ($y/b/2 = -0.75$) for $c_n = 0.996$ (fig. 10(b)) is a typical indication of the interaction of the tunnel wall and boundary layer with a shock wave over the model (ref. 13).

For the lowest Reynolds number data, for which there is considerable laminar boundary-layer flow over the model, the free-transition data (fig. 11) indicate nonuniform transition along the span of the model. However, the situation is improved once the transition is fixed.

Data Repeatability

Since the data for the present test were obtained over two wind-tunnel entries, both the repeatability of the aerodynamics data within each entry and the repeatability of the aerodynamic data from one entry to another are considered.

The repeatability of the airfoil aerodynamic data from the same wind-tunnel entry, with and without transition trips for selected runs, is shown on figures 12(a) to 12(c). Good repeatability is shown except for the higher Mach numbers, where the airfoil is more sensitive to free-stream variations. For example, in figure 12(b), for run 126, the difference in c_d shown at $c_n \approx 0.60$ could be due to changes in transition location from the combined effects of low Reynolds number (7.7×10^6), no transition-trip application, and high test Mach number.

The repeatability of the airfoil aerodynamic data of the two separate tunnel entries is illustrated in figures 13 and 14. For the Reynolds numbers shown, 7.7 and 30.0×10^6, better test-to-test correlation in c_d is indicated at $M_\infty = 0.70$ (figs. 13(a) and 14(a)) than at $M_\infty = 0.76$ (figs. 13(b) and 14(b)). This repeatability is again attributed to the Mach number sensitivity of the airfoil at the higher test Mach numbers.

Overall, the repeatability investigations indicate that, for this experiment, good correlation is likely obtained when any one or a combination of the following conditions is present: (a) subcritical flow over the airfoil, (b) boundary-layer transition location fixed, or (c) comparable tunnel conditions maintained within a run. As discussed previously, the upper surface contour measurements were shown to be within the tolerance of ±0.001 in., and based on a study in reference 14, model contour variation is eliminated as a possible source of data nonrepeatability.

Presentation of Results

The airfoil aerodynamic characteristics are presented as follows:

	Figure
Effects of fixing transition on aerodynamic characteristics of airfoil:	
$R_c = 4.4 \times 10^6$	15
$R_c = 7.7 \times 10^6$	16
Effect of Reynolds number on aerodynamic characteristics of airfoil:	
Free transition	17
Fixed transition	18
Effect of Mach number on aerodynamic characteristics of airfoil:	
Free transition	19
Fixed transition	20
Effect of Mach number on variation of trailing-edge pressure coefficient with normal-force coefficients for fixed transition	21
Effect of transition and Mach number on variation of pitching-moment and normal-force coefficients with Reynolds number for $\alpha = 2°$	22

Discussion of Results

Several aspects of the sectional aerodynamic data are examined in this section. First, effects of boundary-layer tripping, Reynolds number, and Mach number are discussed. Second, variation of the trailing-edge pressure with section normal-force coefficient for several Reynolds number runs as an indicator of the onset of airfoil trailing-edge flow separation is discussed. Third, a discussion of the airfoil stability and performance in the neighborhood of the design condition is presented. Finally, some comments are presented regarding the model and overall test experience.

Basic Aerodynamic Data

Effects of boundary-layer tripping. Figures 15 and 16 show the effect of leading-edge boundary-layer tripping on the basic aerodynamic coefficients for $R_c = 4.4 \times 10^6$ and $R_c = 7.7 \times 10^6$, respectively. For the lower Reynolds number, the boundary-layer transition evaluation was conducted for test Mach numbers of 0.70 and 0.74; for the higher Reynolds number, the test Mach numbers were 0.70, 0.74, and 0.76. A comparison of the data shows that application of the trip to obtain turbulent flow decreased both the section normal-force and nose-down pitching-moment coefficients but increased the section drag coefficient. The thickened boundary layer from tripping has a decambering effect on the airfoil; essentially, the fluid shape of the model is increased, hence there is a reduction of the nose-down pitching-moment coefficient and there is a requirement of higher angles of attack to achieve the same normal-force coefficient. The increase in overall drag level is attributed to higher skin-friction drag associated with the turbulent flow that results from tripping the boundary layer. However, the differences between the fixed- and free-transition data diminish as Reynolds number increases, because the local boundary-layer flow becomes turbulent sooner at higher Reynolds numbers.

Reynolds number effects. The effects of Reynolds number on the basic aerodynamic coefficients for several Mach numbers are presented in figures 17 (free transition) and 18 (fixed transition). These figures show that, below airfoil stall conditions, there was a decrease in drag coefficient and a minor increase in normal force and nose-down pitching-moment with increasing Reynolds number. However, the opposite trend is shown in figures 17(a) and 17(c) as the Reynolds number is increased from 4.4×10^6 to 7.7×10^6. For the low Reynolds number data in figure 17(a), $R_c = 4.4 \times 10^6$; the initial low drag coefficient is attributed to the presence of laminar flow over the airfoil. The abrupt increase in drag coefficient near $c_n = 0.5$ and higher is an indication of increased drag associated with transition from laminar to turbulent flow similar to the increase with the National Advisory Committee on Aeronautics (NACA) laminar-flow airfoils (ref. 15).

Mach number effects. The effects of Mach number on the basic aerodynamic coefficients for the range of test Reynolds numbers are presented in figures 19 (free transition) and 20 (fixed transition). The trends are generally similar for both free and fixed transition and indicate increases in normal-force slopes, drag, and nose-down pitching-moment coefficients with increasing Mach number. The maximum normal-force coefficient and the angle of attack for the maximum normal-force coefficient decreased with increasing Mach number. In the mid-α range ($3^\circ < \alpha < 6^\circ$, nominally) for the Mach number range of 0.70 to 0.76, both the normal-force and pitching-moment curves (for a fixed Mach number) exhibit abrupt slope changes, which indicates possible flow variations over the airfoil. These changes (based on unpublished airfoil pressure data) appear to correspond with the development of a shock wave on the model. The formation of the shock wave resulted in higher section drag coefficients for $M_\infty = 0.78$ (fig. 20) due to momentum loss from boundary-layer separation.

Trailing-Edge Pressure

The trailing-edge pressure was monitored during the initial entry to provide an indication of the onset of trailing-edge flow separation. This separation is indicated by the pressure coefficient becoming more negative. Figure 21 illustrates the effects of Mach number on the trailing-edge pressure coefficient ($C_{p,te}$) with fixed transition at three Reynolds numbers. At each Reynolds number, the data indicate that the section normal-force coefficient associated with separation decreases with increasing Mach number. These coefficients can also be related to the $c_{n,\max}$ when c_n is plotted against α. For example, at $M_\infty = 0.74$ and for $R_c = 7.7 \times 10^6$, the trailing-edge pressure coefficients indicate onset of separation at a normal-force coefficient of 0.94 (fig. 21(b)); the basic aerodynamic data in figure 16(b) indicate a maximum normal-force coefficient of 0.95. Figure 21 also shows that for fixed section normal-force coefficients below flow separation, the trailing-edge pressure coefficients become more positive (i.e., more pressure recovery) with increasing Reynolds number.

Airfoil Stability and Performance

Variation of c_m and c_n with R_c; $\alpha = 2°$. The airfoil pitching-moment and normal-force coefficient characteristics near the design conditions are presented in figure 22 for the test Reynolds number range and for both fixed and free transition. The Mach numbers for these conditions are 0.70 and 0.76. The free-transition data for both Mach numbers and $R_c \geq 7.7 \times 10^6$ show the same trends—increasing both section normal-force and nose-down pitching-moment coefficient with increasing Reynolds number—that were noted in previous discussions. The section normal-force and pitching-moment coefficient data for $M_\infty = 0.70$ indicate little change from $R_c = 4.4$ to 7.7×10^6, whereas the data for $M_\infty = 0.76$ show a decrease in both normal-force and nose-down pitching-moment coefficients. This trend with Reynolds number again illustrates the decambering effect on the fluid shape of the airfoil due to boundary-layer transition. As the Reynolds number is increased from 7.7 to 14.0×10^6, the fixed- and free-transition data are very close for the most part. This result, along with the previous discussion of boundary-layer tripping, suggests that the natural transition has moved forward to the point of fixed transition and occurs in the Reynolds number range from 7.0 to 14.0×10^6.

Variation of normal-force coefficient slopes and stability parameter with Mach number. Figure 23 presents a summary of the variation of section normal-force curve slope $c_{n,\alpha}$ with Mach number for free transition and Reynolds numbers of 14.0, 30.0, and 42.0×10^6. These results illustrate the characteristic increase in section normal-force curve slopes with increasing Mach number and large slope variation as the design Mach number (0.76) is approached. Variation of the stability parameter $\partial c_m/\partial c_n$ with Mach number at $c_n = 0.40$ is presented in figure 24 for the same three Reynolds numbers. The data for $R_c = 14.0$ and 30.0×10^6 show minor variations of $\partial c_m/\partial c_n$ with Mach number up to $M_\infty = 0.70$. However, positive stability (nose-down pitching moment) increases to a large rate for $M_\infty \geq 0.70$ and is attributed to a rapid rearward movement of the developed airfoil shock. The stability variation of the high Reynolds number ($R_c = 42.0 \times 10^6$) data indicates significant shifts of the airfoil center of pressure for $M_\infty \geq 0.70$. The decrease in positive stability in the Mach number range of 0.70 to 0.74 may be due to the presence of laminar flow before becoming fully turbulent at $M_\infty = 0.74$. With regard to the Reynolds number trends, positive stability increases from $R_c = 14.0 \times 10^6$ to $R_c = 30.0 \times 10^6$ for $M_\infty < 0.70$, but no clear trends were evident for $M_\infty > 0.7$.

Variations of c_d with R_c; $c_n = 0.65$ and 0.75. Figure 25 shows the variation of the section drag coefficient with test Reynolds number near the airfoil design section lift condition for fixed and free transition and $M_\infty = 0.70$ and 0.74. The fixed-transition data and free-transition data for $R_c \geq 14.0 \times 10^6$, essentially turbulent flow over the airfoil, illustrate the expected reduction in section drag coefficient with increasing Reynolds number. From the same figure, it is seen that the free-transition data for the lower Reynolds numbers (4.4 and 7.7×10^6) show lower section drag coefficients than the corresponding fixed-transition data. The lower values are attributed to the presence of laminar flow typical of low Reynolds number conditions, and the scatter of the coefficients is likely due to the nonuniform spanwise boundary-layer transition (fig. 11) discussed previously.

Variation of c_d with M_∞, $c_n = 0.55$, 0.65, and 0.75. Figure 26 presents the airfoil drag-rise characteristics for the range of test Reynolds number at normal-force coefficient values of 0.55, 0.65, and 0.75. The open symbols represent the free-transition data from the second tunnel entry, and the solid symbols represent the fixed-transition data from the first tunnel entry. The data show that the section drag coefficient and drag creep[1] increase with increasing normal coefficients. Also, the transition-free, low Reynolds number (4.4×10^6) data show a somewhat higher drag-divergence Mach number than

[1] The term "drag creep" is a description of the moderate drag rise as a result of gradual buildup of boundary layer and shock losses preceding drag divergence (ref. 16) and is dependent upon local boundary-layer condition and the associated fluid shape of the airfoil. This phenomenon had been the subject of advanced airfoil research, and references 16 and 17 are examples of early low Reynolds number investigations concerning a NASA 10-percent-thick supercritical airfoil.

the other test conditions. Interpreting the increased drag-divergence Mach number M_{dd} is difficult because of the inability to determine the transition location on the model. This difficulty is further illustrated in figure 27, which shows little effect of Reynolds number on M_{dd} for the free-transition data except for $R_c = 4.4 \times 10^6$, which has a noticeably higher value of M_{dd}. The area to the left of the drag-divergence Mach number curves represents the test conditions that can be achieved with this airfoil before encountering the transonic drag rise. (Again, these Mach numbers have not been adjusted for tunnel wall interference effects.)

Performance factor and range parameter. The effect of Mach number and Reynolds number on the airfoil, with free transition, is shown in figure 28. For a constant Reynolds number, these results generally indicate small reductions in the performance factor $(n/d)_{\max}$ with increasing Mach number up to transonic drag rise, after which significant performance reductions resulted (sharp break on curves). As expected, increasing the Reynolds number improves the airfoil performance because of the drag reduction associated with progressively smaller boundary-layer thickness. A performance map of the range parameter over the test Mach number range for the airfoil with free transition at $R_c = 30.0 \times 10^6$ is shown in figure 29.

Overall Test and Model Assessment

Primary objectives of the ATAT program were to provide the U.S. industry participants with the opportunity to gain experience in cryogenic testing and cryogenic model design and fabrication. Experience gained from the present airfoil test substantiated previous evidence that the physical stability of models at cryogenic test temperatures is a function of the material, the configuration design, and the overall model fabrication procedures. Model accuracy is also a major consideration for the boundary-layer conditions at high Reynolds numbers. Therefore, a thorough assessment of the accuracy of the model contours and a quantitative definition of the model surface finish, both before and after the test, are considered to be essential.

In general, there were no significant problems encountered with the model design and modified fabrication technique at Boeing. No structural problems were encountered with the load-carrying parts of the model. Post-test examinations of the model did not indicate any obvious distortions or structural failures in the cover plates or associated weld joints, or in the shape and dimension of the model in the spanwise or chordwise direction. There was very little deterioration of the surface finish on the model, in contrast to the model used in the first Boeing 0.3-m TCT test (ref. 3).

The design and fabrication techniques used for this model were shown to be structurally sound and conservative. The model contouring by the wire EDM process helped reduce the cost of the model to about one-half that of the first model (ref. 3); this reduction more than offset the cost for achieving the required stringent surface-finish and dimensional tolerance.

The material used to construct this model, Maraging 200 steel, is susceptible to corrosion. Models made out of this material need to be handled, tested, and stored with care. Minor corrosion had developed near the model trailing edge and the solder-filled upper surface pressure tap trenches (fig. 6(b)); however, nearly all the corrosion was removed by wiping the model with alcohol. The affected part was sufficiently downstream of the leading edge, so as not to have affected the transition location.

Summary of Results

A wind-tunnel investigation, which represents the second Boeing Commercial Airplanes (Boeing) test in the NASA/U.S. industry two-dimensional airfoil study in the Advanced Technology Airfoil Tests (ATAT) program, has been conducted in the Langley 0.3-Meter Transonic Cryogenic Tunnel. This investigation was designed to test a Boeing 12-percent-thick advanced-technology airfoil from low to flight Reynolds numbers and to provide Boeing with additional experience in cryogenic wind-tunnel model design, fabrication, and testing techniques.

All the objectives of this cooperative test were met. Limited analysis of the data from this investigation indicates the following results:

1. Turbulent boundary-layer flow was achieved on the airfoil by using aluminum transition disks at low Reynolds number over the test Mach number range.
2. Increasing Reynolds number resulted in increased normal force, increased nose-down pitching-moment coefficient, and generally decreased drag coefficient. No definite trends with Reynolds number could be determined for lift-curve slope, stability parameter, or drag-divergence Mach number.
3. Increasing Mach number yields increases in normal-force slopes and nose-down pitching-moment coefficients and a decrease of maximum normal-force coefficients.
4. For a given Reynolds number, the normal-force coefficients associated with trailing-edge separation

a fixed normal-force coefficient below airfoil flow separation, the trailing-edge pressure coefficient is more positive with increasing Reynolds number.

5. The data for a Reynolds number of 4.4×10^6 without transition trips had the highest drag-divergence Mach number for moderate values of normal-force coefficient.

NASA Langley Research Center
Hampton, VA 23665-5225
May 1, 1990

References

1. Whitcomb, Richard T.: Review of NASA Supercritical Airfoils. ICAS Paper No. 74-10, Aug. 1974.
2. Ladson, Charles L.; and Ray, Edward J.: Status of Advanced Airfoil Tests in the Langley 0.3-Meter Transonic Cryogenic Tunnel. *Advanced Aerodynamics—Selected NASA Research,* NASA CP-2208, 1981, pp. 37–53.
3. Johnson, William G., Jr.; Hill, Acquilla S.; Ray, Edward J.; Rozendaal, Roger A.; and Butler, Thomas W.: *High Reynolds Number Tests of a Boeing BAC I Airfoil in the Langley 0.3-Meter Transonic Cryogenic Tunnel.* NASA TM-81922, 1982.
4. Kilgore, Robert A.; Adcock, Jerry B.; and Ray, Edward J.: The Cryogenic Transonic Wind Tunnel for High Reynolds Number Research. *Windtunnel Design and Testing Techniques,* AGARD-CP-174, 1976, pp. 1-1–1-20.
5. Kilgore, Robert A.: *Design Features and Operational Characteristics of the Langley 0.3-Meter Transonic Cryogenic Tunnel.* NASA TN D-8304, 1976.
6. Ladson, Charles L.; and Kilgore, Robert A.: *Instrumentation for Calibration and Control of a Continuous-Flow Cryogenic Tunnel.* NASA TM-81825, 1980.
7. Baals, Donald D.; and Mourhess, Mary J.: *Numerical Evaluation of the Wake-Survey Equations for Subsonic Flow Including the Effect of Energy Addition.* NACA WR L-5, 1945. (Formerly NACA ARR L5H27.)
8. Hall, Robert M.; and Adcock, Jerry B.: *Simulation of Ideal-Gas Flow by Nitrogen and Other Selected Gases at Cryogenic Temperatures.* NASA TP-1901, 1981.
9. Adcock, Jerry B.: *Real-Gas Effects Associated With One-Dimensional Transonic Flow of Cryogenic Nitrogen.* NASA TN D-8274, 1976.
10. Adcock, Jerry B.; and Johnson, Charles B.: *A Theoretical Analysis of Simulated Transonic Boundary Layers in Cryogenic-Nitrogen Wind Tunnels.* NASA TP-1631, 1980.
11. Kemp, William B., Jr.: Transonic Assessment of Two-Dimensional Wind Tunnel Wall Interference Using Measured Wall Pressures. *Advanced Technology Airfoil Research—Volume I,* NASA CP-2045, Part 2, 1979, p. 473–486.
12. Sewall, W. G.: The Effects of Sidewall Boundary Layers in Two-Dimensional Subsonic and Transonic Wind Tunnels. AIAA-81-1297, June 1981.
13. Stanewsky, E.; Demurie, F.; Ray, E. J.; and Johnson, C. B.: High Reynolds Number Tests of the CAST 10-2/DOA2 Transonic Airfoil at Ambient and Cryogenic Temperature Conditions. *Wind Tunnels and Testing Techniques,* AGARD-CP-348, Feb. 1984, p. 10-1–10-13.
14. Reaser, J. S.: *Testing of an Advanced Technology Transonic Airfoil in a 2-D Cryogenic Wind Tunnel.* LR 30418, Lockheed-California Co., Feb. 1983.
15. Abbott, Ira H.; and Von Doenhoff, Albert E.: *Theory of Wing Sections.* Dover Publ., Inc., c.1959.
16. Harris, Charles D.: *Aerodynamic Characteristics of an Improved 10-Percent-Thick NASA Supercritical Airfoil.* NASA TM X-2978, 1974.
17. Harris, Charles D.: *Transonic Aerodynamic Characteristics of the 10-Percent-Thick NASA Supercritical Airfoil 31.* NASA TM X-3203, 1975.

Table I. Airfoil Force and Moment Data Tabulation

Pt.	$\overline{M}_{\infty,r}$	$M_{\infty,p}$	R_c	α, deg	c_n	c_m	c_d
Run 1							
1	0.7394	0.7386	4.46×10^6	−2.00	−0.004	−0.105	0.00962
2	.7390	.7388	4.43	.01	.274	−.110	.00961
3	.7391	.7410	4.39	1.03	.429	−.114	.01010
4	.7393	.7406	4.40	2.03	.559	−.113	.01077
5	.7392	.7373	4.41	3.01	.705	−.111	.01179
6	.7393	.7370	4.41	3.55	.803	−.114	[a].01406
7	.7387	.7379	4.41	3.50	.795	−.115	[a].01344
8	.7392	.7398	4.41	4.01	.896	−.126	[a].01777
10	.7391	.7459	4.42	4.54	.956	−.136	.02577
11	.7389	.7417	4.41	4.50	.954	−.131	.02429
12	.7389	.7409	4.40	5.04	.969	−.130	.04400
13	.7389	.7369	4.41	6.00	.965	−.123	.07530
Run 2							
14	0.7818	0.7843	4.42×10^6	−2.00	−0.015	−0.101	(b)
15	.7815	.7784	4.43	−2.00	−.018	−.102	0.01776
16	.7815	.7827	4.43	−1.01	.131	−.113	.01265
17	.7815	.7798	4.43	.03	.281	−.117	.01167
18	.7818	.7868	4.43	1.04	.433	−.127	.01346
19	.7816	.7773	4.43	2.05	.571	−.124	.01811
20	.7815	.7793	4.42	2.52	.628	−.128	.02270
21	.7815	.7809	4.42	3.01	.673	−.129	.03010
Run 3							
1	0.6984	0.6968	4.41×10^6	−2.00	0.007	−1.101	0.00905
2	.6981	.6973	4.42	.08	.282	−.104	.00918
3	.6981	.6959	4.40	1.13	.419	−.106	.00950
4	.6983	.6982	4.40	2.10	.548	−.109	.00996
5	.7030	.7030	4.42	3.08	.679	−.107	.01089
6	.7032	.7050	4.40	3.60	.756	−.106	.01186
7	.7032	.7008	4.40	4.08	.816	−.102	.01414
8	.7031	.7030	4.40	4.05	.811	−.102	.01402
9	.7029	.7023	4.39	4.57	.901	−.104	.01836
10	.7032	.7034	4.40	5.05	.986	−.105	.02490
11	.7031	.7058	4.39	6.05	1.104	−.110	.04290
12	.7031	.7014	4.40	7.05	1.129	−.107	.06620
Run 4							
13	0.7820	0.7788	7.69×10^6	−2.10	−0.019	−0.105	[a]0.02040
14	.7822	.7863	7.69	−.94	.184	−.125	[a].01231
15	.7817	.7804	7.70	.08	.330	−.129	.01198
16	.7817	.7790	7.69	1.14	.466	−.129	.01405
17	.7819	.7843	7.70	2.10	.594	−.137	.01976
18	.7821	.7835	7.68	2.57	.640	−.138	.02480
19	.7817	.7833	7.69	3.05	.680	−.135	.02870
20	.7817	.7838	7.68	3.55	.714	−.133	.03540

[a] Extrapolated airfoil wake profile used.

[b] Insufficient data for evaluation of associated coefficient.

Table I. Continued

Pt.	$\overline{M}_{\infty,r}$	$M_{\infty,p}$	R_c	α, deg	c_n	c_m	c_d
Run 5							
22	0.7624	0.7599	7.73×10^6	−2.02	−0.001	−0.109	[a]0.01098
23	.7620	.7622	7.71	−.99	.160	−.116	.00929
25	.7623	.7620	7.73	.01	.299	−.119	.00938
28	.7634	.7609	7.71	.99	.444	−.124	.01050
29	.7634	.7614	7.72	2.03	.609	−.127	.01252
30	.7634	.7629	7.68	3.03	.759	−.138	[a].02210
31	.7636	.7608	7.69	3.53	.803	−.137	.02870
32	.7636	.7601	7.71	4.04	.835	−.835	.03590
Run 6							
33	0.7438	0.7439	7.73×10^6	−2.04	0.025	−0.114	0.00922
34	.7437	.7437	7.72	.03	.312	−.119	.00897
35	.7437	.7478	7.73	1.02	.455	−.121	.00951
36	.7434	.7440	7.72	2.04	.596	−.121	.01017
37	.7437	.7452	7.71	3.30	.786	−.130	.01210
38	.7434	.7425	7.73	3.53	.855	−.134	[a].01622
39	.7433	.7429	7.74	4.02	.918	−.136	[a].02220
40	.7435	.7443	7.73	4.56	.944	−.136	[a].03260
41	.7438	.7475	7.73	4.57	.946	−.137	[a].03240
42	.7436	.7439	7.72	5.03	.938	−.129	[a].05080
Run 7							
44	0.7036	0.7030	7.71×10^6	−2.05	0.030	−0.109	0.00845
45	.7037	.7023	7.72	.04	.303	−.113	.00848
46	.7037	.7929	7.71	1.03	.429	−.113	(b)
47	.7035	.7005	7.71	1.03	.426	−.113	.00870
48	.7032	.7025	7.70	2.03	.562	−.115	.00928
49	.7036	.7037	7.70	3.03	.698	−.113	.00992
50	.7035	.7008	7.71	3.52	.764	−.112	.01120
51	.7037	.7024	7.72	4.03	.854	−.110	.01394
52	.7037	.7045	7.72	4.54	.956	−.113	[a].01928
53	.7036	.7059	7.72	5.03	1.043	−.116	.02720
54	.7036	.7048	7.72	6.05	1.143	−.120	.05230
55	.7035	.7034	7.71	7.05	1.117	−.119	[a].07820
Run 8							
4	0.7796	0.7849	4.42×10^6	−2.00	−0.022	−0.096	(b)
5	.7796	.7801	4.41	.02	.294	−.120	[a]0.01208
6	.7795	.7832	4.42	1.03	.438	−.125	.01397
7	.7792	.7793	4.42	2.06	.584	−.129	.01907
8	.7796	.7811	4.43	2.58	.633	−.131	.02480
Run 9							
9	0.7617	0.7592	7.74×10^6	−0.03	0.300	−0.120	0.00962
10	.7624	.7669	7.71	2.16	.637	−.134	[a].01305
11	.7626	.7616	7.71	2.57	.697	−.134	[a].01597
12	.7625	.7662	7.71	3.06	.752	−.140	[a].02110

[a] Extrapolated airfoil wake profile used.
[b] Insufficient data for evaluation of associated coefficient.

Table I. Continued

Pt.	$\overline{M}_{\infty,r}$	$M_{\infty,p}$	R_c	α, deg	c_n	c_m	c_d
			Run 10				
13	0.7426	0.7437	7.72×10^6	−0.03	0.302	−0.118	0.00918
14	.7426	.7443	7.73	2.06	.597	−.122	.01052
15	.7425	.7398	7.73	3.04	.746	−.120	[a].01213
16	.7426	.7462	7.73	3.55	.852	−.133	[a].01518
17	.7426	.7413	7.73	4.05	.916	−.135	[a].02110
18	.7427	.7434	7.73	4.52	.954	−.136	.02950
			Run 11				
19	0.7819	0.7816	14.05×10^6	−0.98	0.190	−0.129	[a]0.01233
20	.7819	.7856	14.06	.06	.342	−.137	[a].01231
21	.7821	.7802	14.05	1.06	.487	−.140	.01530
22	.7819	.7824	14.05	2.04	.611	−.144	.02210
23	.7822	.7793	14.05	2.55	.656	−.142	(b)
			Run 12				
24	0.7612	0.7611	14.04×10^6	−2.02	0.028	−0.119	[a]0.01036
25	.7609	.7616	14.04	−.98	.191	−.125	[a].00870
26	.7611	.7617	14.04	.03	.337	−.128	(b)
27	.7610	.7617	14.05	.04	.332	−.126	.00883
28	.7611	.7610	14.05	1.04	.479	−.131	[a].00983
29	.7611	.7615	14.05	2.04	.635	−.134	.01136
30	.7608	.7626	14.15	2.54	.705	−.140	.01420
31	.7632	.7631	14.06	3.00	.770	−.146	.02140
32	.7634	.7665	14.06	3.53	.798	−.142	[a].02920
			Run 13				
1	0.7026	0.7040	14.01×10^6	−2.00	0.038	−0.113	0.00792
2	.7027	.7008	14.03	.02	.324	−.117	.00802
3	.7022	.7020	14.03	1.03	.447	−.117	.00816
4	.7024	.7024	14.03	2.02	.572	−.117	.00859
5	.7024	.7049	14.04	3.02	.716	−.118	.00929
6	.7024	.7070	14.02	3.52	.786	−.116	.01041
7	.7023	.7007	14.02	4.02	.849	−.112	.01320
8	.7026	.7037	14.02	4.52	.950	−.117	.01793
9	.7022	.7050	14.02	5.02	1.012	−.114	.02460
10	.7025	.7007	14.02	6.02	1.106	−.113	.04160
			Run 14				
11	0.7429	0.7391	14.03×10^6	−1.98	0.038	−0.114	0.00863
12	.7433	.7465	14.00	.02	.327	−.124	.00861
13	.7433	.7406	14.02	1.03	.465	−.124	.00896
14	.7433	.7444	14.02	2.01	.609	−.126	.00967
15	.7432	.7434	14.02	3.02	.758	−.126	[a].01124
16	.7430	.7462	14.02	3.52	.833	−.130	[a].01390
17	.7432	.7431	14.02	4.02	.887	−.133	[a].01821
18	.7434	.7433	14.02	4.52	.939	−.135	.02520
19	.7431	.7409	14.02	5.02	.975	−.133	.03490
20	.7433	.7455	14.02	6.02	.943	−.124	[a].07770

[a] Extrapolated airfoil wake profile used.
[b] Insufficient data for evaluation of associated coefficient.

Table I. Continued

Pt.	$\overline{M}_{\infty,r}$	$M_{\infty,p}$	R_c	α, deg	c_n	c_m	c_d
Run 15							
1	0.7833	0.7863	7.72×10^6	−2.00	−0.027	−0.100	0.01647
2	.7828	.7861	7.71	−.97	.155	−.125	.01185
3	.7832	.7840	7.70	.03	.302	−.131	.01195
4	.7829	.7820	7.70	1.03	.458	−.137	.01504
5	.7831	.7841	7.70	2.02	.585	−.142	.02140
6	.7829	.7807	7.71	2.55	.642	−.139	.02910
Run 16							
7	0.7057	0.7049	7.66×10^6	−2.00	0.011	−0.104	0.00831
8	.7058	.7069	7.71	.02	.289	−.112	.00782
9	.7057	.7066	7.70	1.02	.422	−.115	.00824
10	.7061	.7080	7.68	2.01	.557	−.118	.00808
12	.7059	.7068	7.72	3.02	.697	−.116	.00888
13	.7057	.7055	7.71	3.52	.764	−.114	.01001
14	.7060	.7031	7.71	4.02	.838	−.110	.01300
15	.7060	.7038	7.72	4.52	.926	−.111	.01823
16	.7058	.7074	7.71	5.02	1.038	−.120	.02600
17	.7059	.7023	7.71	6.02	1.154	−.124	.05090
18	.7058	.7047	7.71	7.03	1.157	−.128	.08000
Run 17							
19	0.7026	0.7005	30.09×10^6	−2.01	0.045	−0.112	0.00704
20	.7025	.7062	30.06	.02	.323	−.120	.00712
21	.7027	.7040	30.07	1.02	.459	−.123	.00721
22	.7023	.7002	30.18	2.02	.577	−.119	.00761
23	.7002	.7026	30.17	3.02	.728	−.121	[a].00826
24	.7035	.7034	30.21	3.52	.799	−.119	[a].00981
25	.7036	.7081	30.22	4.02	.900	−.119	.01270
26	.7068	.7076	30.16	4.52	.986	−.122	.01878
27	.7060	.7043	30.13	5.02	1.061	−.124	.02640
28	.7020	.6989	30.00	6.03	1.180	−.127	.04910
Run 18							
29	0.6019	0.6023	7.72×10^6	−2.00	0.032	−0.098	0.00774
30	.6028	.6021	7.74	0	.271	−.102	[a].00787
31	.6025	.6040	7.73	1.01	.384	−.102	[a].00787
32	.6013	.6039	7.71	0	.504	−.104	.00738
33	.6022	.6048	7.72	3.01	.641	−.111	.00766
34	.5981	.5976	7.67	3.52	.688	−.108	.00807
35	.5997	.6003	7.67	4.01	.742	−.106	.00830
36	.6021	.6029	7.70	4.51	.811	−.106	.00870
37	.6036	.6052	7.71	5.01	.865	−.105	.00935
38	.6013	.6008	7.70	6.01	.980	−.095	.01213
39	.6025	.6058	7.71	7.02	1.123	−.090	.02100
40	.6019	.5973	7.71	8.01	1.190	−.084	.03560
41	.5997	.6034	7.66	9.03	(b)	(b)	.04910

[a] Extrapolated airfoil wake profile used.
[b] Insufficient data for evaluation of associated coefficient.

Table I. Continued

Pt.	$\overline{M}_{\infty,r}$	$M_{\infty,p}$	R_c	α, deg	c_n	c_m	c_d
Run 19							
42	0.7665	0.7702	30.04×10^6	0	0.344	−0.138	[a]0.00851
43	.7658	.7664	30.08	2.02	.646	−.145	[a].01264
44	.7644	.7663	29.66	2.53	.715	−.150	[a].01706
45	.7602	.7613	30.06	3.02	.792	−.150	[a].01935
Run 20							
1	0.7026	0.7036	4.40×10^6	−2.00	0.063	−0.118	0.00710
2	.7024	.7018	4.40	−1.98	.055	−.114	.00723
3	.7023	.7000	4.39	.03	.315	−.118	.00710
4	.7022	.7007	4.41	1.03	.447	−.119	.00672
5	.7022	.7011	4.41	2.02	.559	−.116	.00811
6	.7023	.7024	4.41	3.04	.696	−.114	.00868
7	.7024	.7043	4.41	3.54	.774	−.114	.00964
8	.7022	.7017	4.41	4.05	.850	−.111	.01246
9	.7022	.7020	4.41	4.52	.936	−.111	.01760
10	.7023	.7008	4.41	5.04	1.024	−.114	.02560
11	.7025	.7049	4.40	6.02	1.172	−.126	.04760
12	.7023	.7046	4.40	7.04	1.206	−.122	.06350
Run 21							
13	0.7432	0.7427	4.40×10^6	−2.13	0.033	−0.120	0.00782
14	.7427	.7412	4.40	.04	.341	−.127	.00709
15	.7429	.7351	4.40	1.02	.463	−.124	.00772
16	.7430	.7441	4.40	2.01	.608	−.127	.00844
17	.7435	.7444	4.41	3.02	.792	−.134	[a].00946
18	.7431	.7469	4.40	3.53	.906	−.152	[a].01266
19	.7431	.7441	4.40	4.03	.955	−.149	[a].01873
20	.7430	.7399	4.40	4.52	.996	−.147	[a].02820
21	.7429	.7434	4.40	5.03	1.017	−.150	[a].04310
22	.7407	.7399	4.39	6.04	1.071	−.144	.06360
Run 22							
23	0.7601	0.7605	4.40×10^6	−1.99	0.049	−0.123	[a]0.00888
24	.7599	.7609	4.39	−.98	.203	−.129	[a].00788
25	.7593	.7608	4.39	.01	.352	−.134	[a].00733
26	.7629	.7632	4.40	1.02	.508	−.139	[a].00783
27	.7625	.7591	4.40	2.01	.648	−.137	.00896
28	.7615	.7636	4.40	2.52	.743	−.149	[a].01096
29	.7603	.7611	4.39	3.02	.817	−.153	[a].01534
30	.7632	.7635	4.40	3.51	.857	−.157	[a].02720
31	.7618	.7638	4.40	4.02	.871	−.155	.03830

[a] Extrapolated airfoil wake profile used.

Table I. Continued

Pt.	$\overline{M}_{\infty,r}$	$M_{\infty,p}$	R_c	α, deg	c_n	c_m	c_d
			Run 23				
32	0.7471	0.7453	7.75×10^6	−2.01	0.023	−0.113	[a]0.00944
33	.7406	.7433	7.72	.02	.312	−.123	.00896
34	.7414	.7424	7.73	1.03	.454	−.123	.00909
35	.7444	.7442	7.75	2.03	.588	−.121	.00979
36	.7397	.7405	7.67	3.04	.764	−.126	.01067
38	.7431	.7438	7.70	3.53	.858	−.136	[a].01431
39	.7449	.7443	7.71	4.02	.930	−.148	[a].02140
40	.7411	.7437	7.68	4.53	.975	−.147	[a].02890
41	.7437	.7454	7.73	5.02	.947	−.136	.05530
			Run 24				
43	0.7656	0.7659	7.73×10^6	−2.01	0.014	−0.116	[a]0.01166
44	.7653	.7649	7.73	−.99	.179	−.123	[a].00946
45	.7641	.7667	7.72	0	.322	−.127	.00922
46	.7634	.7666	7.71	1.01	.474	−.131	.01026
47	.7635	.7644	7.74	2.01	.625	−.136	.01113
48	.7632	.7649	7.72	2.52	.703	−.139	.01408
49	.7632	.7658	7.73	3.02	.762	−.143	.01940
			Run 101				
2	0.7596	0.7610	29.97×10^6	−0.99	0.1748	−0.1248	0.00762
3	.7589	.7590	29.94	.03	.3165	−.1268	.00762
4	.7577	.7570	29.91	1.04	.4689	−.1321	.00810
5	.7567	.7567	29.95	2.03	.6051	−.1302	.00861
7	.7603	.7621	30.01	2.53	.6817	−.1339	.01079
8	.7597	.7574	30.01	3.02	.7436	−.1335	.01213
9	.7599	.7585	30.04	3.53	.8004	−.1359	[a].01522
10	.7596	.7572	30.03	4.04	.8586	−.1386	.01999
			Run 102				
1	0.7037	0.7027	29.96×10^6	−2.02	0.0452	−0.1131	0.00710
2	.7004	.6977	29.96	.01	.3079	−.1175	.00705
3	.7010	.6999	30.01	.04	.3109	−.1170	.00709
4	.7004	.7017	29.99	1.01	.4294	−.1171	.00717
5	.6986	.6977	29.97	2.05	.5687	−.1189	.00736
6	.6991	.7013	30.06	3.02	.6919	−.1167	.00778
7	.6989	.7032	29.98	3.12	.7108	−.1170	.00805
8	.7017	.7038	30.06	3.52	.7680	−.1151	.00898
9	.6987	.6971	29.98	4.04	.8418	−.1123	.01081
10	.6982	.6971	29.97	4.54	.9128	−.1089	.01494
11	.7013	.6993	30.11	5.03	.9963	−.1091	.02190

[a] Extrapolated airfoil wake profile used.

Table I. Continued

Pt.	$\overline{M}_{\infty,r}$	$M_{\infty,p}$	R_c	α, deg	c_n	c_m	c_d
Run 103							
12	0.7593	0.7595	13.98×10^6	−2.01	0.0256	−0.1178	0.00960
13	.7589	.7611	13.99	.99	.1781	−.1227	.00853
14	.7573	.7541	13.97	.89	.1934	−.1227	.00847
15	.7607	.7609	14.03	0	.3248	−.1276	.00869
16	.7584	.7589	14.01	1.00	.4620	−.1281	.00918
18	.7597	.7614	14.03	1.12	.4821	−.1299	(b)
20	.7595	.7589	13.97	2.03	.6166	−.1310	(b)
21	.7607	.7626	14.01	2.18	.6424	−.1340	(b)
22	.7594	.7600	14.00	2.54	.7019	−.1386	(b)
23	.7587	.7592	14.00	3.03	.7690	−.1395	(b)
24	.7598	.7614	14.00	3.51	.8135	−.1433	(b)
25	.7610	.7618	14.02	4.05	.8479	−.1367	(b)
26	.7619	.7643	14.03	3.98	.8261	−.1386	(b)
27	.7621	.7653	14.04	4.01	.8247	−.1373	(b)
Run 104							
28	0.7443	0.7447	14.07×10^6	−1.98	0.0290	−0.1164	[a]0.00845
29	.7412	.7424	14.03	.02	.3173	−.1224	(b)
30	.7414	.7412	14.04	.03	.3172	−.1220	.00815
31	.7405	.7405	14.04	1.02	.4535	−.1239	.00842
32	.7403	.7405	14.04	2.05	.5935	−.1226	[a].00925
33	.7413	.7418	14.02	2.18	.6171	−.1238	.00920
34	.7431	.7434	14.01	2.51	.6716	−.1238	[a].00954
35	.7413	.7407	14.01	3.03	.7556	−.1242	[a].01051
36	.7401	.7431	14.02	3.54	.8461	−.1320	[a].01420
37	.7392	.7406	14.03	4.03	.9173	−.1357	(b)
38	.7391	.7352	13.89	4.55	.9832	−.1395	(b)
39	.7389	.7409	13.95	4.05	.9647	−.1399	(b)
Run 105							
1	0.7702	0.7721	4.43×10^6	−1.99	0.0414	−0.1242	(b)
2	.7684	.7692	4.42	−1.00	.1901	−.1288	[a]0.00716
3	.7703	.7711	4.41	.02	.3365	−.1335	.00749
4	.7707	.7705	4.40	1.04	.4841	−.1376	.00869
5	.7694	.7701	4.39	2.03	.6193	−.1371	.00977
6	.7727	.7707	4.40	2.56	.6862	−.1402	.01282
7	.7719	.7697	4.40	3.02	.7390	−.1413	[a].01518
8	.7725	.7714	4.40	3.51	.7841	−.1418	(b)
9	.7714	.7692	4.39	4.02	.8358	−.1421	(b)

[a] Extrapolated airfoil wake profile used.
[b] Insufficient data for evaluation of associated coefficient.

Table I. Continued

Pt.	$\overline{M}_{\infty,r}$	$M_{\infty,p}$	R_c	α, deg	c_n	c_m	c_d
Run 107							
10	0.7580	0.7607	4.41×10^6	−2.01	0.0451	−0.1227	[a]0.00720
11	.7571	.7598	4.41	−1.00	.1893	.1264	.00645
12	.7600	.7607	4.42	.01	.3275	−.1289	.00666
13	.7598	.7579	4.42	1.00	.4616	−.1294	.00763
14	.7596	.7598	4.41	2.01	.6042	−.1297	.00829
15	.7625	.7641	4.42	2.50	.6820	−.1350	.00932
16	.7594	.7605	4.41	3.01	.7509	−.1351	.01020
17	.7614	.7604	4.42	3.50	.7985	−.1350	[a].01410
18	.7608	.7628	4.41	4.00	.8465	−.1355	(b)
Run 108							
19	0.6984	0.7012	4.40×10^6	−2.00	0.0576	−0.1142	0.00641
20	.7000	.7023	4.41	.01	.3071	−.1167	[a].00647
22	.7005	.7005	4.40	1.00	.4290	−.1169	[a].00674
23	.7005	.7016	4.41	2.02	.5471	−.1148	.00745
24	.6998	.7009	4.41	2.99	.6616	−.1101	.00865
25	.7008	.7029	4.41	3.49	.7325	−.1090	.00911
26	.7012	.7026	4.41	3.99	.8098	−.1078	.01057
27	.7018	.7031	4.41	4.50	.8932	−.1064	[a].01400
28	.7016	.7011	4.40	4.99	.9754	−.1073	[a].01985
29	.6996	.7007	4.41	6.02	1.1188	−.1121	.03707
30	.6998	.7004	4.41	7.00	1.1717	−.1088	.05427
Run 109							
31	0.6001	0.6014	4.41×10^6	−1.99	0.0597	−0.1042	0.00577
33	.6007	.6013	4.42	.01	.2903	−.1066	.00604
34	.5998	.6002	4.41	1.00	.4017	−.1068	.00621
35	.5989	.5990	4.41	2.01	.5047	−.1044	.00708
36	.6006	.6021	4.41	2.99	.6153	−.1040	.00779
37	.6010	.6019	4.42	3.49	.6741	−.1046	.00840
39	.6004	.6013	4.42	4.00	.7310	−.1028	(b)
40	.5987	.5984	4.41	4.49	.7797	−.1008	.00918
41	.5992	.5999	4.42	5.00	.8333	−.0977	.00961
42	.5990	.5987	4.41	6.00	.9453	−.0891	.01252
43	.6016	.6027	4.42	7.01	1.0706	−.0830	.01982
44	.5995	.5998	4.41	8.00	1.1758	−.0778	.03227
Run 110							
3	0.7730	0.7746	7.73×10^6	−1.98	0.0110	−0.1153	[a]0.01265
4	.7708	.7713	7.72	−1.00	.1629	−.1238	.00929
5	.7708	.7694	7.72	.01	.3014	−.1252	.00901
6	.7712	.7792	7.70	1.01	.4484	−.1294	.00996
7	.7738	.7637	7.70	2.01	.5970	−.1364	.01307
8	.7708	.7693	7.68	2.53	.6788	−.1389	.01547
9	.7711	.7687	7.69	3.03	.7407	−.1418	.02027
10	.7713	.7697	7.68	3.52	.7836	−.1429	.02527

[a] Extrapolated airfoil wake profile used.
[b] Insufficient data for evaluation of associated coefficient.

Table I. Continued

Pt.	$\overline{M}_{\infty,r}$	$M_{\infty,p}$	R_c	α, deg	c_n	c_m	c_d
Run 111							
11	0.7608	0.7613	7.72×10^6	−2.00	0.0169	−0.1166	0.00940
12	.7603	.7617	7.71	−1.00	.1666	−.1213	.00819
13	.7595	.7590	7.71	.01	.3058	−.1242	.00807
14	.7624	.7626	7.72	1.00	.4482	−.1271	.00883
15	.7610	.7597	7.71	2.00	.5922	−.1271	.00937
16	.7642	.7632	7.73	2.51	.6776	−.1325	.01216
17	.7624	.7616	7.72	3.00	.7496	−.1369	.01491
18	.7583	.7622	7.70	3.50	.8123	−.1399	.01732
19	.7590	.7576	7.69	4.01	.8756	−.1429	.02327
20	.7593	.7564	7.70	4.51	.9086	−.1407	.03198
Run 112							
21	0.6989	0.6997	7.69×10^6	−2.01	0.0315	−0.1082	0.00805
22	.7018	.7015	7.71	.01	.2946	−.1141	.00742
23	.7004	.7012	7.70	1.01	.4166	−.1140	.00763
24	.7000	.6999	7.70	2.01	.5445	−.1148	.00770
25	.7027	.7030	7.70	3.02	.6765	−.1129	.00842
26	.7008	.7000	7.68	3.50	.7454	−.1121	.00932
27	.6971	.6971	7.66	4.01	.8112	−.1081	.01051
28	.7014	.7014	7.69	4.51	.8966	−.1068	.01457
29	.7015	.7028	7.69	5.01	.9868	−.1089	.02069
30	.7008	.7000	7.69	6.02	1.1180	−.1117	.03828
Run 113							
31	0.5989	0.6004	13.94×10^6	−1.98	0.0460	−0.1021	0.00741
32	.6039	.6030	14.04	0	.2810	−.1056	.00744
33	.6018	.6013	14.01	.99	.3922	−.1061	.00753
34	.6020	.6020	14.01	2.01	.5138	−.1071	.00762
35	.5993	.5962	13.96	3.00	.6319	−.1078	.00792
36	.6011	.6000	13.99	4.01	.7502	−.1072	.00827
37	.6034	.6033	14.03	4.51	.8092	−.1059	.00855
38	.5990	.6005	13.96	5.01	.8586	−.1036	.00896
39	.6031	.6050	14.04	5.51	.9208	−.1010	.01014
40	.6027	.6015	14.03	6.02	.9810	−.0954	.01210
41	.5991	.5995	13.97	7.02	1.0746	−.0883	.01941
42	.6020	.6056	14.02	8.01	1.1668	−.0753	.03240
Run 114							
43	0.7003	0.7005	13.99×10^6	−0.20	0.0373	−0.1111	0.00775
44	.7001	.7003	13.99	.01	.2994	−.1153	.00766
45	.7004	.7018	14.00	1.01	.4289	−.1172	.00768
46	.6986	.7004	13.97	2.01	.5525	−.1159	.00806
47	.7002	.7010	13.99	3.01	.6863	−.1150	.00876
48	.7013	.7002	14.00	3.50	.7561	−.1139	.00954
49	.7000	.6979	13.99	4.01	.8273	−.1108	.01142
50	.7001	.7003	13.99	4.51	.9142	−.1095	.01529
51	.6993	.6996	13.97	5.01	.9885	−.1088	.02078
52	.7001	.6981	13.99	6.03	1.1249	−.1121	.03975

Table I. Continued

Pt.	$\overline{M}_{\infty,r}$	$M_{\infty,p}$	R_c	α, deg	c_n	c_m	c_d
			Run 115				
1	0.7706	0.7695	30.00×10^6	−2.00	0.0400	−0.1228	0.01059
2	.7709	.7688	30.00	−1.00	.1905	−.1296	.00833
3	.7714	.7709	30.03	.01	.3418	−.1353	.00879
4	.7716	.7747	30.02	1.01	.4843	−.1411	.01043
5	.7717	.7711	29.88	1.04	.4855	−.1392	.01020
6	.7715	.7711	30.00	2.03	.6283	−.1417	.01285
7	.7735	.7756	30.00	2.53	.6822	−.1443	.01712
8	.7687	.7664	30.01	3.02	.7532	−.1445	.01758
9	.7721	.7716	30.01	3.54	.7902	−.1452	.02329
			Run 117				
1	0.7609	0.7608	29.91×10^6	−1.98	0.0390	−0.1220	0.00878
2	.7612	.7622	30.00	−1.00	.1881	−.1280	.00765
3	.7616	.7634	29.98	.01	.3342	−.1314	.00784
4	.7599	.7588	29.97	1.01	.4737	−.1325	.00746
5	.7621	.7631	30.03	2.03	.6227	−.1347	.01015
6	.7629	.7632	30.05	2.53	.7003	−.1399	.01139
7	.7597	.7591	30.03	3.01	.7648	−.1416	.01398
8	.7599	.7645	29.99	3.52	.8105	−.1443	.01749
9	.7594	.7584	29.98	4.02	.8682	−.1435	.02083
10	.7608	.7594	29.96	4.53	.9051	−.1419	.03016
			Run 118				
11	0.7419	0.7410	29.97×10^6	−2.00	0.0472	−0.1203	0.00765
12	.7397	.7413	29.88	.01	.3298	−.1264	.00727
13	.7411	.7408	29.95	1.01	.4701	−.1283	.00761
14	.7384	.7393	29.95	2.03	.6081	−.1268	.00799
15	.7442	.7441	30.25	2.53	.6906	−.1275	.00862
16	.7436	.7441	29.88	3.01	.7661	−.1293	.00992
17	.7416	.7418	29.86	3.51	.8363	−.1300	.01214
18	.7407	.7392	29.94	4.03	.9061	−.1326	.01592
19	.7383	.7392	30.07	5.01	.9912	−.1333	.02815
20	.7433	.7440	30.00	6.04	.9772	−.1285	.06816
			Run 119				
21	0.6019	0.6026	30.00×10^6	−1.98	0.0612	−0.1043	0.00702
22	.6025	.6015	30.09	0	.2940	−.1079	.00670
23	.6022	.6024	30.09	1.00	.4114	−.1090	.00680
25	.6026	.6035	30.04	2.02	.5321	−.1098	.00681
26	.6006	.5969	29.99	3.00	.6469	−.1104	.00720
27	.6011	.5975	29.96	4.01	.7661	−.1099	.00763
28	.6016	.6018	30.01	4.51	.8187	−.1068	.00804
29	.6013	.5982	29.95	5.01	.8764	−.1064	.00865
30	.6018	.6024	30.00	5.52	.9343	−.1015	.00973
31	.6017	.6022	29.96	6.03	.9978	−.0971	.01181
32	.6018	.6023	29.94	7.03	1.0959	−.0886	.02027
34	.6024	.6025	29.93	8.03	1.1772	−.0772	.03300

Table I. Continued

Pt.	$\overline{M}_{\infty,r}$	$M_{\infty,p}$	R_c	α, deg	c_n	c_m	c_d
Run 120							
36	0.7410	0.7426	30.00×10^6	−0.02	0.3328	−0.1262	0.00738
37	.7428	.7451	29.94	2.53	.6858	−.1257	.00873
38	.7397	.7402	29.93	3.02	.7647	−.1264	.00936
39	.7425	.7452	30.01	3.52	.8523	−.1357	.01287
40	.7392	.7397	29.88	4.04	.9088	−.1338	.01602
Run 121							
41	0.5027	0.5021	30.04×10^6	−2.01	0.0604	−0.0979	0.00685
42	.5025	.5031	30.00	0	.2804	−.1005	.00668
43	.5022	.5013	30.03	2.00	.5000	−.1030	.00678
44	.5021	.5008	30.05	3.00	.6090	−.1039	.00705
45	.5019	.5001	30.16	4.01	.7207	−.1042	.00748
46	.5020	.5011	30.08	4.50	.7706	−.1033	.00760
47	.5021	.5021	30.06	5.01	.8266	−.1030	.00789
48	.5024	.5027	30.05	5.51	.8858	−.1041	.00832
49	.5022	.5033	30.02	6.00	.9276	−.1011	.00862
50	.5025	.5008	30.04	7.00	1.0214	−.0961	.01015
51	.5025	.5023	30.04	8.01	1.0847	−.0850	.01534
52	.5025	.5012	30.04	8.98	1.1370	−.0757	.02519
Run 122							
54	0.7021	0.6994	42.10×10^6	0.01	0.3190	−0.1190	0.00684
55	.7018	.7012	42.09	1.02	.4538	−.1212	.00699
56	.7020	.7006	41.93	2.01	.5869	−.1229	.00724
57	.6981	.7001	41.87	3.07	.7202	−.1186	.00788
58	.7020	.7033	42.07	4.02	.8672	−.1144	.01173
59	.7032	.7053	42.12	3.52	.7961	−.1180	.00920
Run 123							
60	0.7420	0.7423	42.08×10^6	−2.02	0.0494	−0.1213	0.00746
61	.7417	.7420	42.07	.02	.3388	−.1275	.00721
62	.7424	.7384	42.09	1.02	.4749	−.1281	.00760
64	.7370	.7355	42.11	2.05	.6192	−.1286	.00805
Run 124							
65	0.7637	0.7607	42.12×10^6	−2.07	0.0300	−0.1221	0.00958
66	.7606	.7619	42.02	−.98	.1978	−.1291	.00775
67	.7627	.7645	42.07	.02	.3486	−.1346	.00797
Run 125							
69	0.7735	0.7725	13.95×10^6	−2.00	0.0268	−0.1191	0.01195
70	.7700	.7703	13.96	−.98	.1834	−.1262	.00911
71	.7697	.7706	13.99	.02	.3368	−.1320	.00929
72	.7697	.7692	14.00	1.01	.4751	−.1343	.01076
73	.7707	.7757	14.01	2.02	.6217	−.1385	[a].01380
74	.7691	.7695	14.00	2.52	.6939	−.1412	.01694
75	.7714	.7638	14.01	3.02	.7546	−.1409	.02457
76	.7658	.7658	13.96	3.51	.7998	−.1410	.02586
77	.7726	.7740	14.03	1.51	.5516	−.1389	.01256

[a] Extrapolated airfoil wake profile used.

Table I. Continued

Pt.	$\overline{M}_{\infty,r}$	$M_{\infty,p}$	R_c	α, deg	c_n	c_m	c_d
			Run 126				
78	0.7601	0.7626	7.73×10^6	0.01	0.3174	−0.1226	0.00922
79	.7681	.7677	7.80	2.03	.6097	−.1324	[a].01211
81	.7572	.7570	7.71	2.51	.6628	−.1254	.01126
82	.7617	.7610	7.74	3.00	.7455	−.1345	.01645
83	.7582	.7604	7.65	2.01	.5911	−.1264	.01014
			Run 127				
1	0.7683	0.7695	14.04×10^6	0.01	0.2995	−0.1260	0.00905
2	.7708	.7713	14.05	1.58	.5225	−.1304	.01125
3	.7693	.7711	14.01	2.04	.5997	−.1351	.01166
4	.7733	.7695	14.04	2.52	.6696	−.1385	.01686
5	.7743	.7760	13.98	3.02	.7126	−.1419	.02220
			Run 128				
6	0.7401	0.7401	13.98×10^6	0.03	0.3134	−0.1226	0.00821
7	.7403	.7374	13.98	2.50	.6470	−.1224	.00949
8	.7425	.7439	13.99	3.02	.7368	−.1239	.00999
9	.7412	.7387	13.99	3.52	.8037	−.1202	.01184
10	.7435	.7400	14.02	4.01	.8810	−.1274	.01653
			Run 129				
11	0.5998	0.5994	14.00×10^6	0.02	0.2828	−0.1061	0.00747
12	.6014	.6008	14.04	2.01	.5136	−.1071	.00777
13	.6058	.6040	14.10	4.01	.7394	−.1051	.00833
14	.6007	.6054	14.03	5.51	.9200	−.1009	.01036
15	.5990	.6001	14.00	5.00	.8642	−.1051	.00914
16	.5976	.5971	13.98	6.02	.9666	−.0964	.01204
			Run 130				
17	0.5001	0.5016	7.65×10^6	−1.98	0.0493	−0.0948	0.00790
18	.4987	.4984	7.70	0	.2659	−.0976	.00776
19	.5003	.4987	7.73	.98	.3745	−.0990	.00790
20	.5005	.4994	7.73	2.00	.4834	−.1000	.00763
21	.5003	.5003	7.73	3.00	.5920	−.1011	.00793
22	.5010	.4993	7.73	4.00	.7014	−.1012	.00830
23	.5009	.4994	7.74	4.50	.7489	−.1005	.00848
24	.5006	.4992	7.73	5.00	.8041	−.1007	.00885
25	.5018	.5000	7.75	5.49	.8620	−.1011	.00902
26	.5022	.5018	7.75	6.01	.9115	−.0994	.00931
27	.5021	.5016	7.73	7.01	1.0024	−.0923	.01110
28	.5023	.5006	7.75	8.00	1.0634	−.0811	.01563
29	.5027	.5041	7.76	9.01	1.1097	−.0711	.02338
30	.5029	.5006	7.76	10.16	1.1406	−.0616	.03890

[a] Extrapolated airfoil wake profile used.

Table I. Continued

Pt.	$\overline{M}_{\infty,r}$	$M_{\infty,p}$	R_c	α, deg	c_n	c_m	c_d
Run 131							
31	0.7015	0.7021	7.71×10^6	0.02	0.2978	−0.1139	0.00835
32	.7004	.6996	7.71	2.01	.5490	−.1152	.00860
33	.7007	.6988	7.71	3.01	.6797	−.1143	.00908
34	.7007	.7011	7.71	3.50	.7466	−.1117	.00993
35	.7006	.6993	7.71	4.00	.8208	−.1099	.01190
36	.7006	.6988	7.71	4.51	.9024	−.1081	.01563
Run 132							
37	0.7024	0.7021	4.43×10^6	0.02	0.3172	−0.1194	0.00603
38	.7027	.7036	4.44	2.01	.5515	−.1172	.00775
39	.7006	.7023	4.41	3.00	.6661	−.1119	.00850
40	.6990	.6995	4.41	3.49	.7312	−.1101	.00909
41	.6983	.6983	4.41	3.99	.8043	−.1080	.01048
42	.7011	.7011	4.42	4.50	.8911	−.1077	.01461
Run 133							
43	0.7017	0.7015	22.03×10^6	−1.98	0.0290	−0.1106	0.00734
44	.7014	.7033	22.04	.03	.2977	−.1170	.00736
45	.6994	.7002	22.01	1.02	.4265	−.1184	.00757
46	.6981	.6939	21.98	2.03	.5542	−.1190	.00779
47	.7010	.7036	22.02	2.05	.5567	−.1182	.00778
48	.7007	.6985	22.02	3.03	.6888	−.1178	.00832
49	.6968	.6970	21.96	3.53	.7502	−.1140	.00894
50	.7009	.7017	22.05	4.05	.8313	−.1122	.01151
51	.7013	.7029	22.05	4.52	.9183	−.1115	.01564
52	.7011	.6989	22.05	5.04	1.0002	−.1116	.02201
53	.7005	.7001	22.03	6.03	1.1232	−.1163	.03848
Run 134							
57	0.7416	0.7424	22.01×10^6	0.02	0.3260	−0.1261	0.00778
58	.7416	.7444	22.02	1.01	.4633	−.1280	.00810
59	.7422	.7437	22.05	2.02	.6036	−.1285	.00871
60	.7423	.7439	22.03	2.51	.6806	−.1278	.00910
61	.7397	.7406	21.99	3.01	.7472	−.1248	.00970
62	.7408	.7408	22.08	3.52	.8342	−.1307	.01210
63	.7394	.7417	21.99	4.01	.9040	−.1351	.01606
64	.7380	.7406	21.88	5.01	.9946	−.1388	.02865
Run 135							
2	0.6982	0.6981	42.12×10^6	3.56	0.7707	−0.1165	0.00859
3	.7025	.7033	42.45	3.99	.8456	−.1141	[a].01113
4	.7008	.6986	42.15	4.52	.9229	−.1123	.01475
5	.7017	.7002	42.39	5.04	1.0071	−.1125	.02170

[a] Extrapolated airfoil wake profile used.

Table I. Concluded

Pt.	$\overline{M}_{\infty,r}$	$M_{\infty,p}$	R_c	α, deg	c_n	c_m	c_d
Run 136							
6	0.7406	0.7421	42.22×10^6	2.00	0.6032	−0.1281	0.00790
7	.7409	.7420	42.33	2.52	.6775	−.1268	.00816
9	.7403	.7388	42.16	3.02	.7584	−.1272	.00881
10	.7385	.7380	41.52	3.51	.8301	−.1293	.01029
11	.7388	.7414	41.74	4.00	.8968	−.1341	.01457
Run 137							
12	0.7620	0.7645	42.34×10^6	−0.99	0.1975	−0.1313	0.00752
13	.7635	.7639	42.23	0	.3434	−.1361	.00802
14	.7629	.7605	42.30	1.02	.4847	−.1371	[a].00914
15	.7580	.7572	41.35	2.05	.6340	−.1366	.00954
16	.7590	.7546	40.89	2.53	.7092	−.1395	.01168
Run 138							
18	0.7719	0.7710	42.10×10^6	−1.01	0.1892	−0.1326	0.00854
19	.7698	.7691	42.04	0	.3470	−.1390	.00866
21	.7693	.7670	42.08	1.02	.4945	−.1427	.01031
22	.7693	.7693	41.49	1.54	.5674	−.1442	.01035
23	.7682	.7663	41.18	2.02	.6393	−.1469	.01184

[a] Extrapolated airfoil wake profile used.

Table II. Sample Tunnel Free-Stream Mach Number Deviation

Pt.	R_c	$\overline{M}_{\infty,r}$	σ
Run 1			
1	4.4×10^6	0.7393	0.0027
2	↓	.7390	.0024
3		.7390	.0023
4		.7393	.0022
5		.7391	.0020
6		.7392	.0019
7		.7386	.0020
8		.7391	.0022
10		.7393	.0047
11		.7389	.0022
12		.7389	.0027
13		.7388	.0024
Run 6			
33	7.7×10^6	0.7437	0.0022
34	↓	.7437	.0026
35		.7437	.0022
36		.7433	.0031
37		.7437	.0020
38		.7434	.0023
39		.7432	.0029
40		.7434	.0029
42		.7436	.0024
Run 14			
11	14.0×10^6	0.7429	0.0022
12	↓	.7432	.0018
13		.7433	.0019
14		.7432	.0024
15		.7431	.0019
16		.7429	.0022
17		.7432	.0019
18		.7434	.0025
19		.7431	.0026
20		.7432	.0025
Run 102			
1	30.0×10^6	0.7037	0.0018
2	↓	.7004	.0017
3		.7010	.0017
4		.7004	.0014
5		.6986	.0019
6		.6991	.0017
7		.6989	.0016
8		.7017	.0023
9		.6987	.0020
10		.6982	.0016
11		.7013	.0018

Table II. Continued

Pt.	R_c	$\overline{M}_{\infty,r}$	σ
		Run 115	
1	30.0×10^6	0.7706	0.0016
2	↓	.7709	.0017
3		.7714	.0013
4		.7716	.0022
5		.7717	.0019
6		.7715	.0017
7		.7735	.0021
8		.7687	.0020
9		.7721	.0022
		Run 117	
1	30.0×10^6	0.7609	0.0017
2	↓	.7612	.0012
3		.7616	.0014
4		.7599	.0018
5		.7621	.0020
6		.7629	.0021
7		.7597	.0020
8		.7599	.0023
9		.7594	.0019
10		.7608	.0023
		Run 118	
11	30.0×10^6	0.7419	0.0022
12	↓	.7397	.0016
13		.7411	.0019
14		.7384	.0018
15		.7442	.0022
16		.7436	.0017
17		.7416	.0017
18		.7407	.0019
19		.7383	.0021
20		.7433	.0027
		Run 119	
21	30.0×10^6	0.6019	0.0006
22	↓	.6025	.0008
23		.6022	.0006
25		.6026	.0006
26		.6006	.0014
27		.6011	.0021
28		.6016	.0014
29		.6013	.0015
30		.6018	.0016
31		.6017	.0017
32		.6018	.0016
34		.6024	.0015

Table II. Concluded

Pt.	R_c	$\overline{M}_{\infty,r}$	σ
Run 120			
36	30.0×10^6	0.7410	0.0008
37	↓	.7428	.0019
38		.7397	.0017
39		.7425	.0017
40		.7392	.0024
Run 121			
41	30.0×10^6	0.5027	0.0006
42	↓	.5025	.0006
43		.5022	.0006
44		.5021	.0005
45		.5019	.0007
46		.5020	.0010
47		.5021	.0015
48		.5024	.0012
49		.5022	.0010
50		.5025	.0013
51		.5025	.0011
52		.5025	.0014

ORIGINAL PAGE
BLACK AND WHITE PHOTOGRAPH

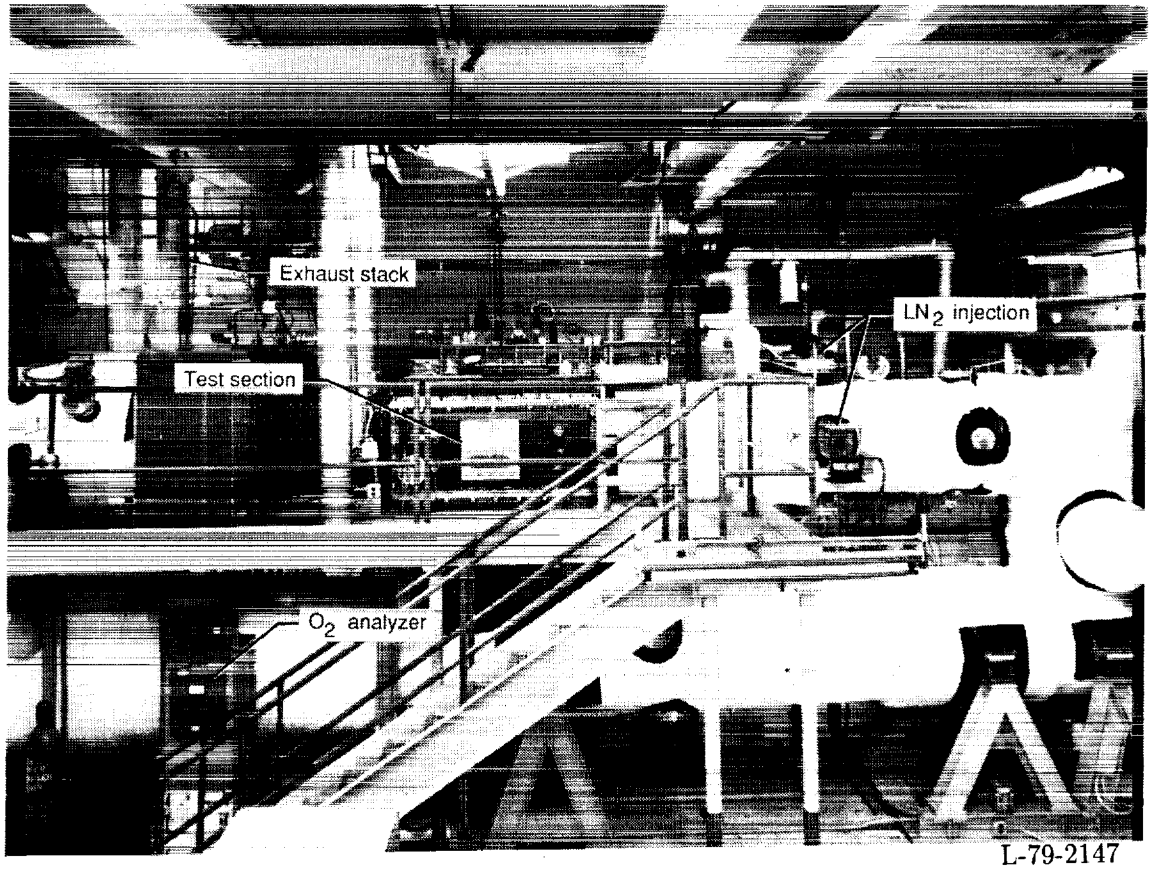

(a) Photograph.

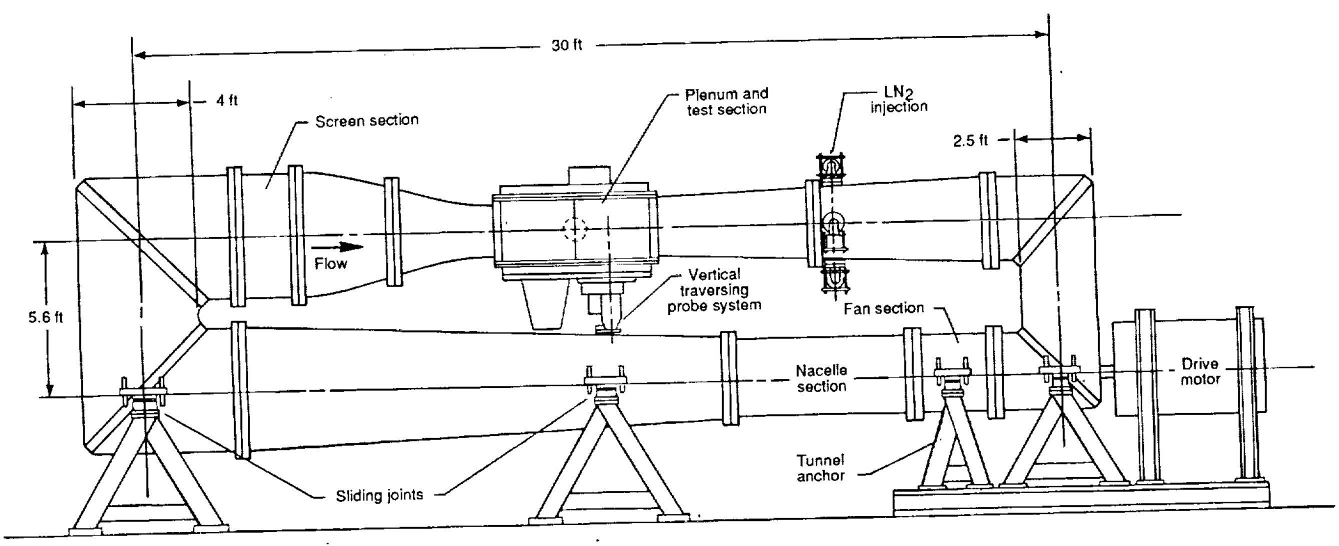

(b) Schematic drawing.

Figure 1. Elevation view of 0.3-Meter Transonic Cryogenic Tunnel with two-dimensional test section installed.

ORIGINAL PAGE
BLACK AND WHITE PHOTOGRAPH

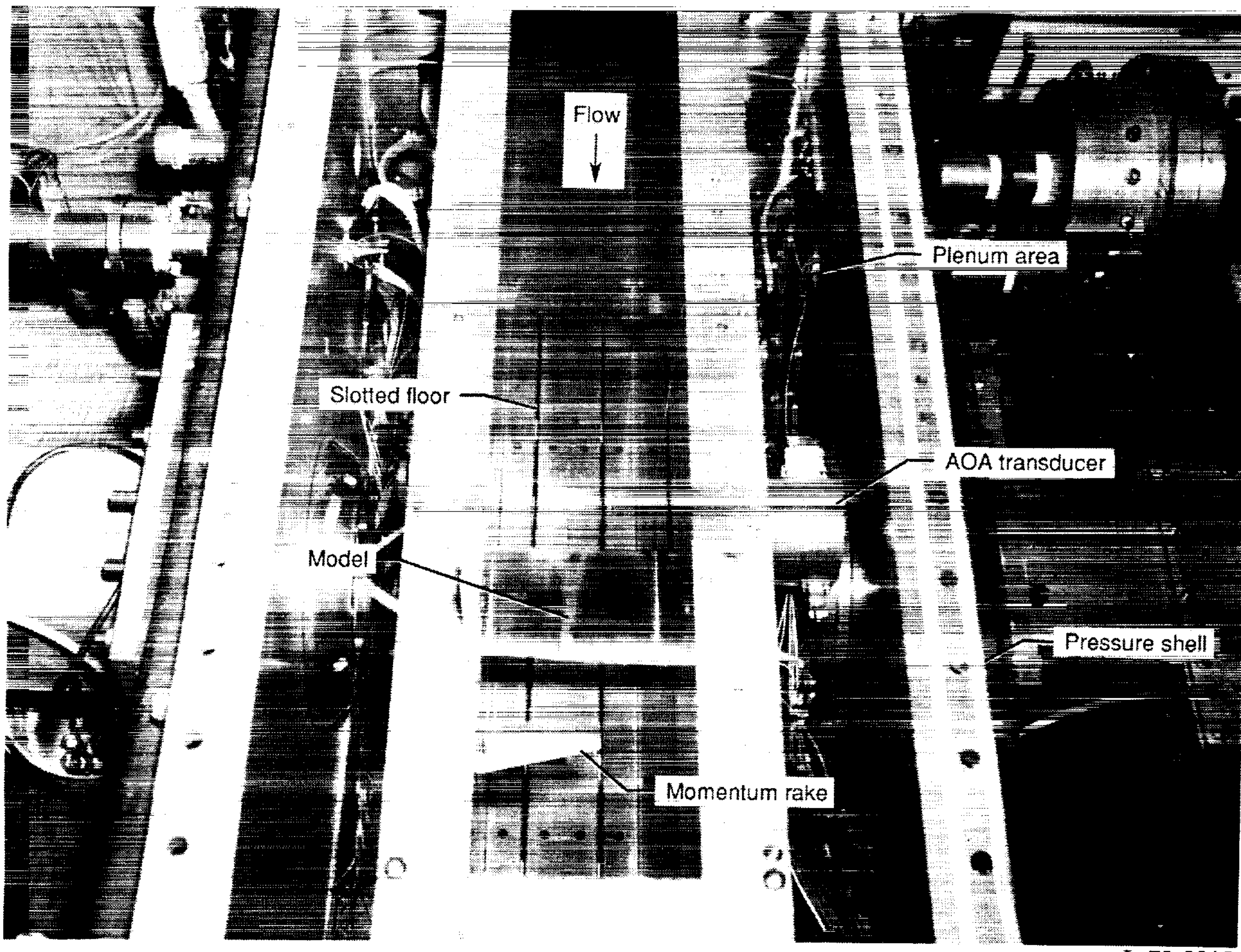

L-79-8913

Figure 2. Photograph of model in two-dimensional test section.

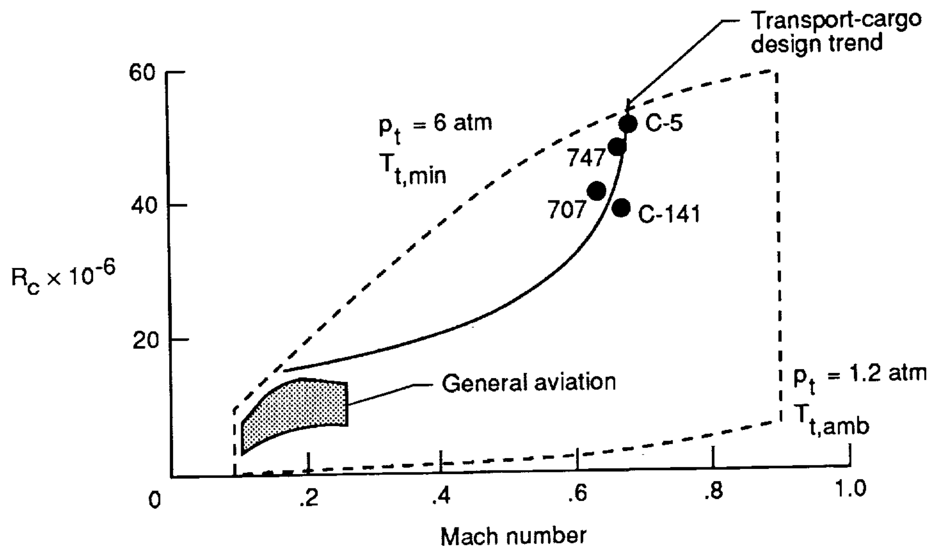

Figure 3. Reynolds number capability of two-dimensional test section of Langley 0.3-Meter Transonic Cryogenic Tunnel.

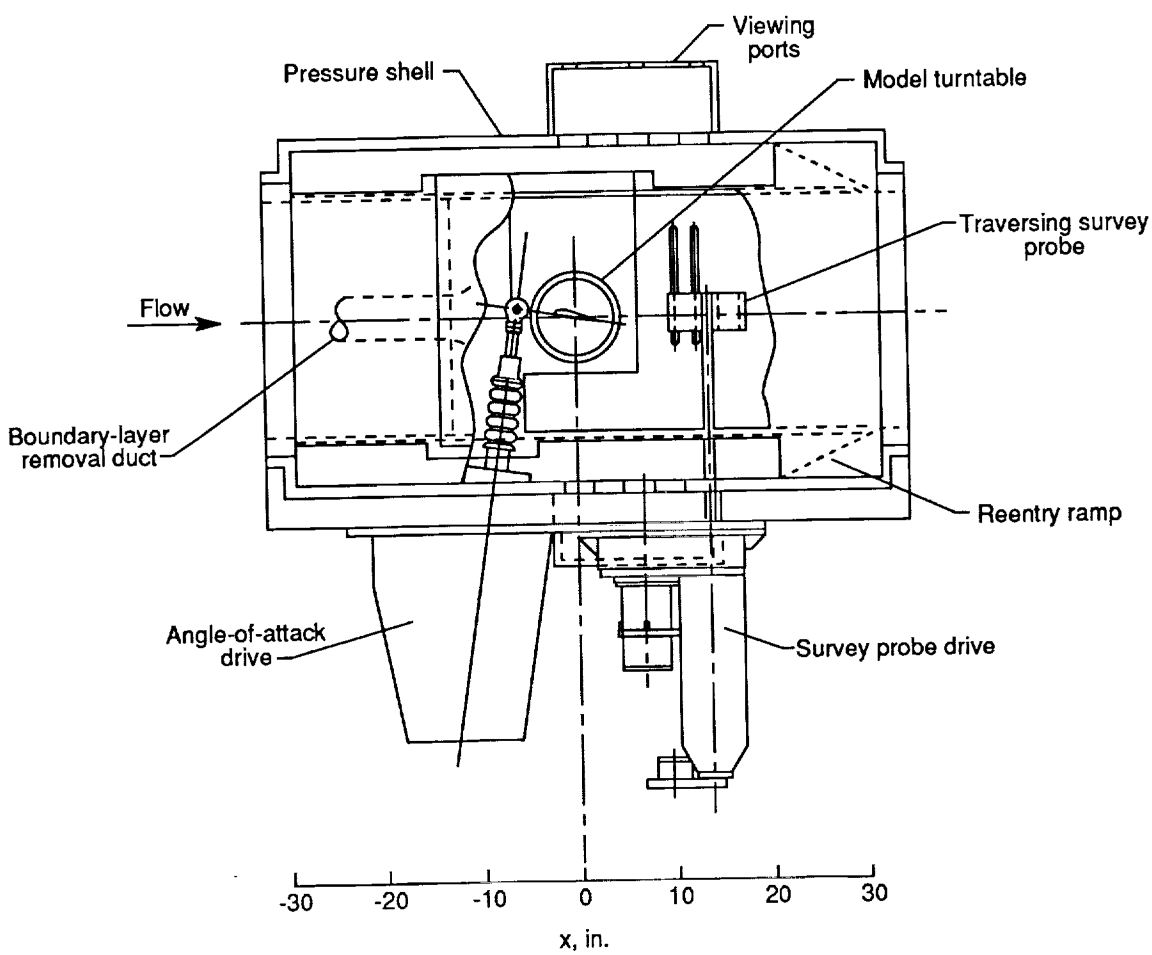

Figure 4. Schematic drawing of major components inside two-dimensional test section.

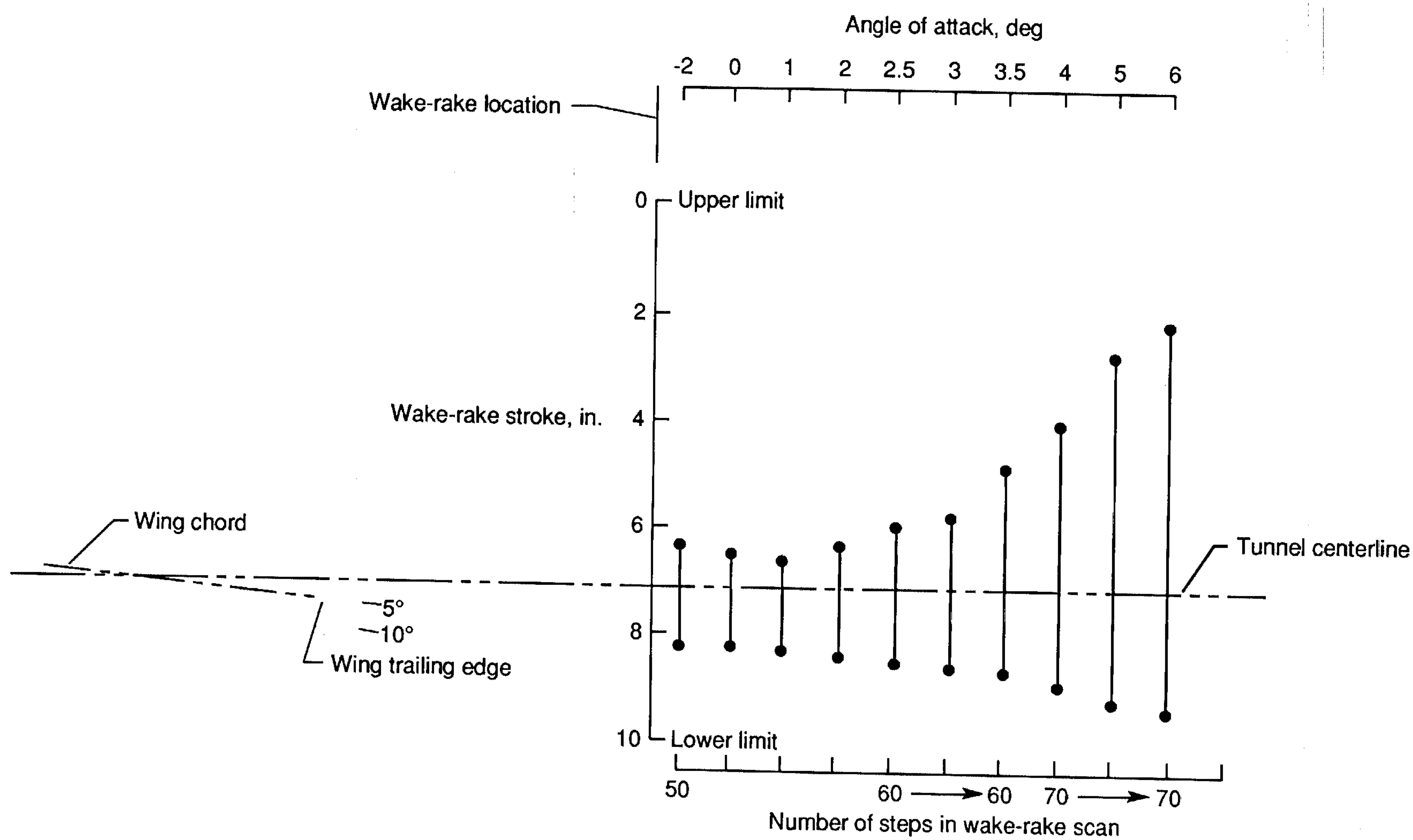

Figure 5. Sample variation of wake-rake stroke with angle of attack. $M_\infty = 0.76$.

ORIGINAL PAGE
BLACK AND WHITE PHOTOGRAPH

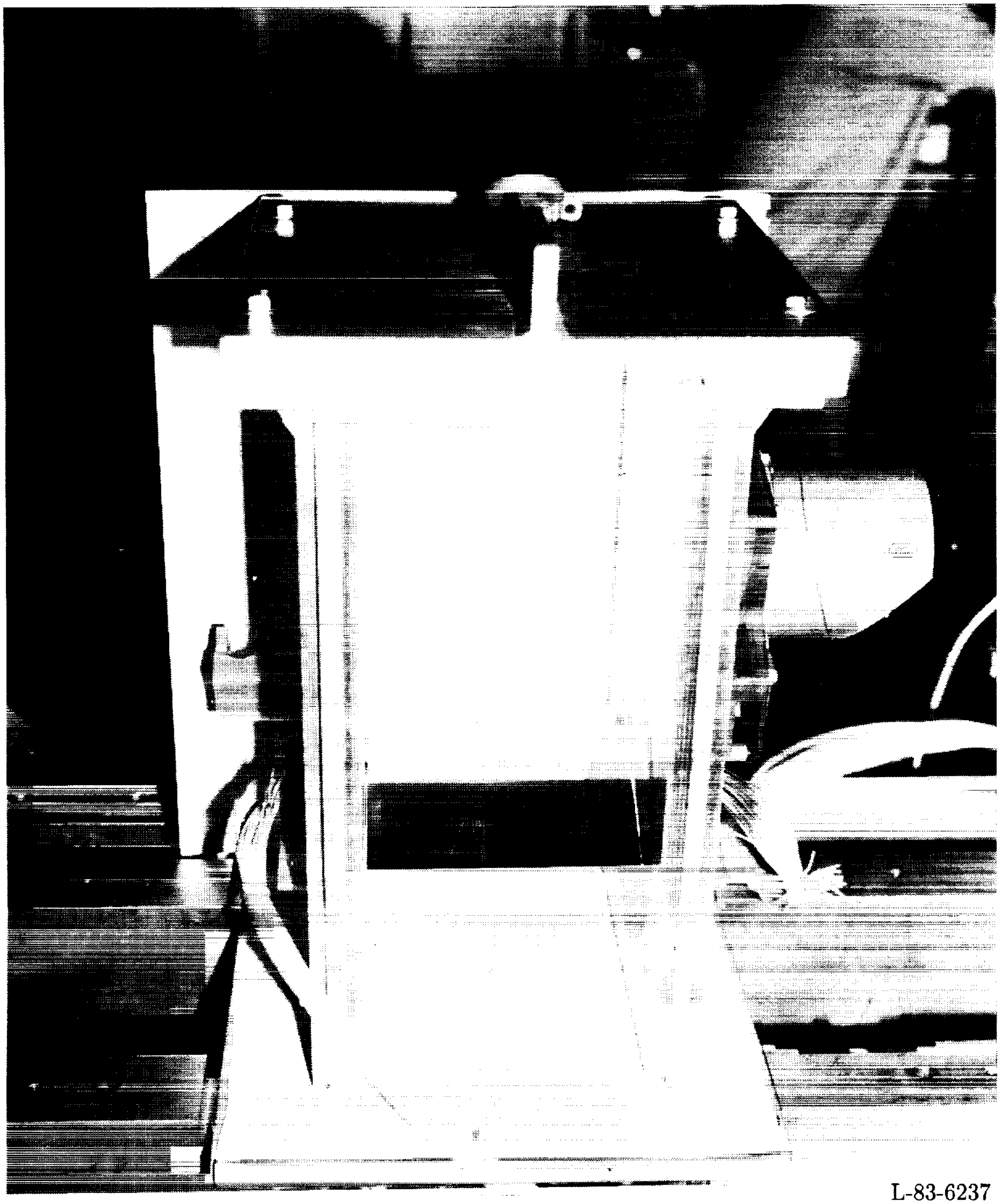

L-83-6237

(a) Airfoil installed in turntable module.

Figure 6. Details of Boeing TR77 airfoil model.

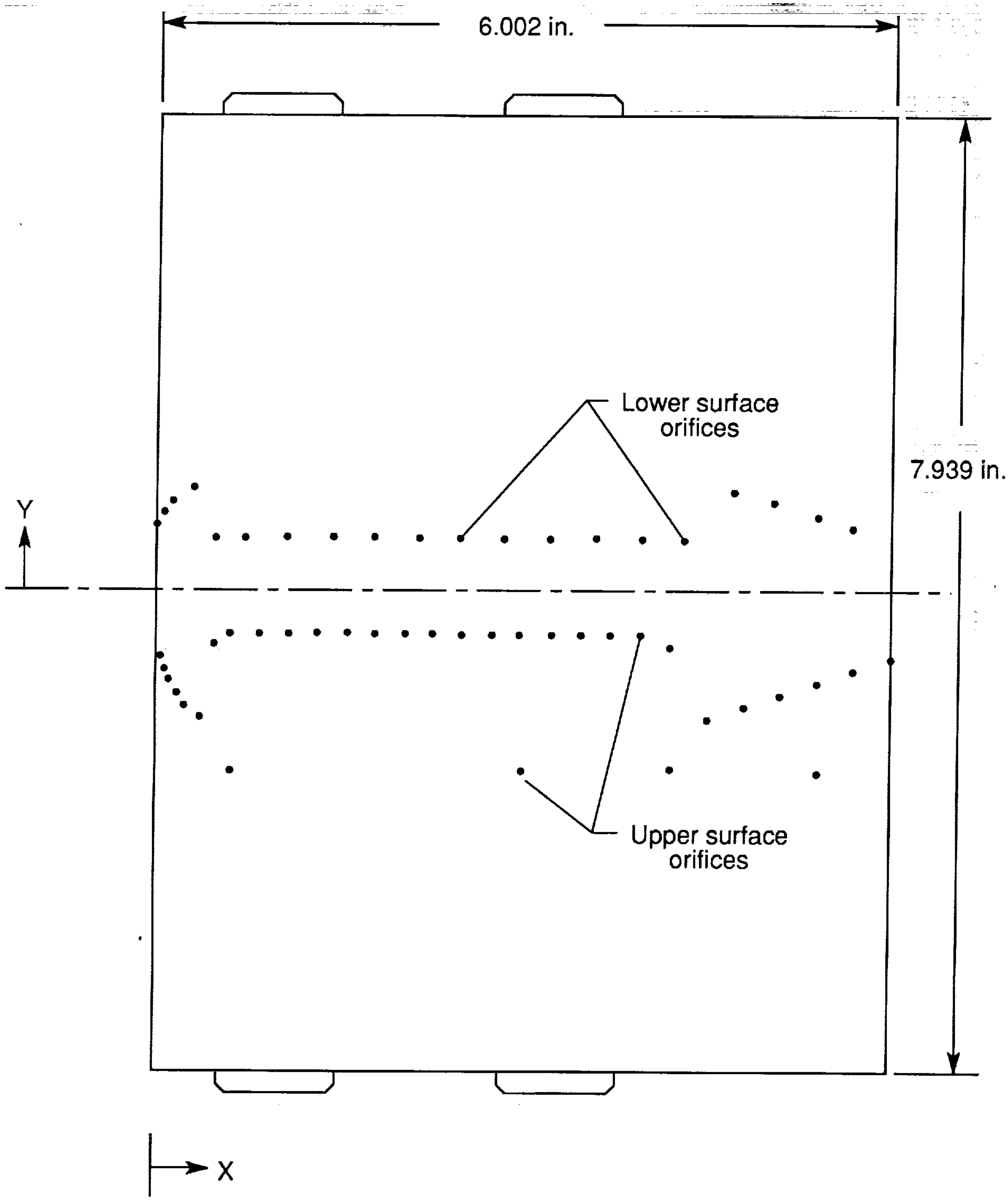

(b) Schematic drawings of airfoil.

Figure 6. Concluded.

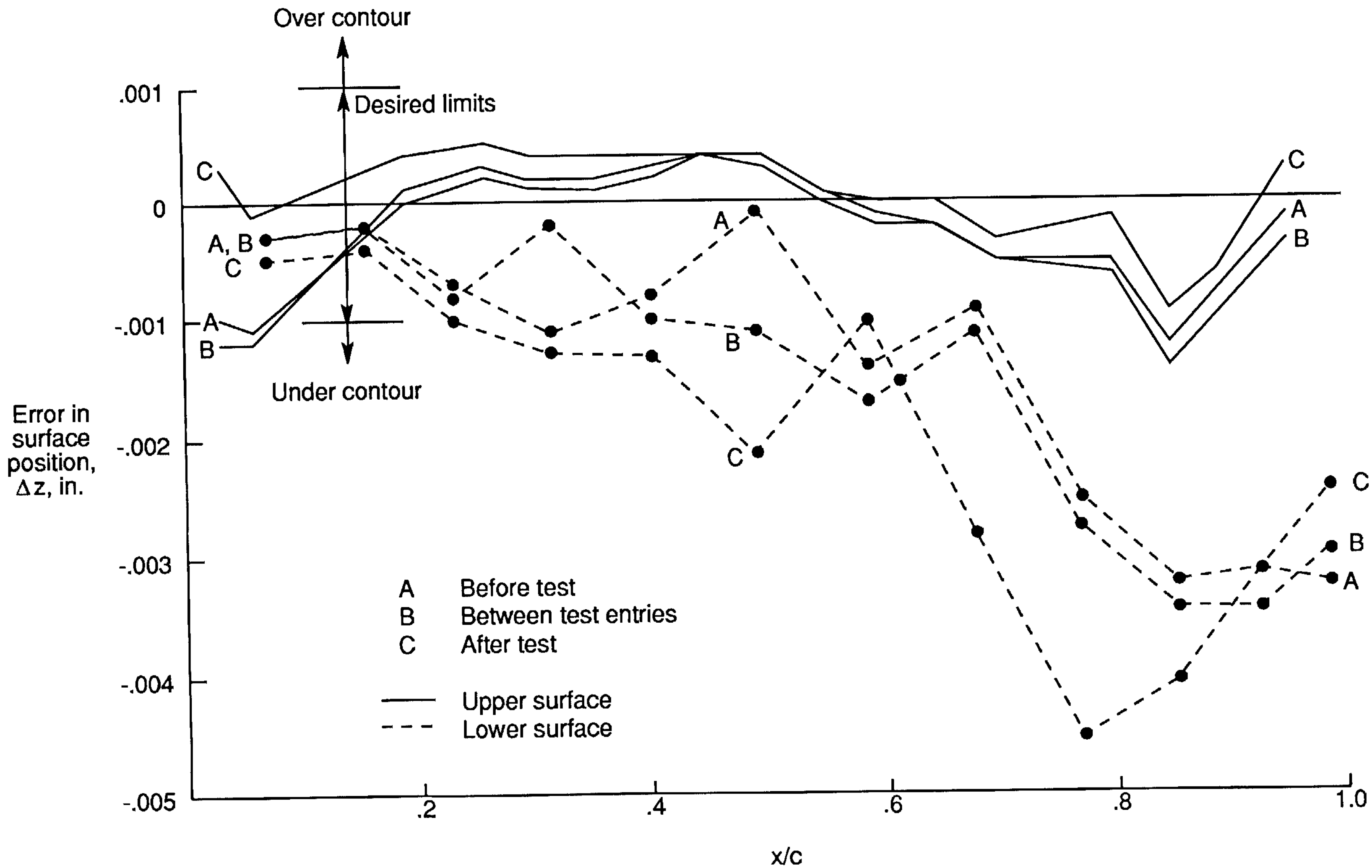

Figure 7. Variation of model contour x/c measurements with tunnel entries. Midspan station.

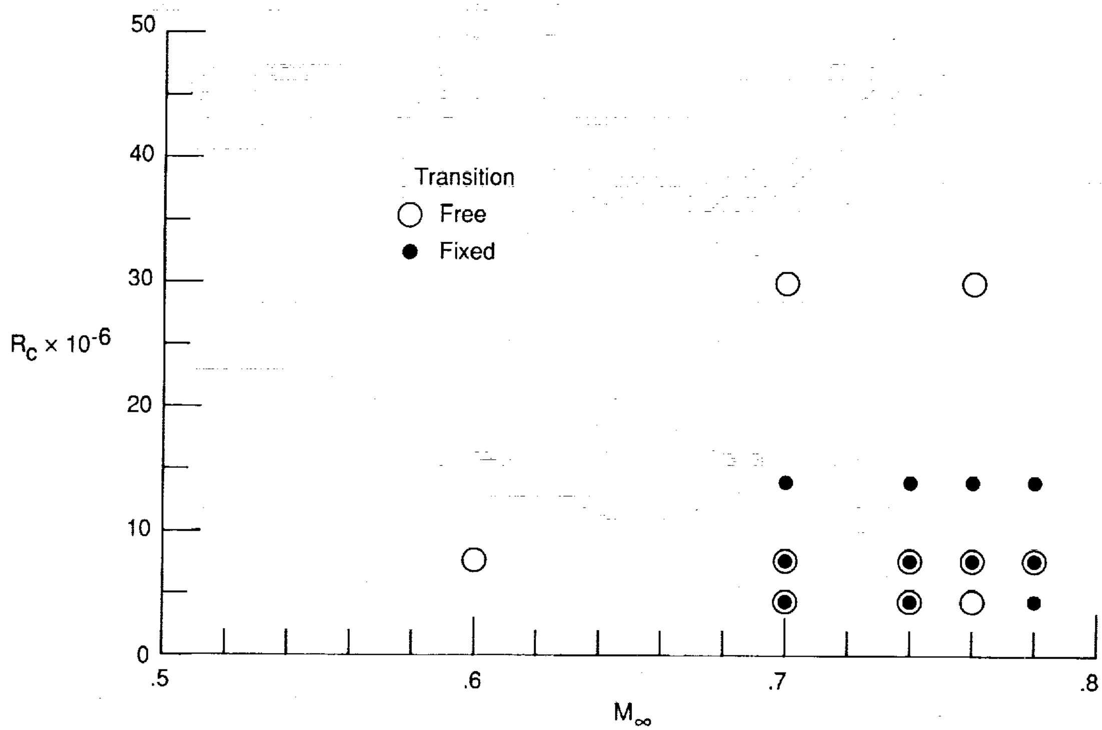

(a) First entry.

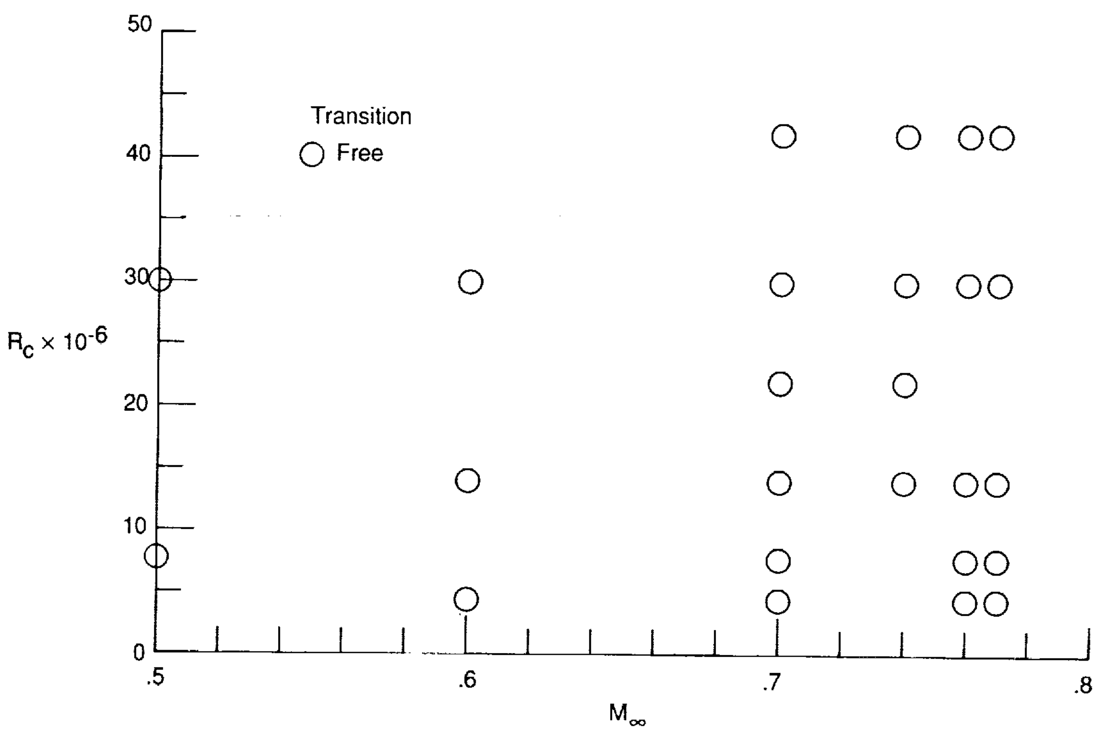

(b) Second entry.

Figure 8. Airfoil tet program for Boeing TR77 model.

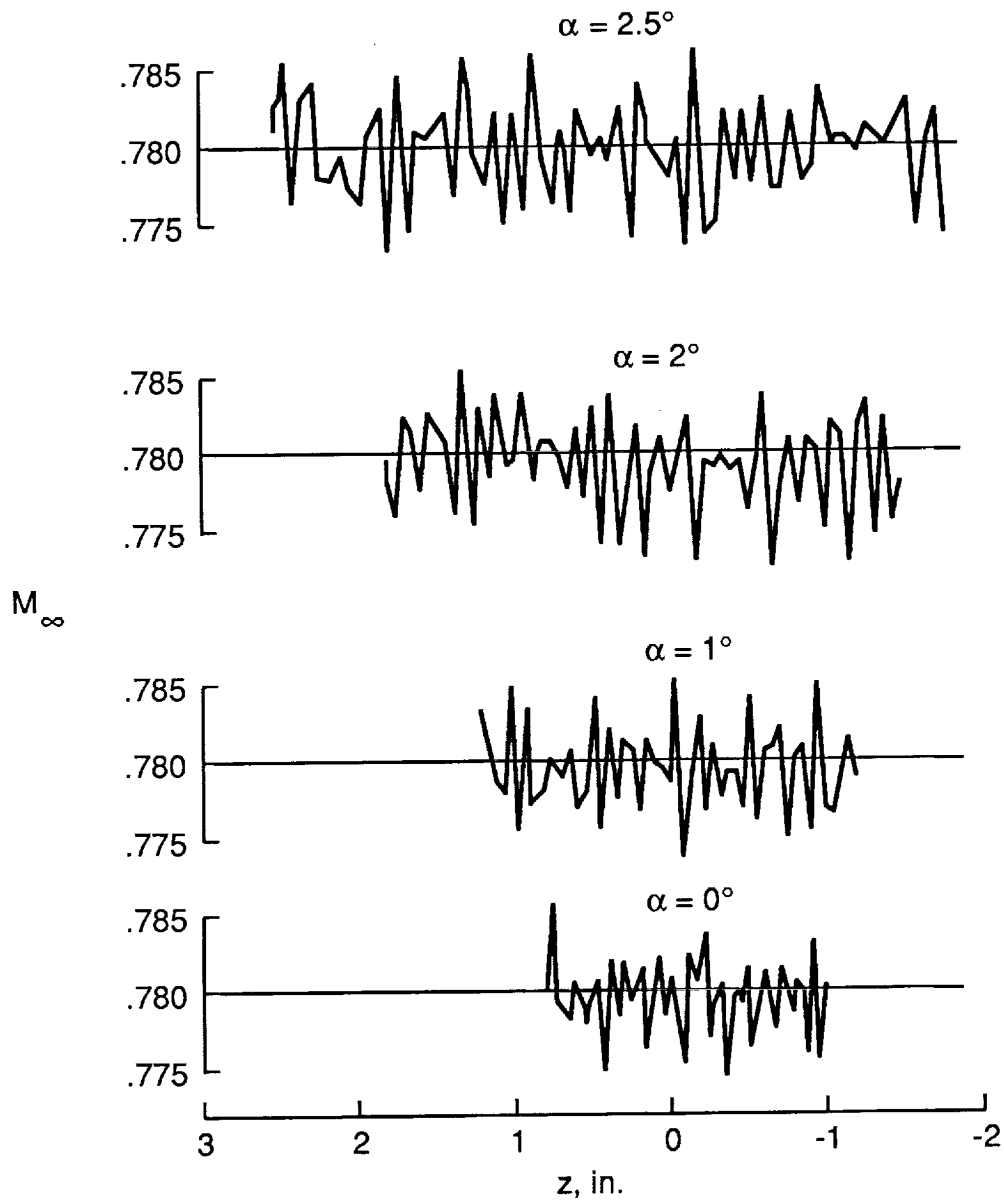

(a) Run 8.

Figure 9. Tunnel Mach number variation on test point.

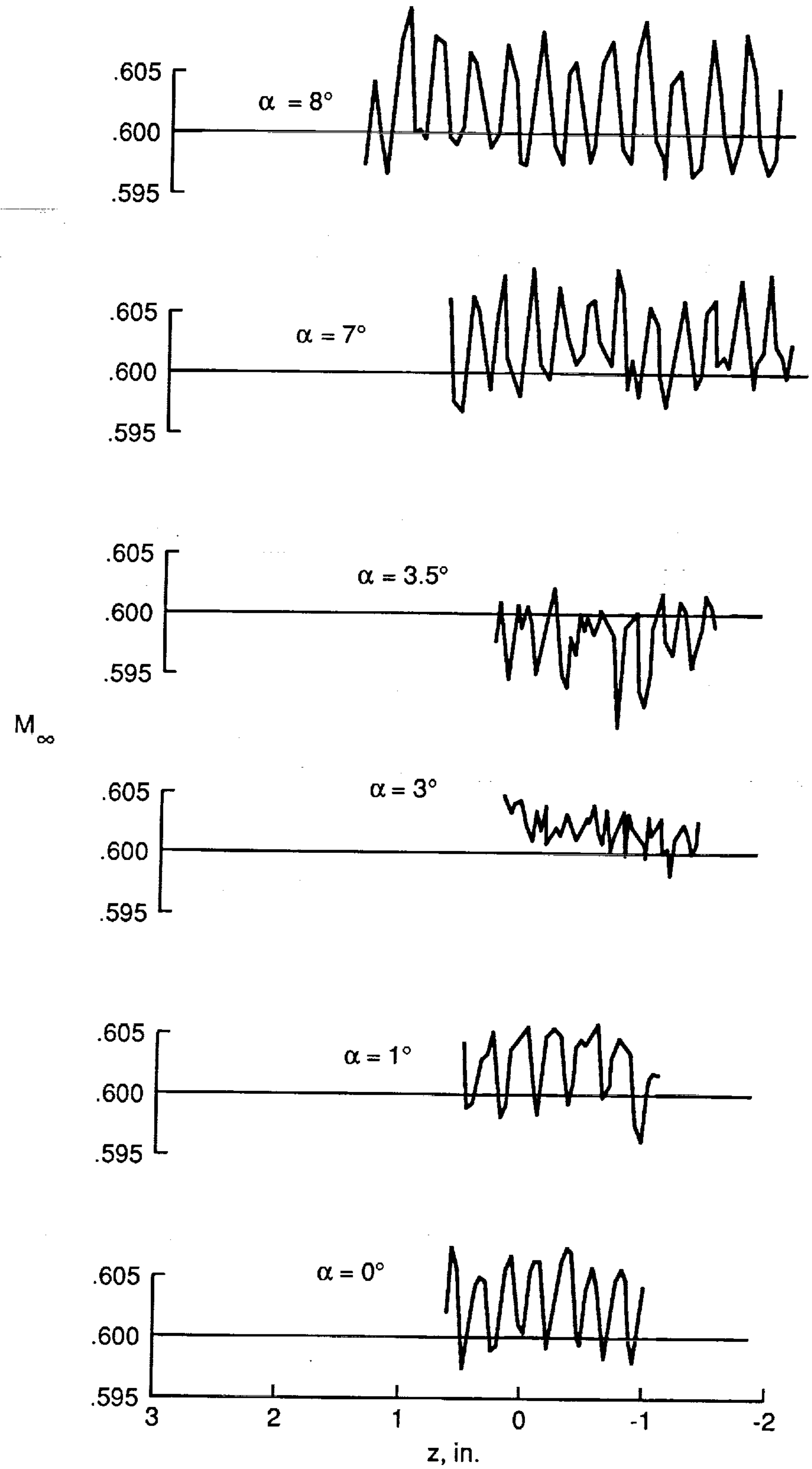

(b) Run 18.

Figure 9. Continued.

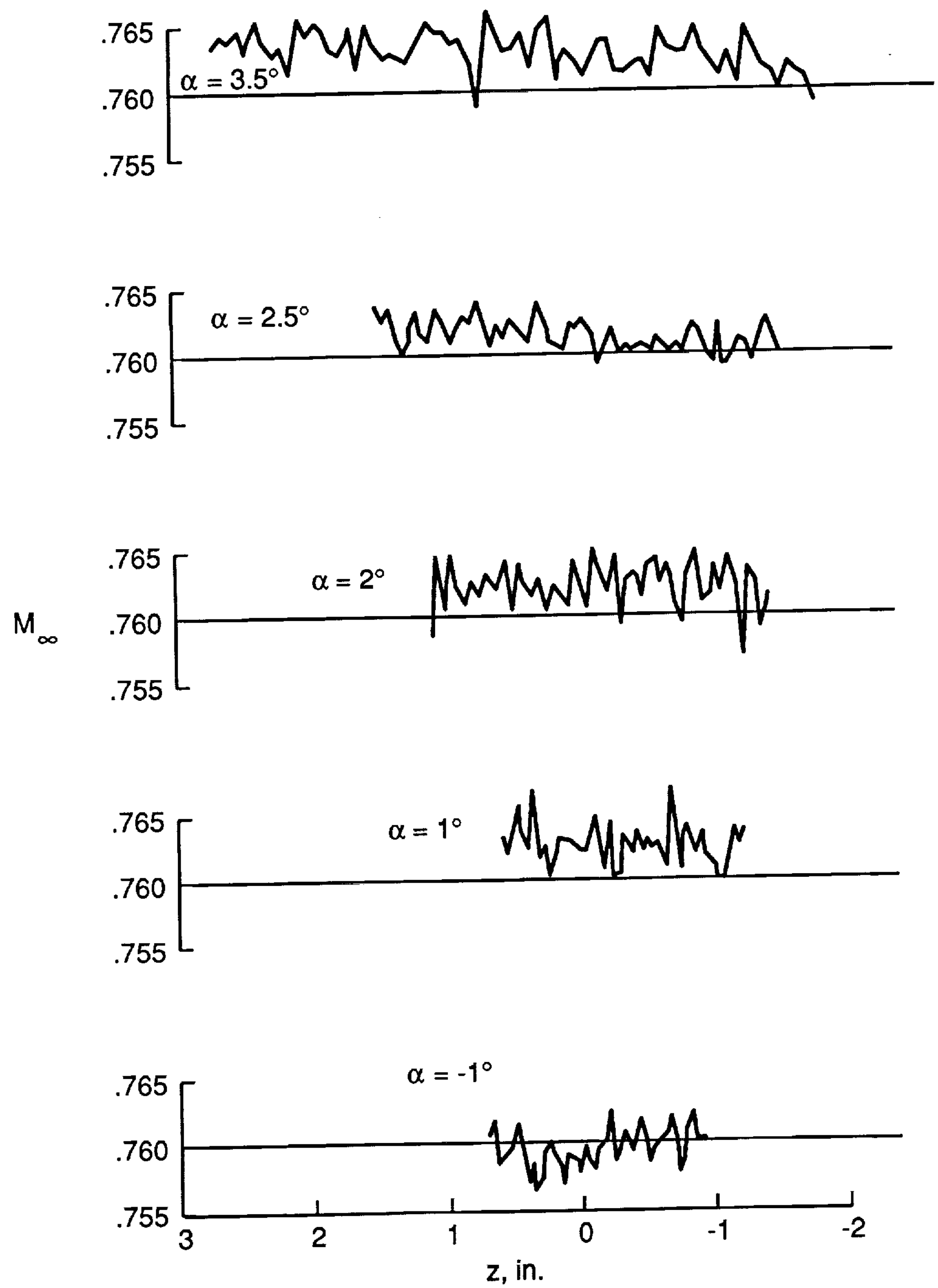

(c) Run 22.

Figure 9. Concluded.

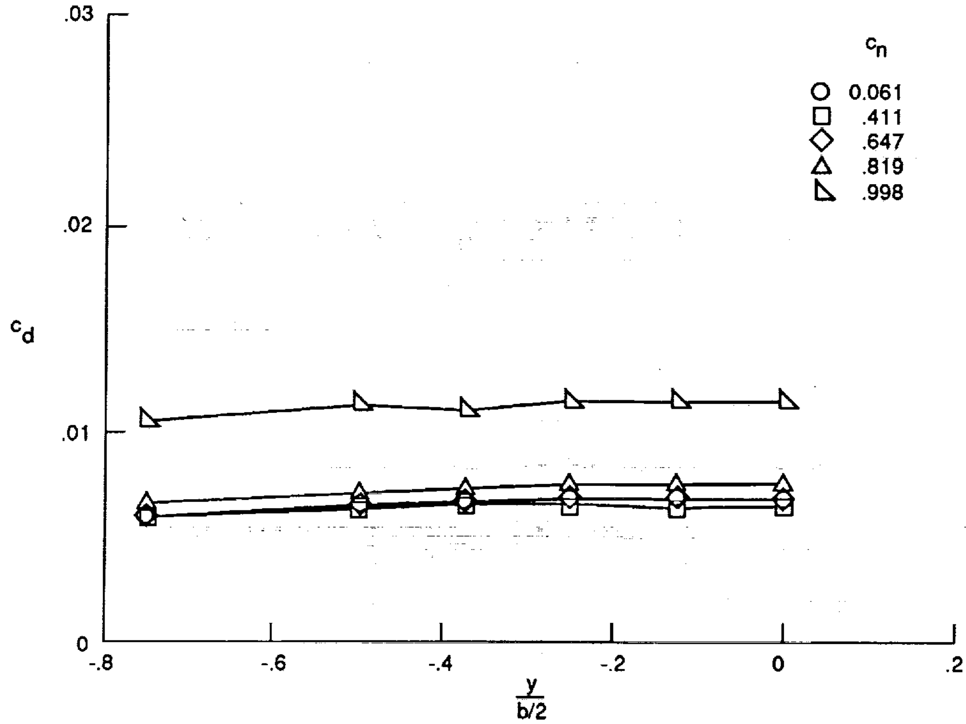

(a) $M_\infty = 0.60$.

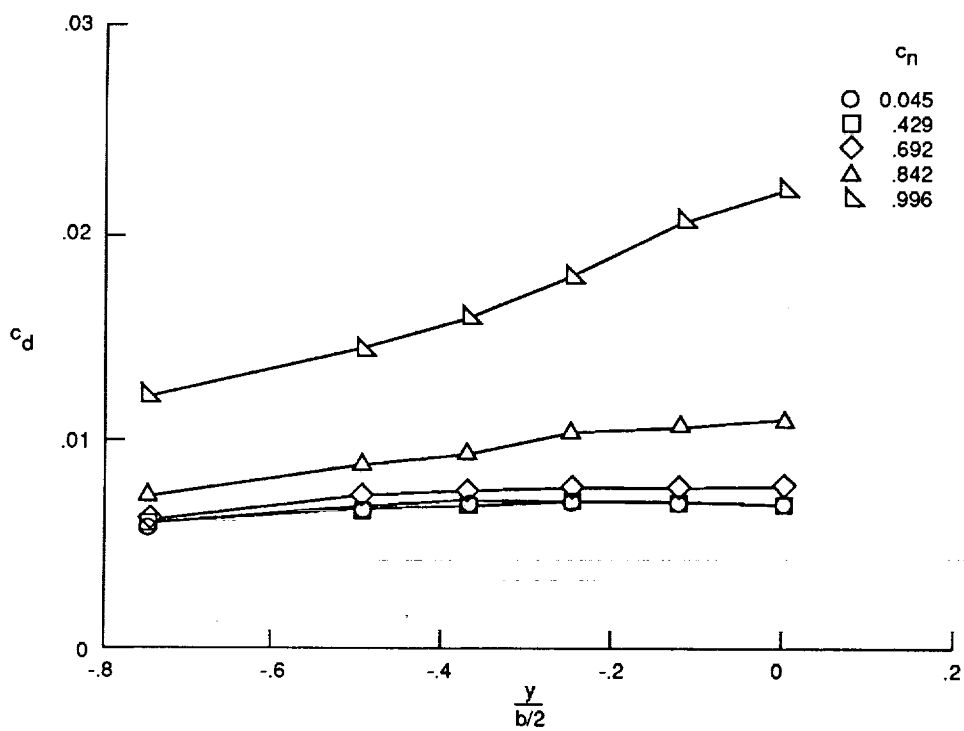

(b) $M_\infty = 0.70$.

Figure 10. Variation of drag coefficient with span for constant normal-force coefficient. Free transition; $R_c = 30 \times 10^6$.

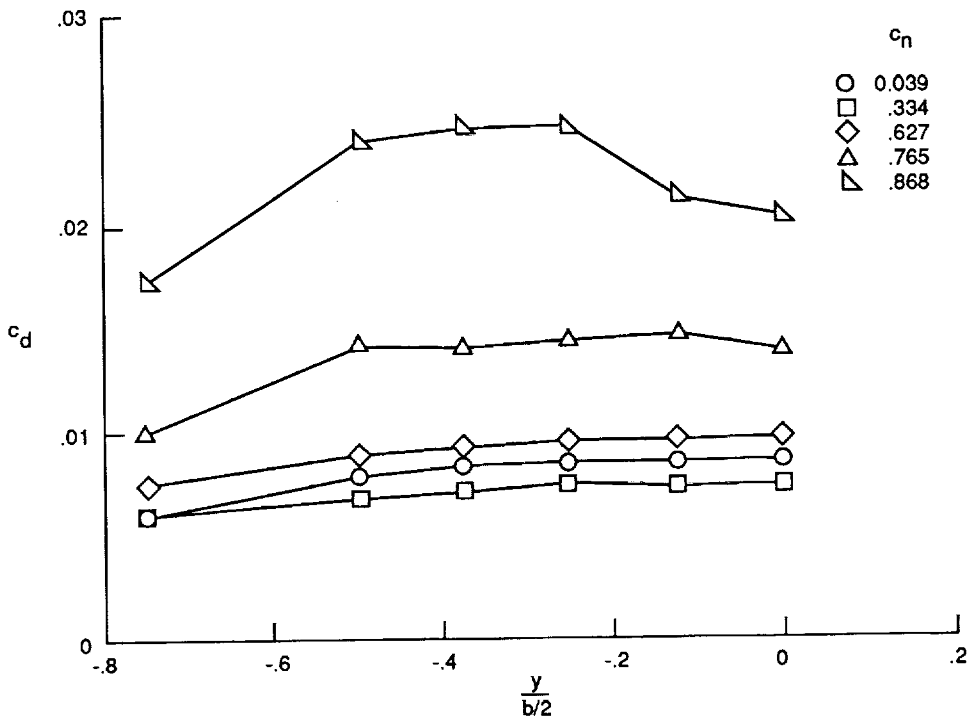

(c) $M_\infty = 0.76$.

Figure 10. Concluded.

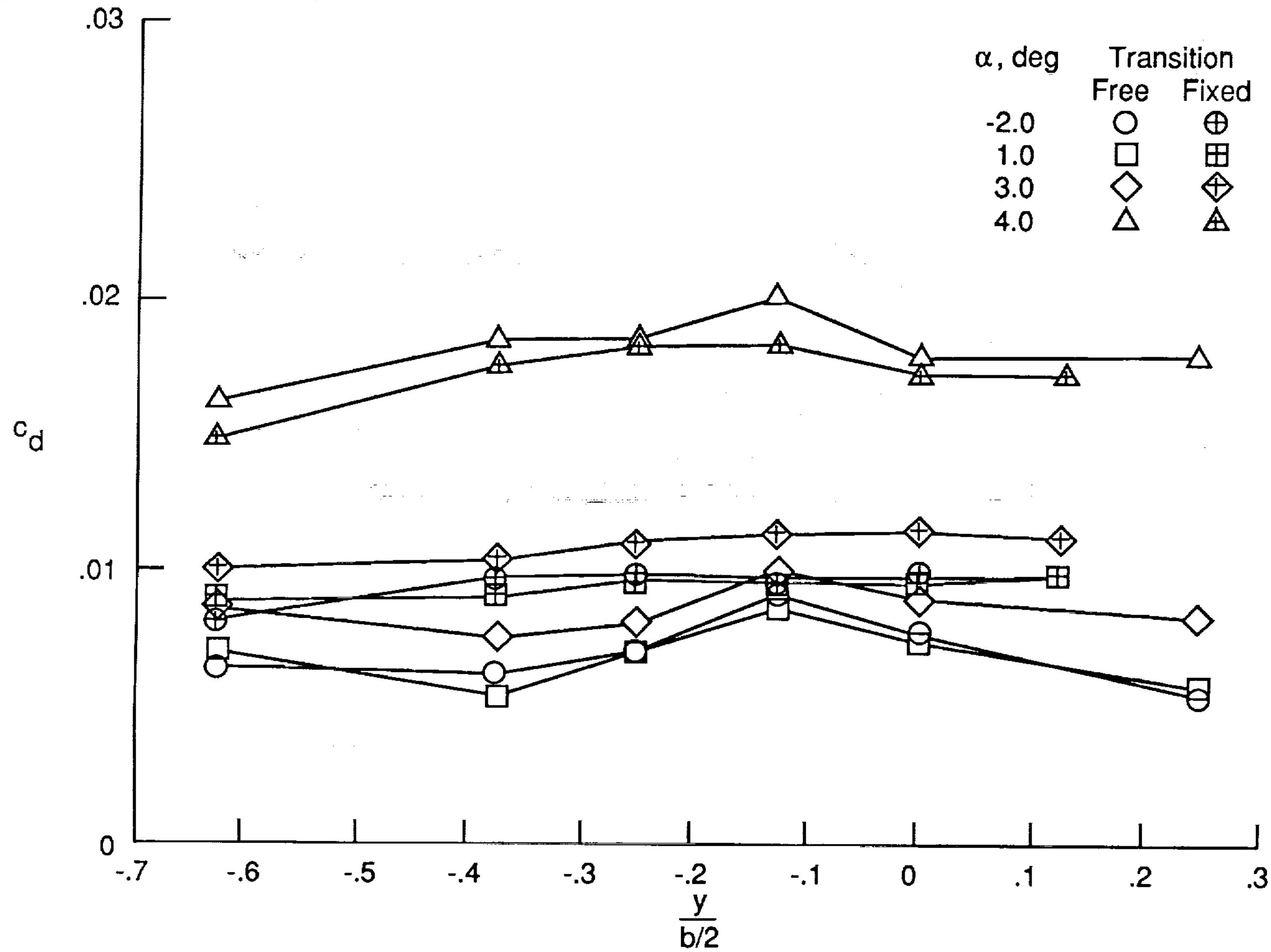

Figure 11. Effect of transition on variation of drag coefficient with span. $M_\infty = 0.76$; $R_c = 4.4 \times 10^6$.

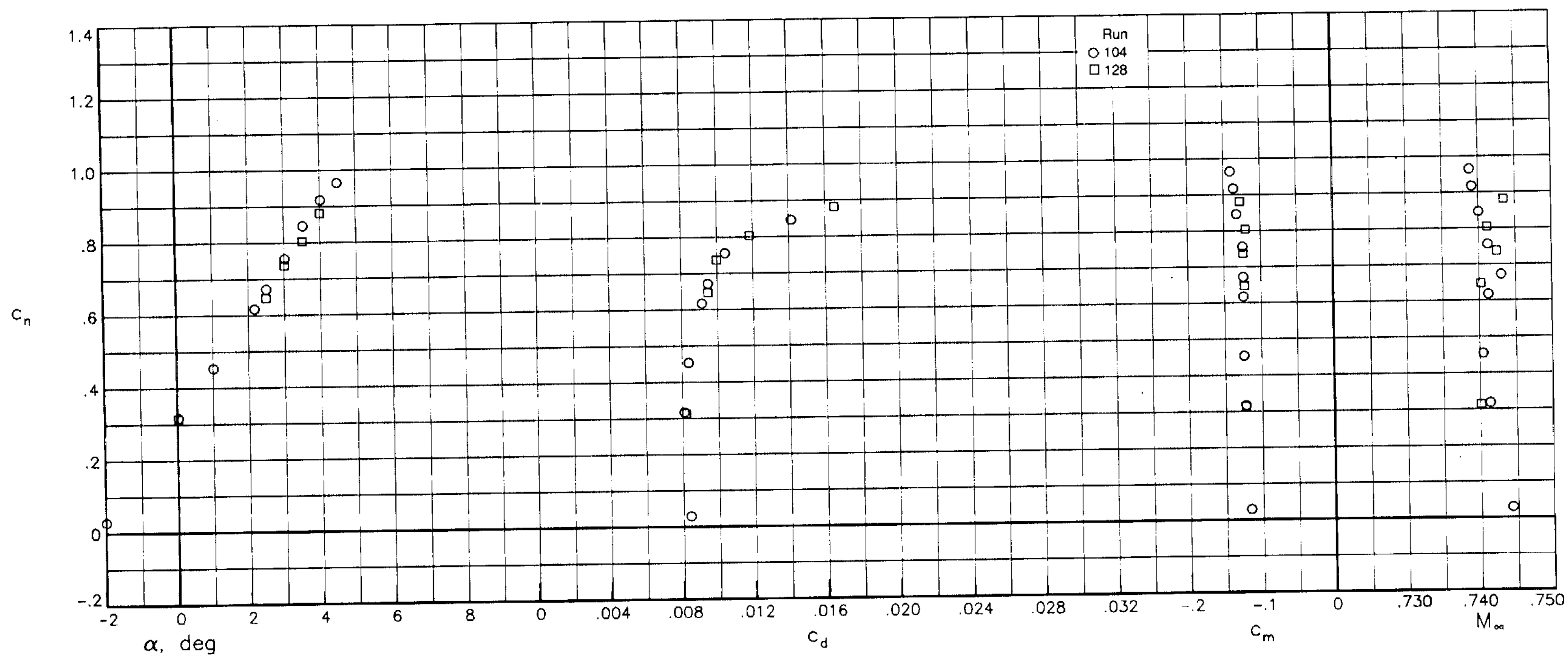

(a) Free transition; $M_\infty = 0.74$; $R_c = 14.0 \times 10^6$.

Figure 12. Repeatability of airfoil aerodynamic data.

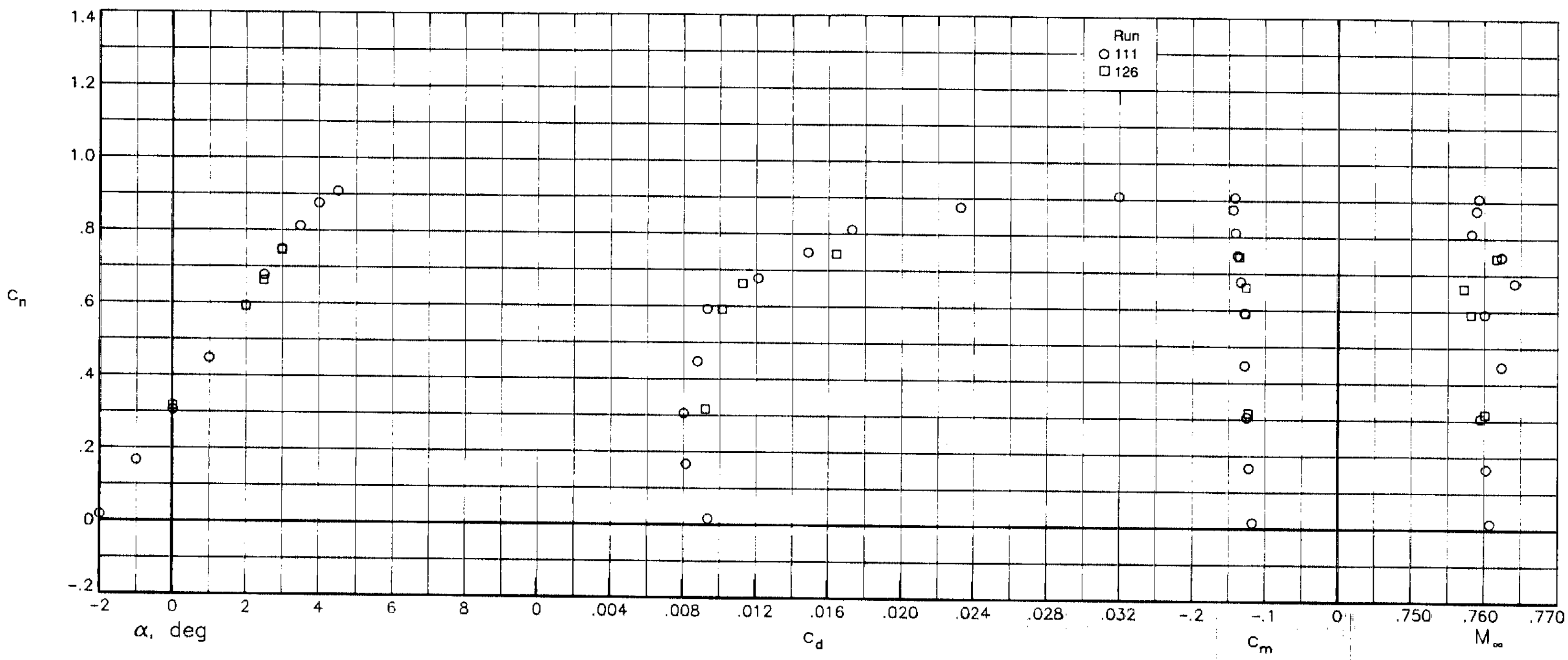

(b) Free transition; $M_\infty = 0.76$; $R_c = 7.7 \times 10^6$.

Figure 12. Continued.

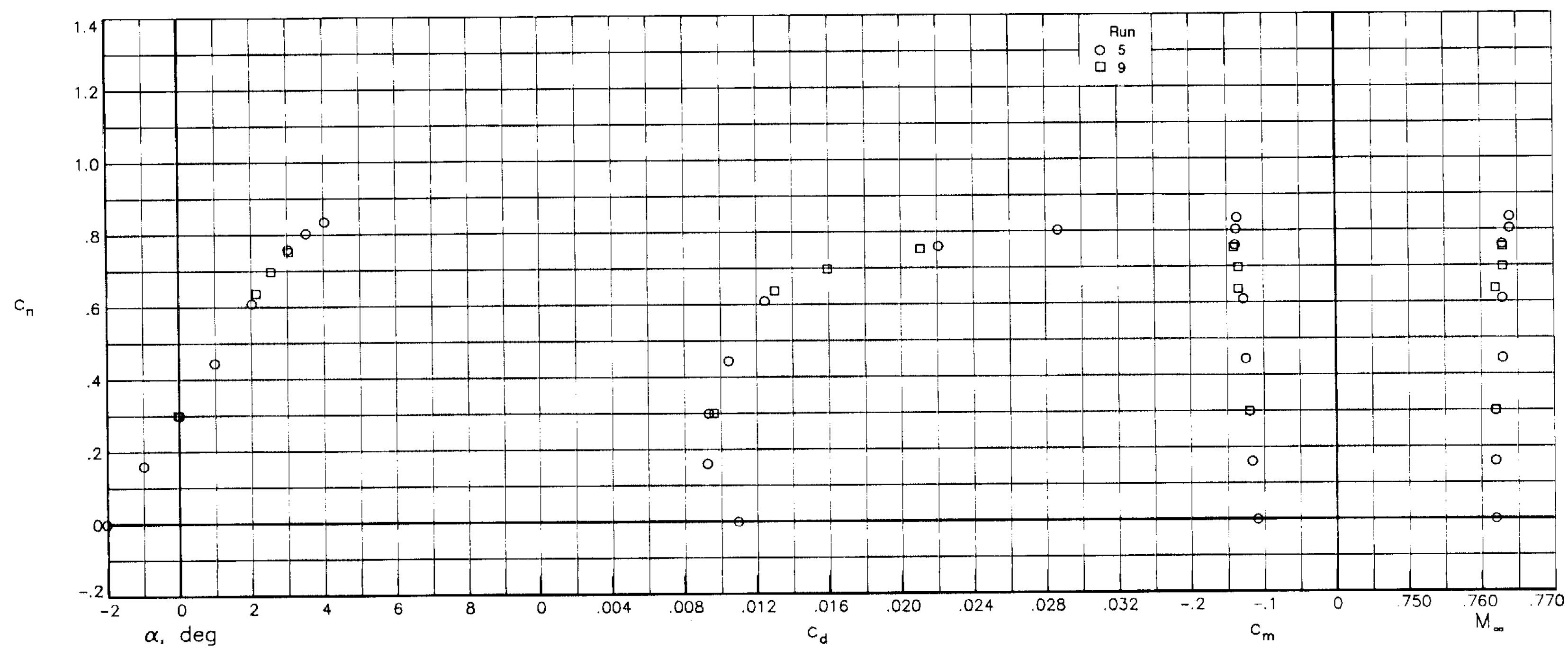

(c) Fixed transition; $M_\infty = 0.76$; $R_c = 7.7 \times 10^6$.

Figure 12. Concluded.

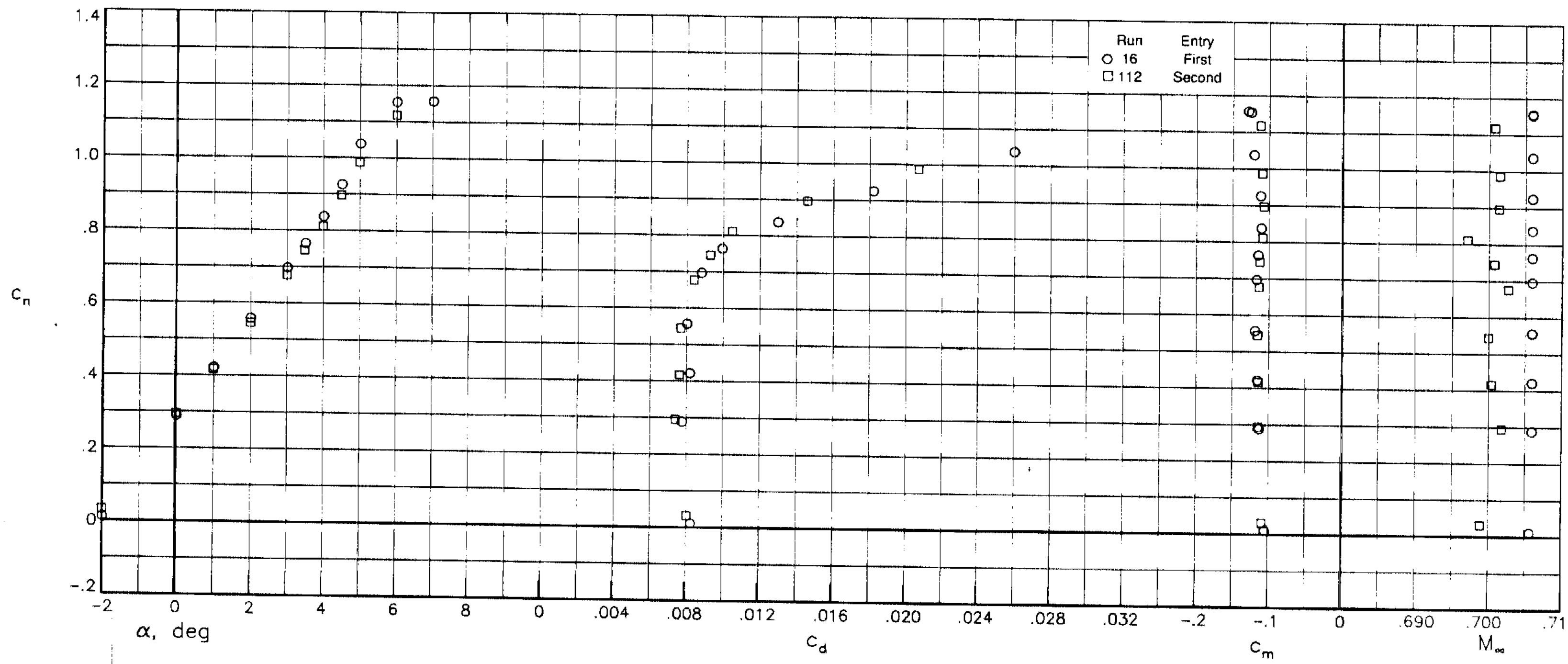

(a) $M_\infty = 0.70$.

Figure 13. Test-to-test correlation of repeatability of airfoil aerodynamic data with free transition at $R_c = 7.7 \times 10^6$.

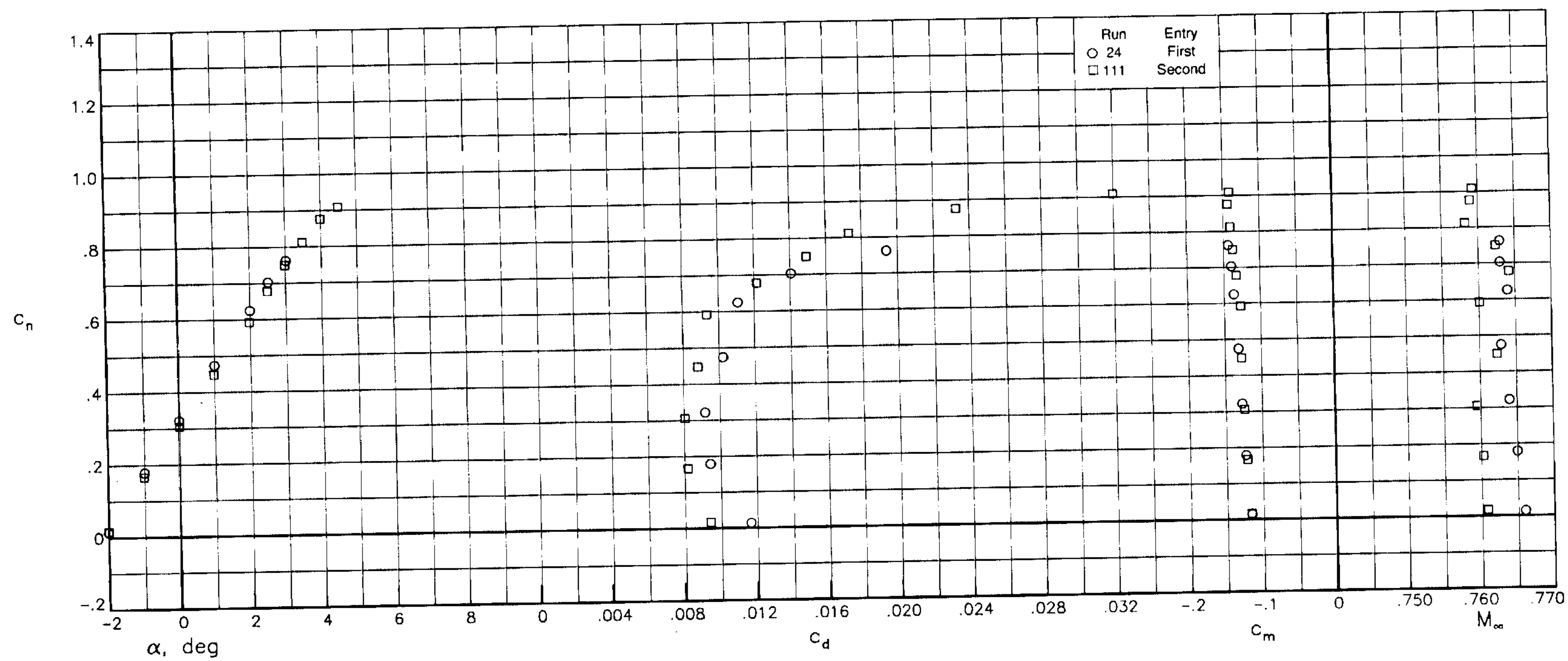

(b) $M_\infty = 0.76$.

Figure 13. Concluded.

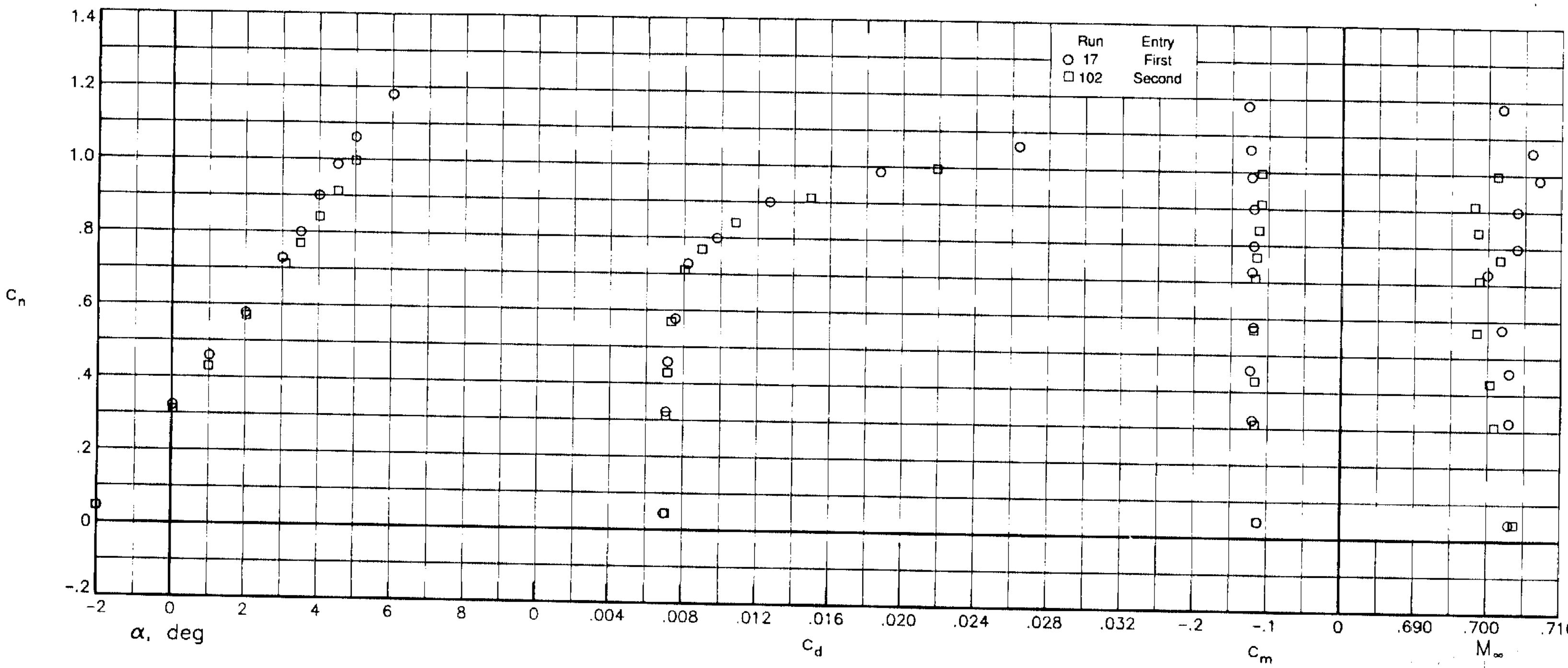

(a) $M_\infty = 0.70$.

Figure 14. Test-to-test correlation of repeatability of airfoil aerodynamic data with free transition at $R_c = 30.0 \times 10^6$.

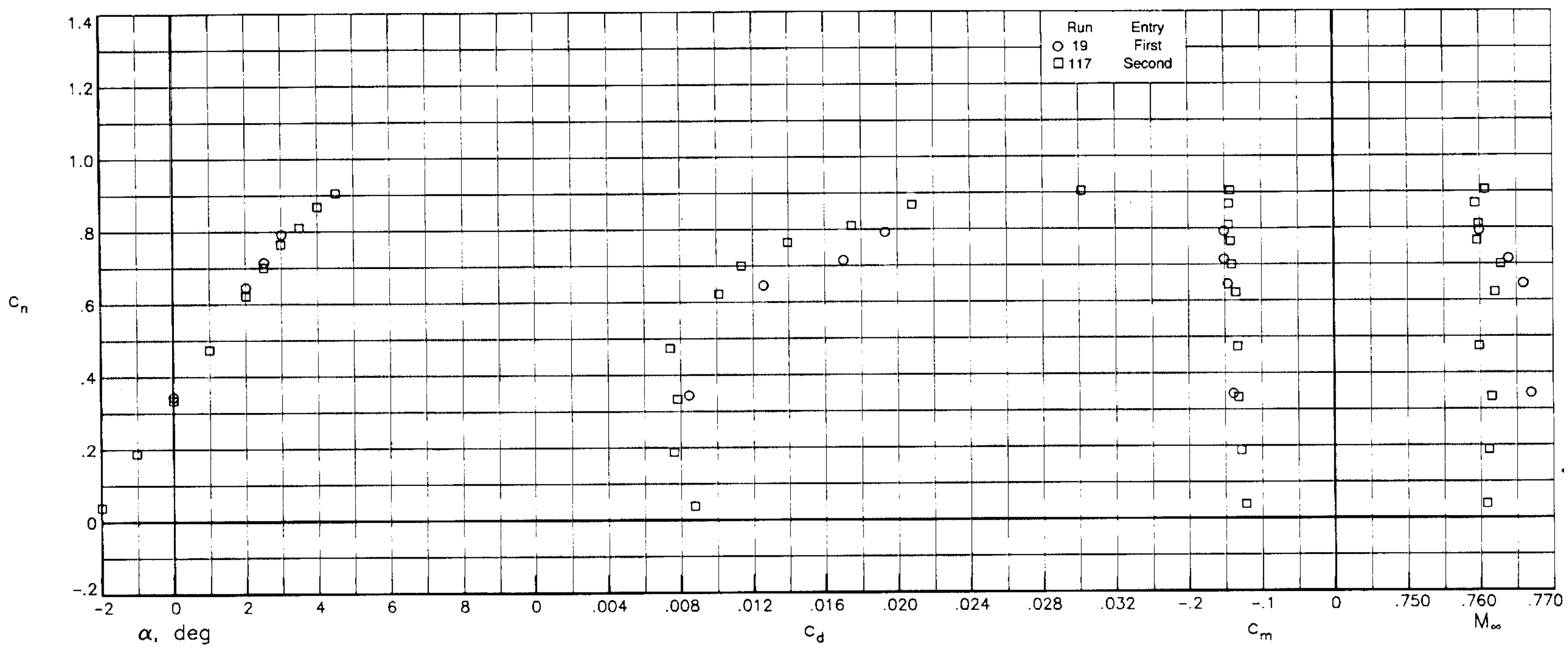

(b) $M_\infty = 0.76$.

Figure 14. Concluded.

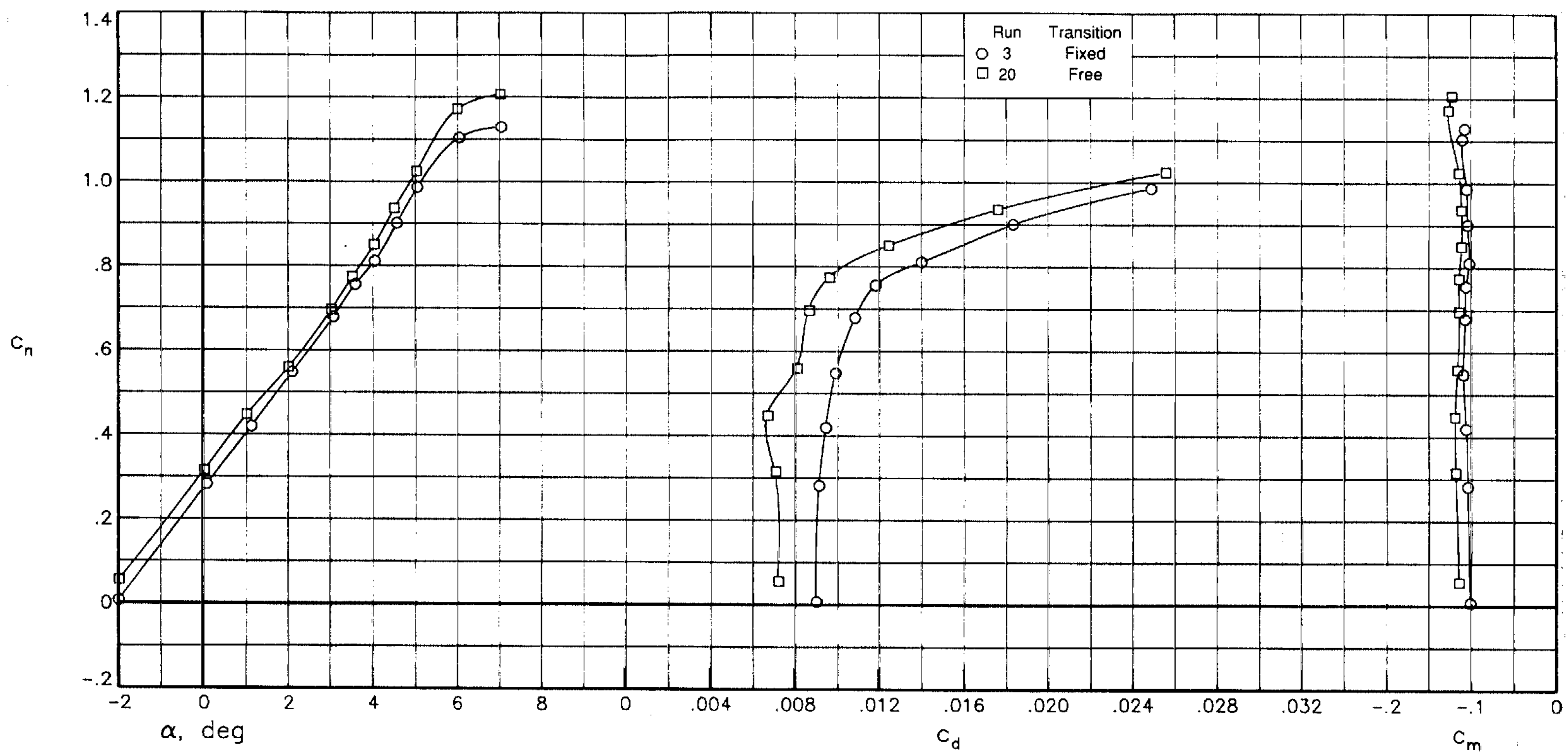

(a) $M_\infty = 0.70$.

Figure 15. Effect of transition on airfoil aerodynamic characteristics at $R_c = 4.4 \times 10^6$.

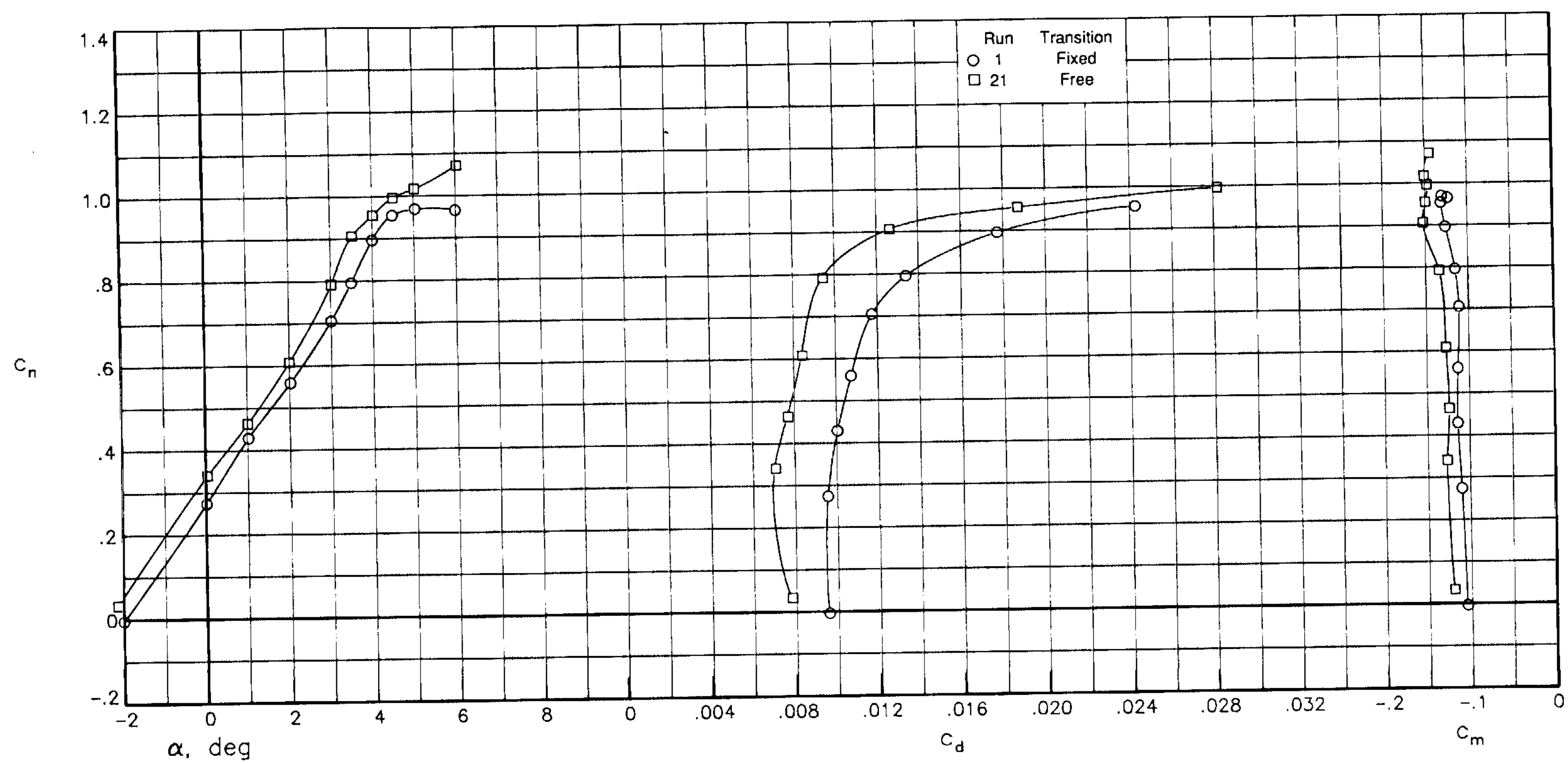

(b) $M_\infty = 0.74$.

Figure 15: Concluded.

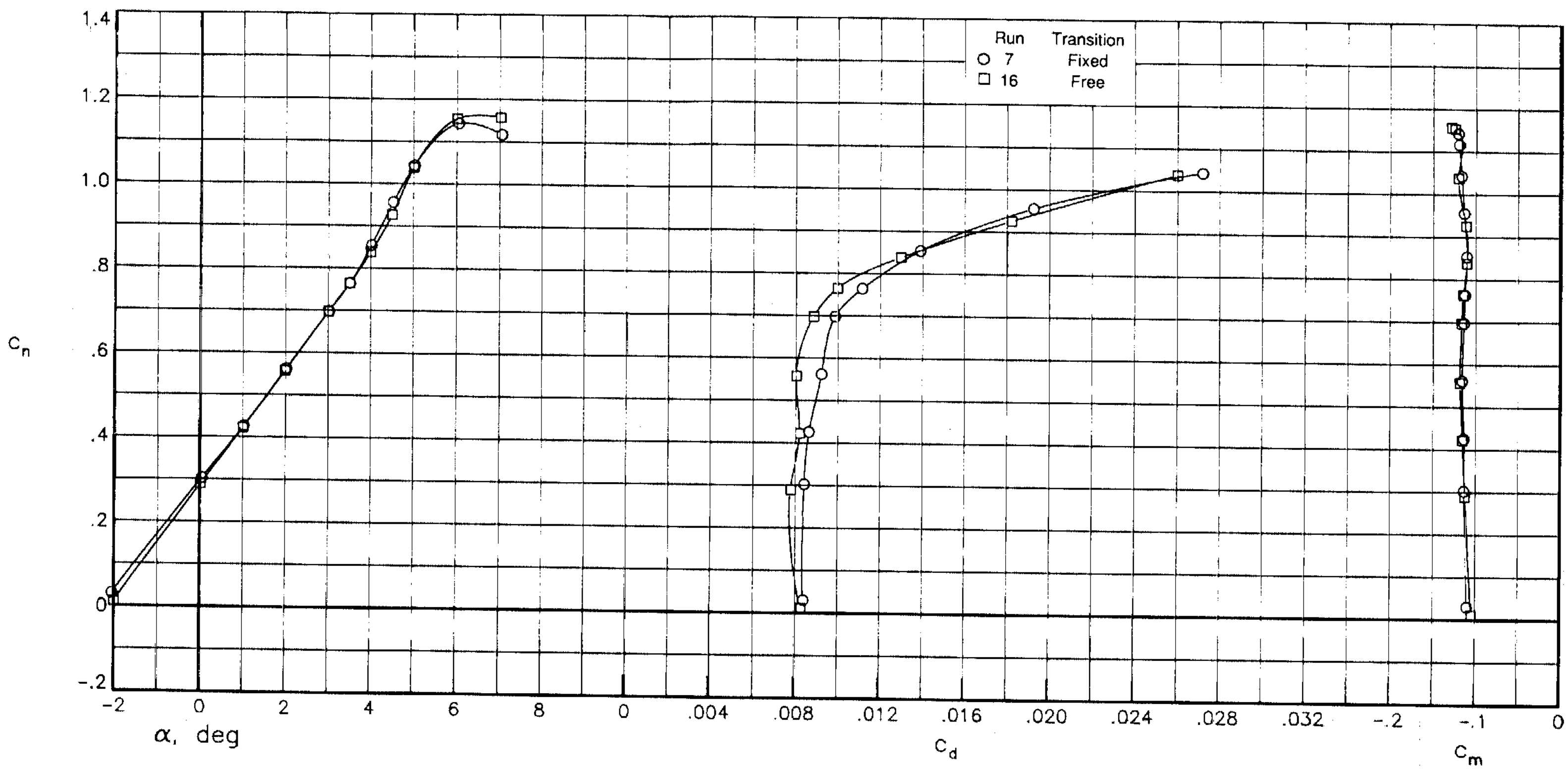

(a) $M_\infty = 0.70$.

Figure 16. Effect of transition on airfoil aerodynamic characteristics at $R_c = 7.7 \times 10^6$.

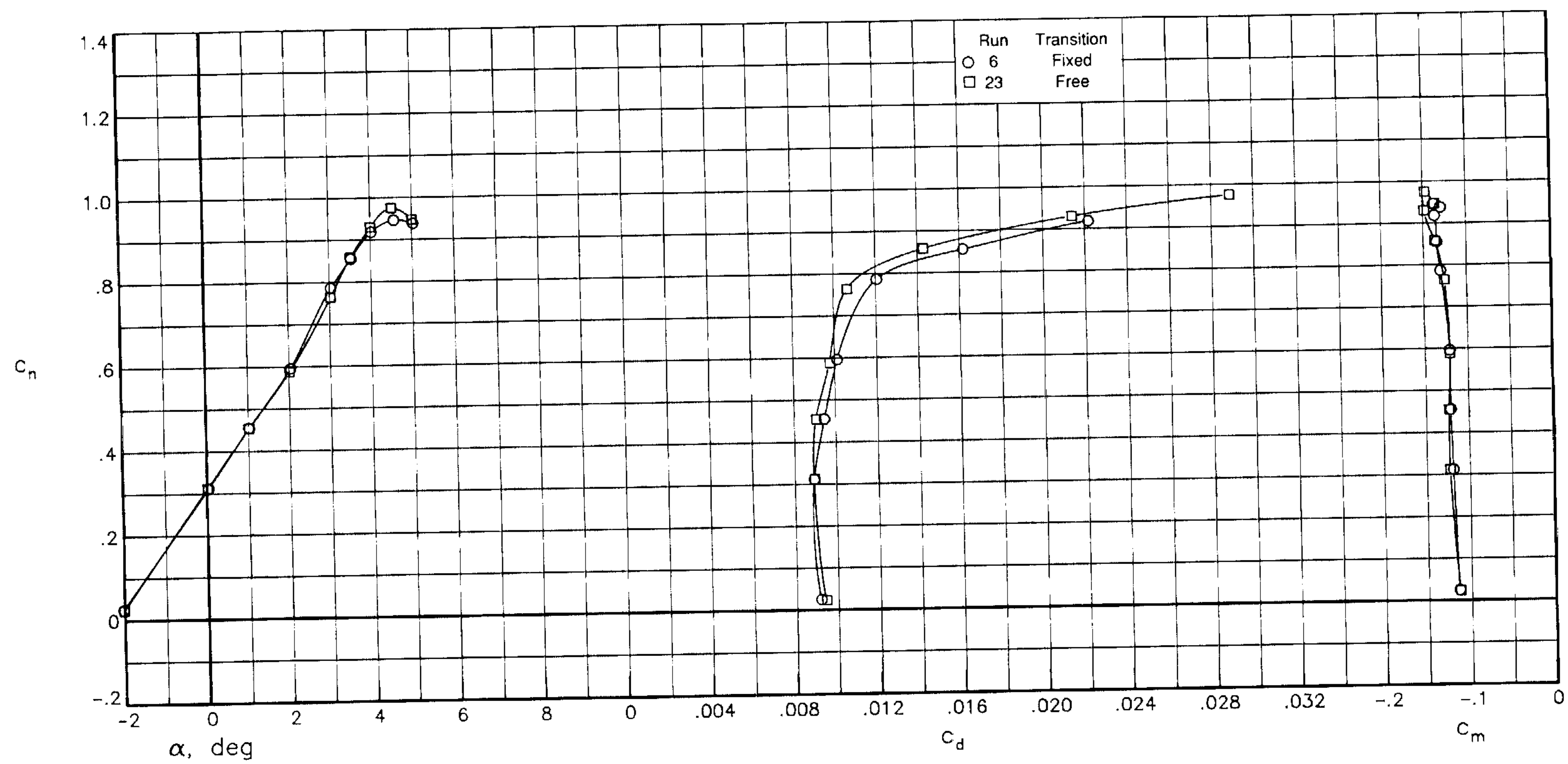

(b) $M_\infty = 0.74$.

Figure 16. Continued.

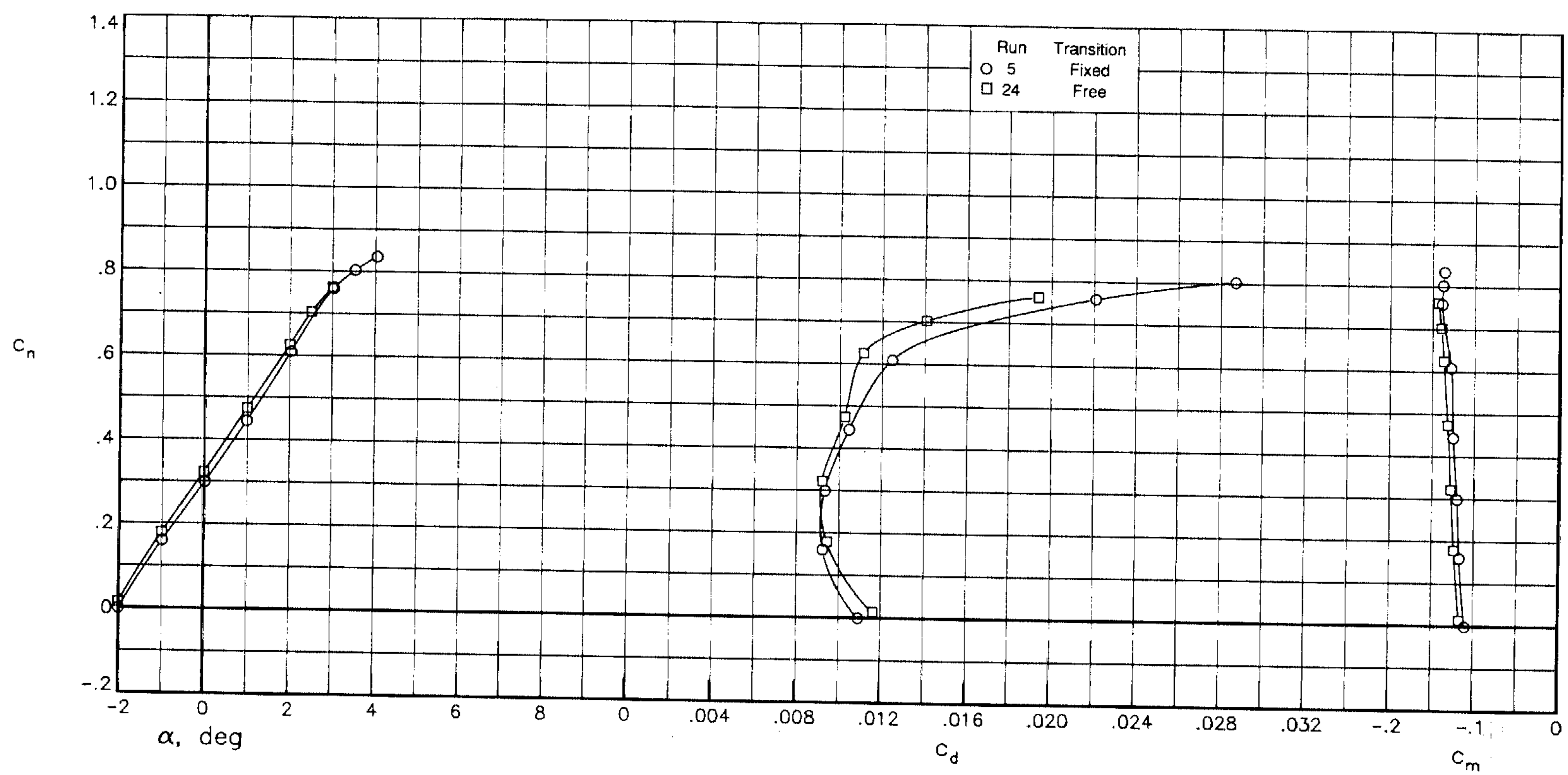

(c) $M_\infty = 0.76$.

Figure 16. Concluded.

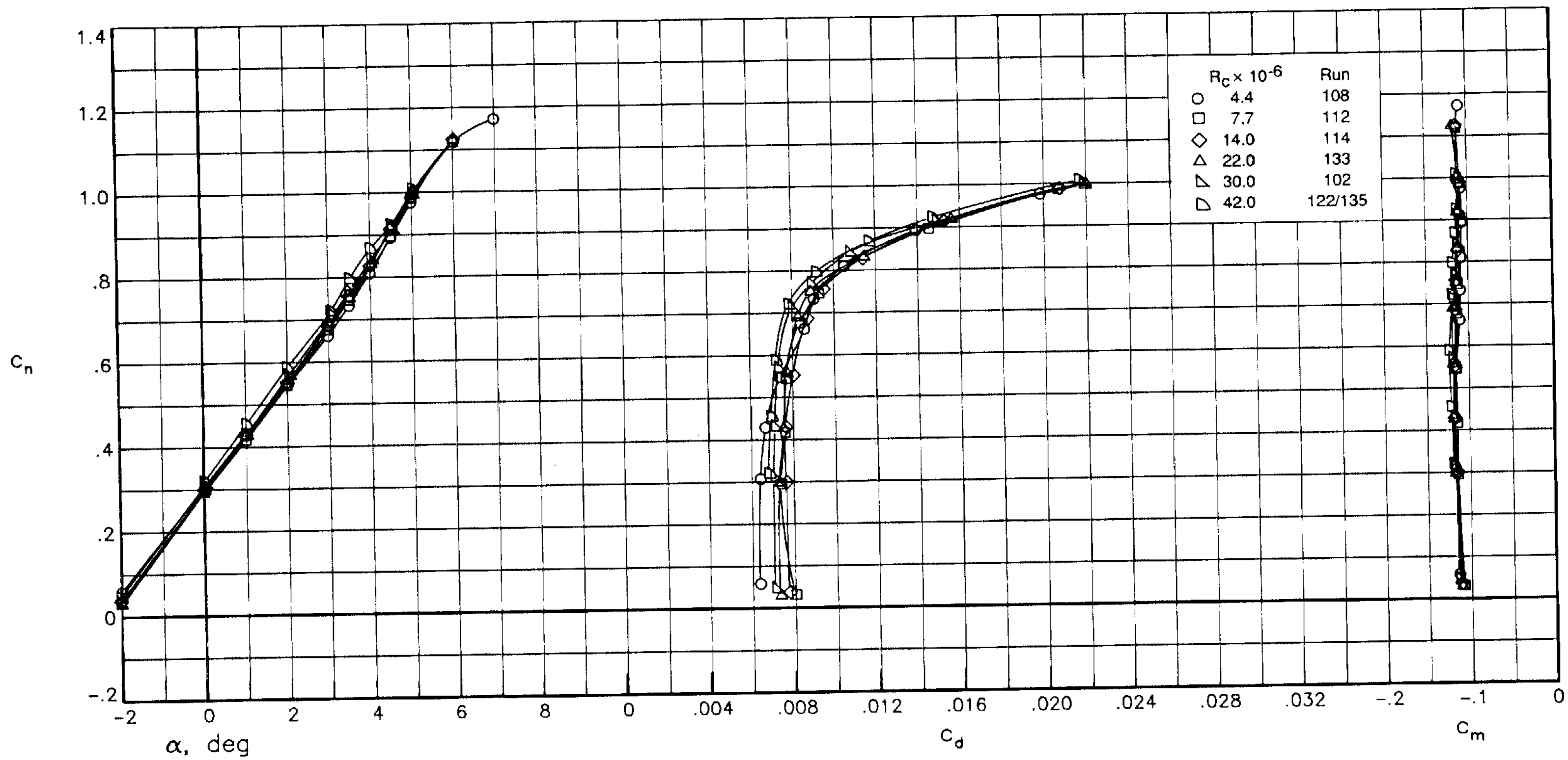

(a) $M_\infty = 0.70$.

Figure 17. Effect of Reynolds number on airfoil aerodynamic characteristics with free transition.

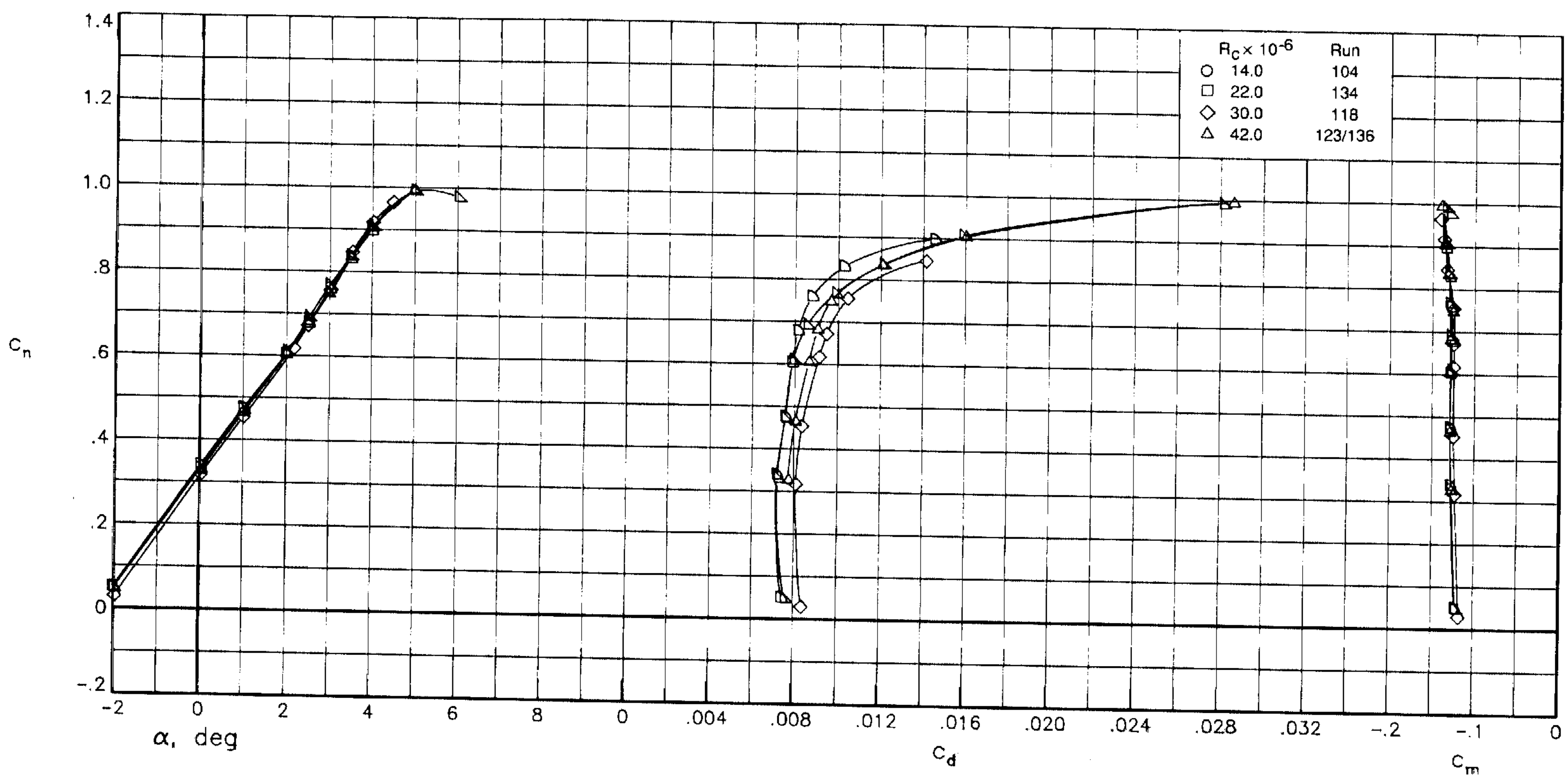

(b) $M_\infty = 0.74$.

Figure 17. Continued.

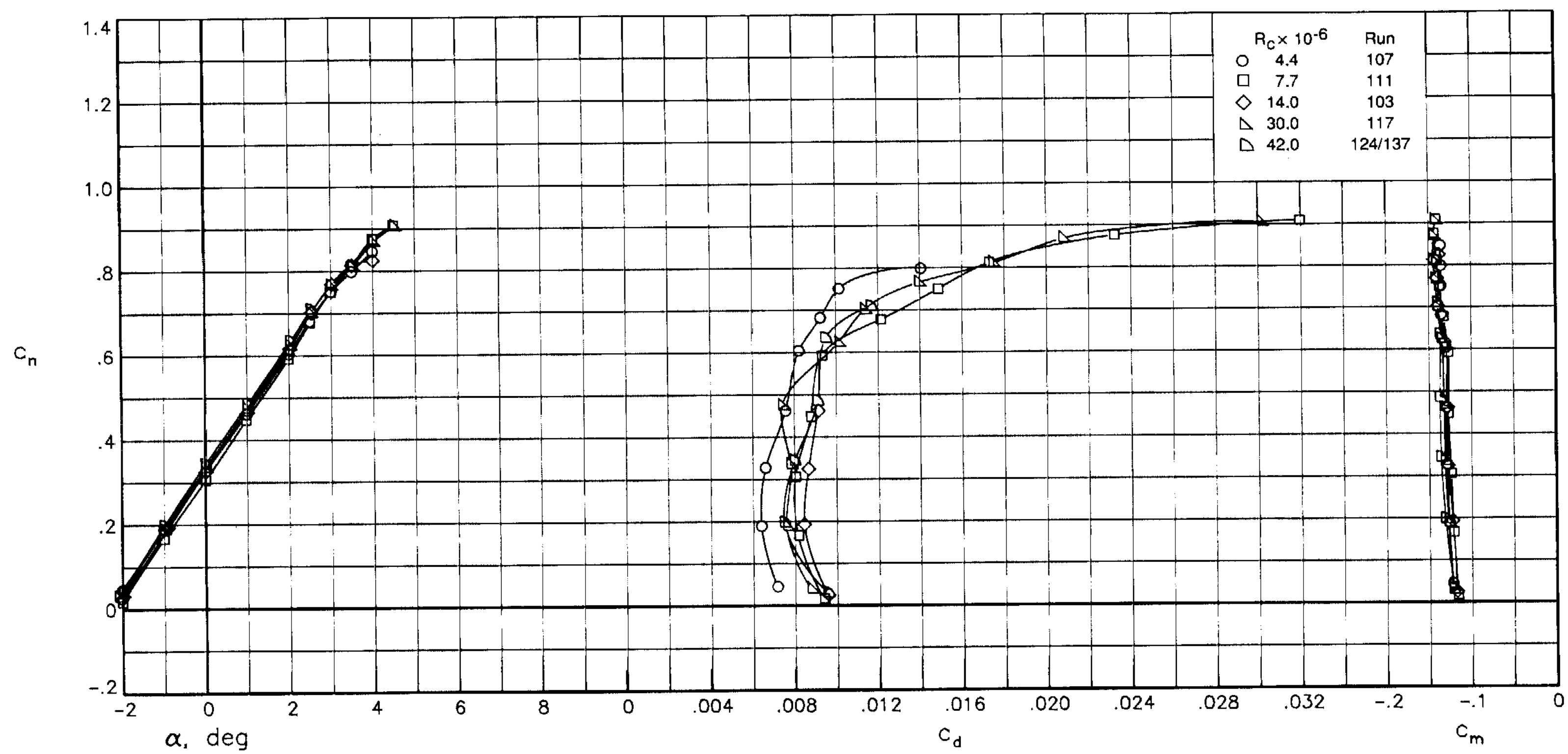

(c) $M_\infty = 0.76$.

Figure 17. Concluded.

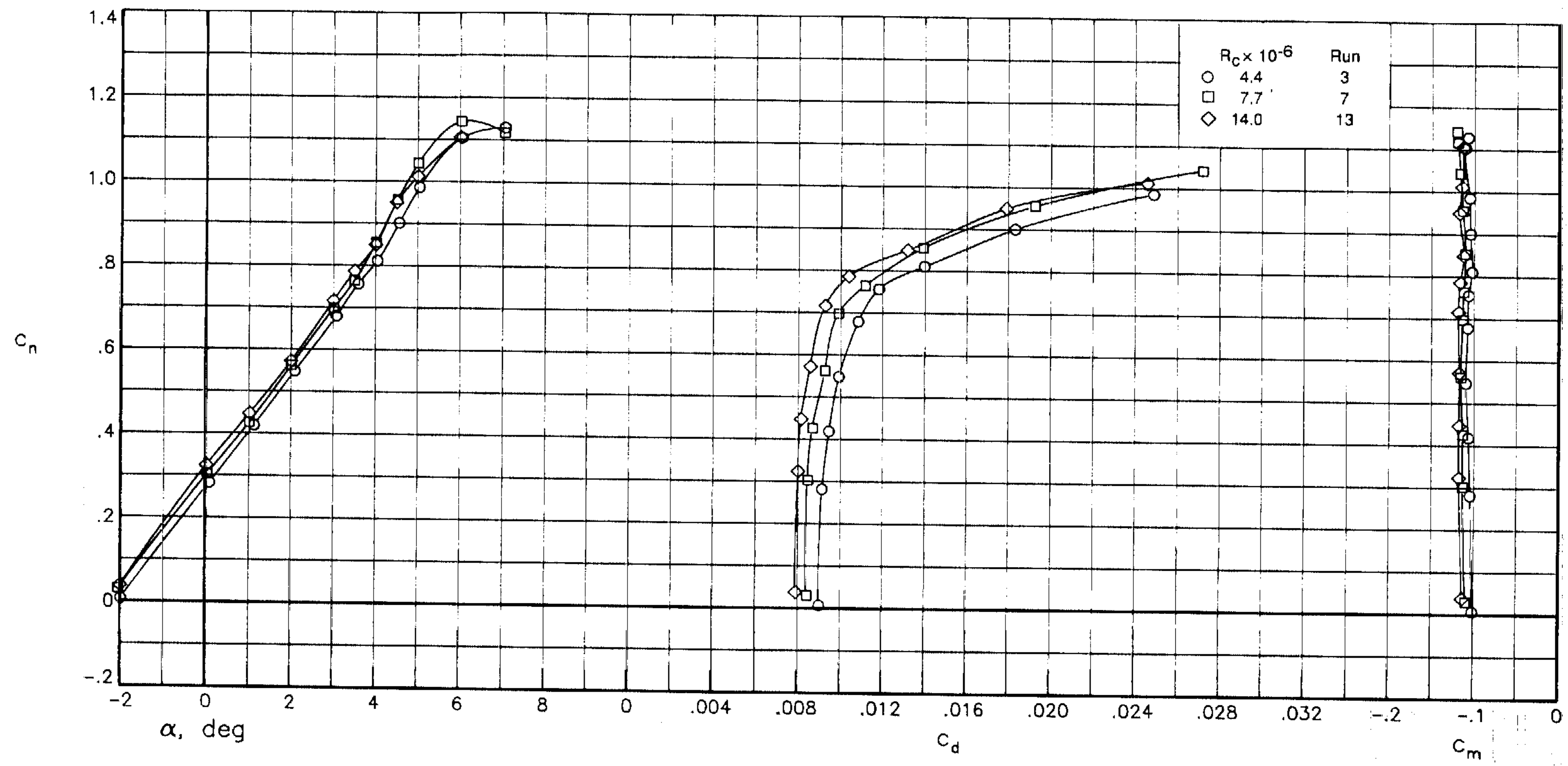

(a) $M_\infty = 0.70$.

Figure 18. Effect of Reynolds number on airfoil aerodynamic characteristics with fixed transition.

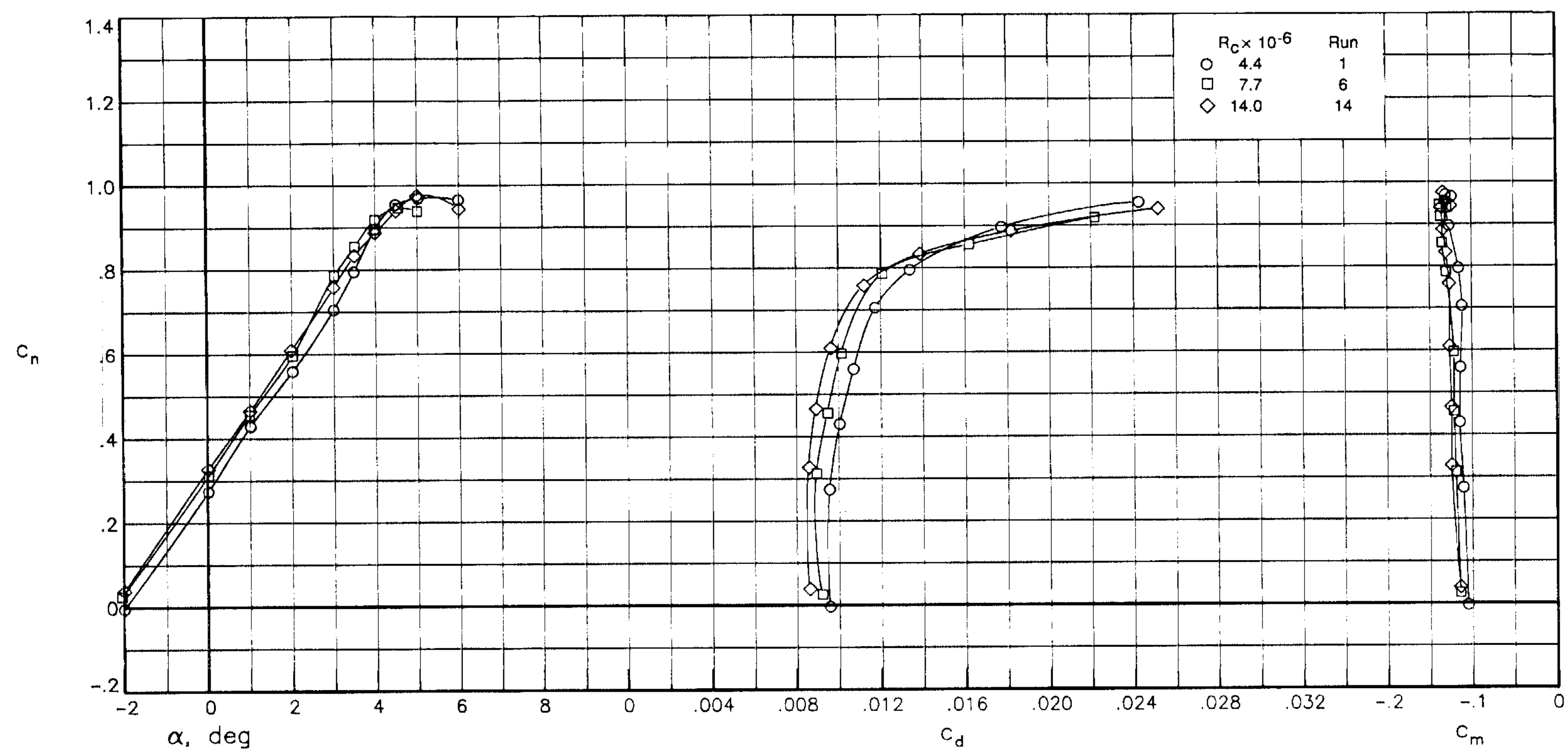

(b) $M_\infty = 0.74$.

Figure 18. Continued.

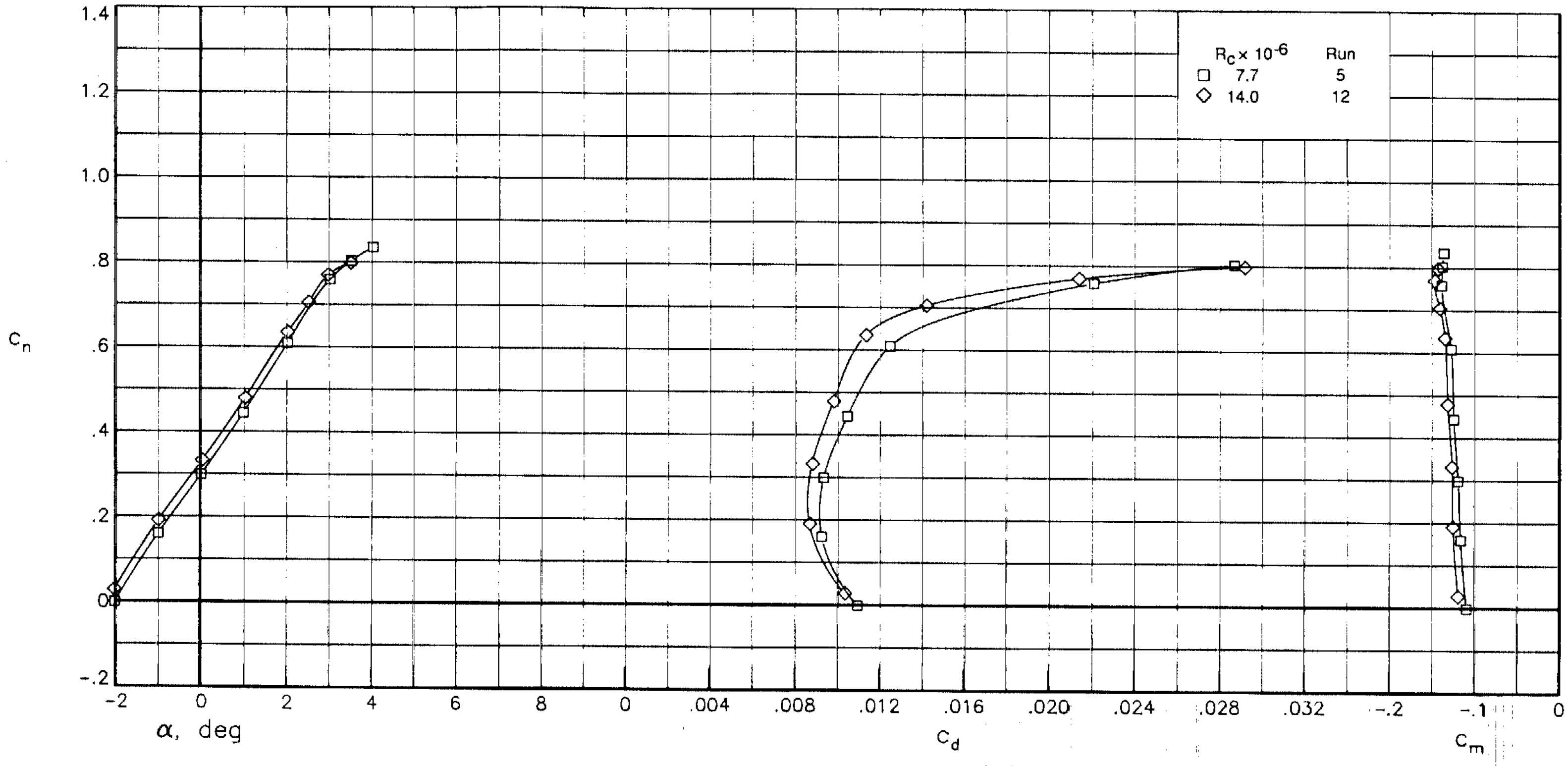

(c) $M_\infty = 0.76$.

Figure 18. Concluded.

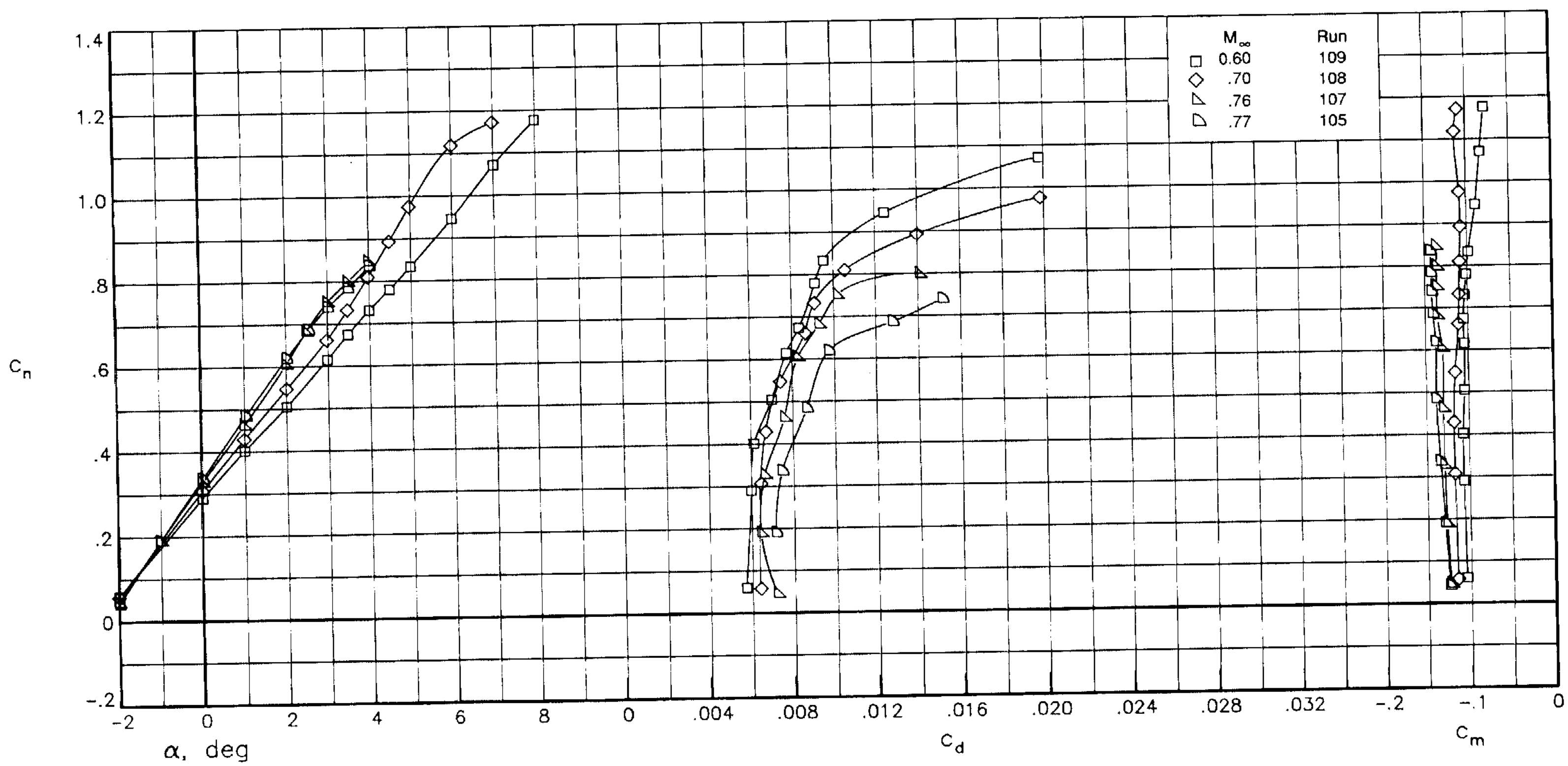

(a) $R_c = 4.4 \times 10^6$.

Figure 19. Effect of Mach number on airfoil aerodynamic characteristics with free transition.

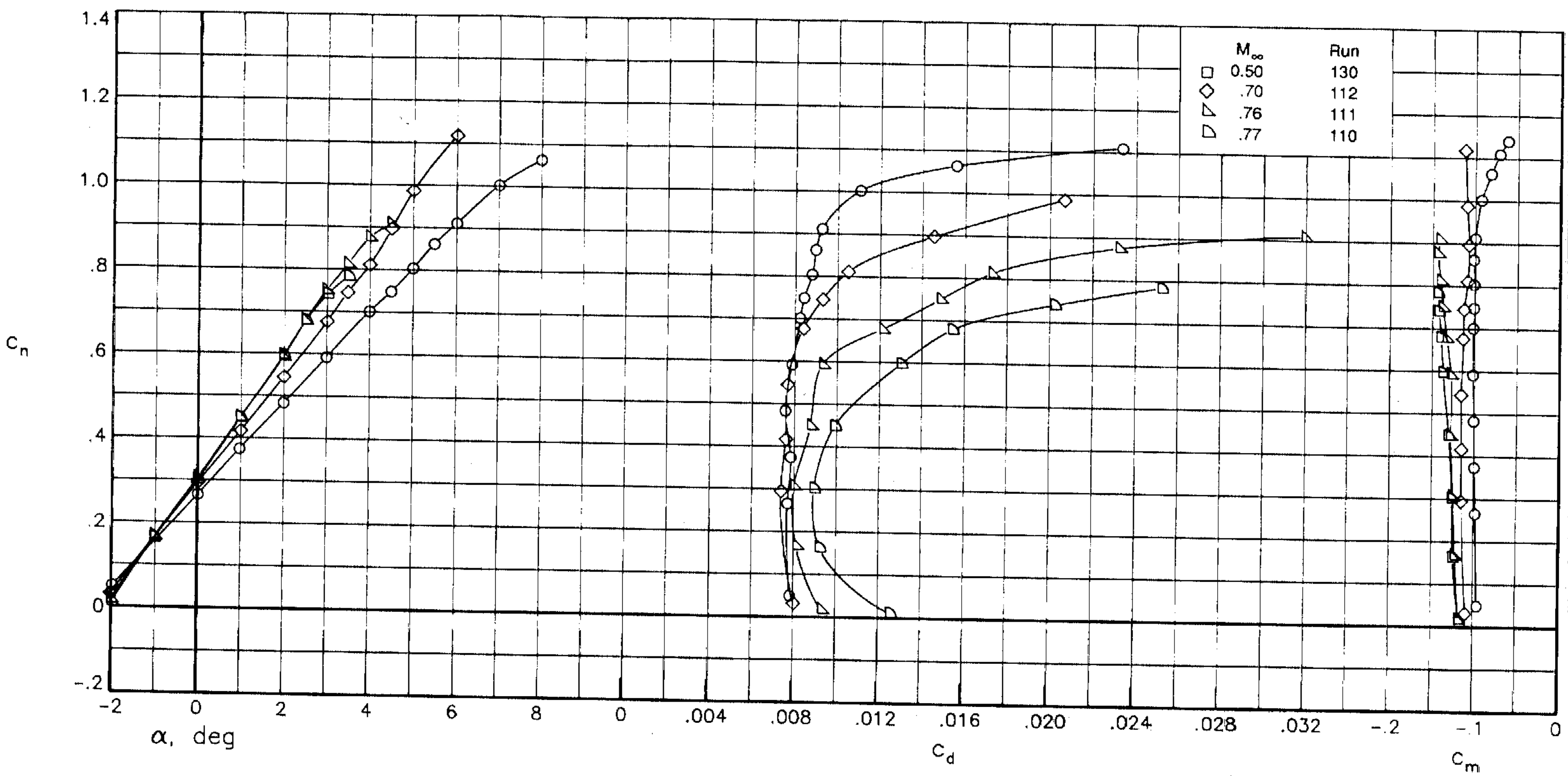

(b) $R_c = 7.7 \times 10^6$.

Figure 19. Continued.

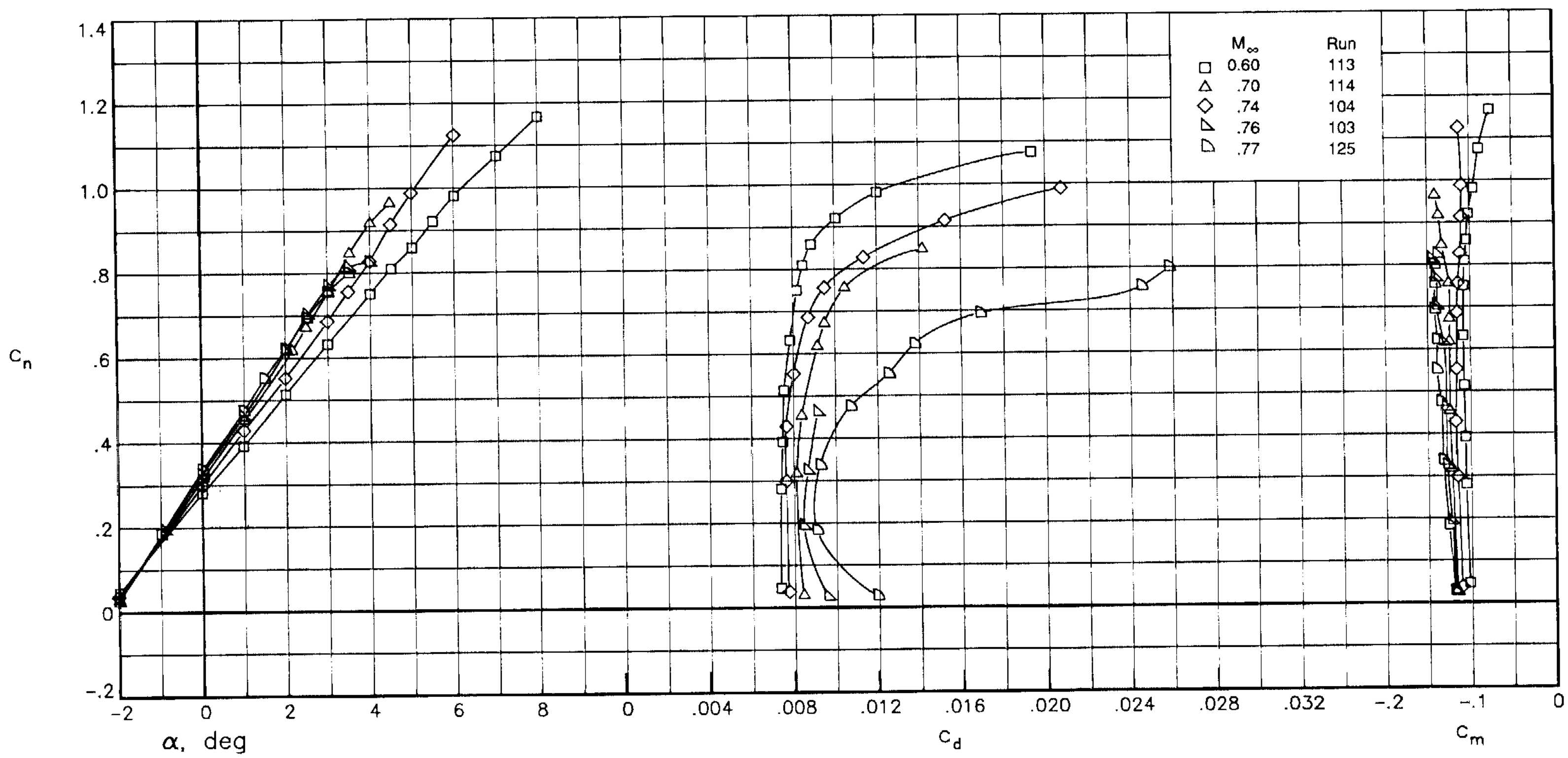

(c) $R_c = 14.0 \times 10^6$.

Figure 19. Continued.

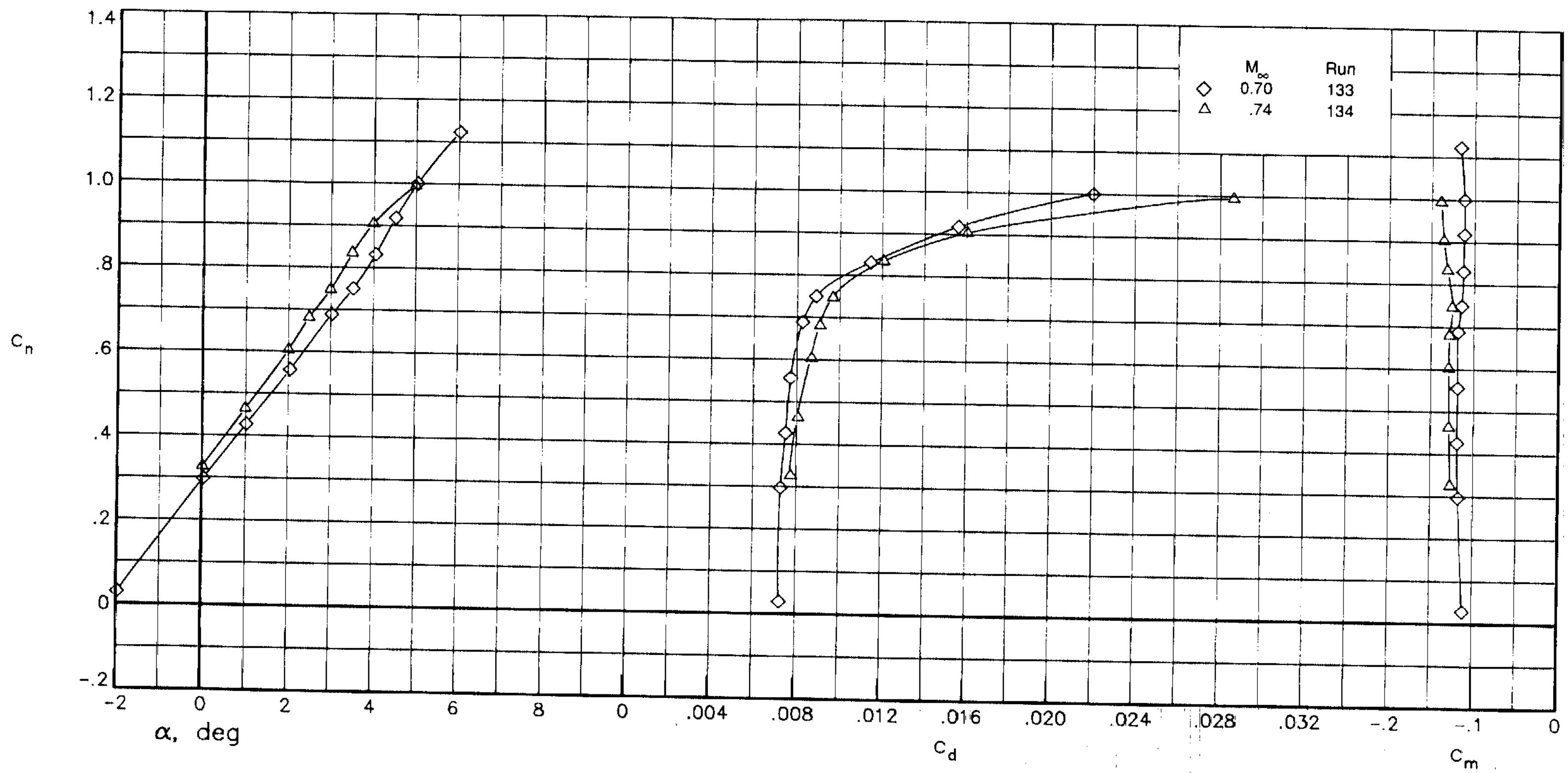

(d) $R_c = 22.0 \times 10^6$.

Figure 19. Continued.

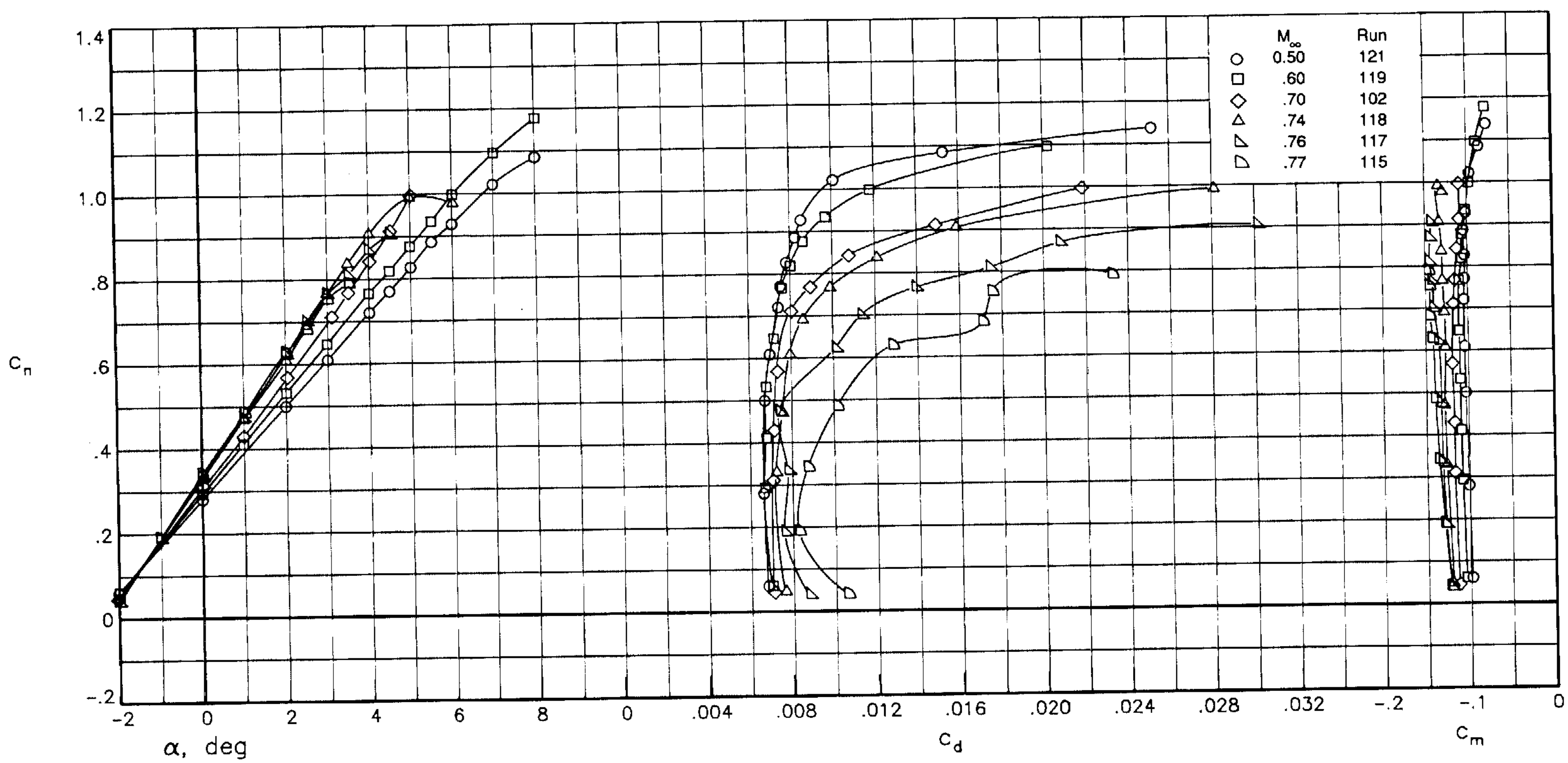

(e) $R_c = 30.0 \times 10^6$.

Figure 19. Continued.

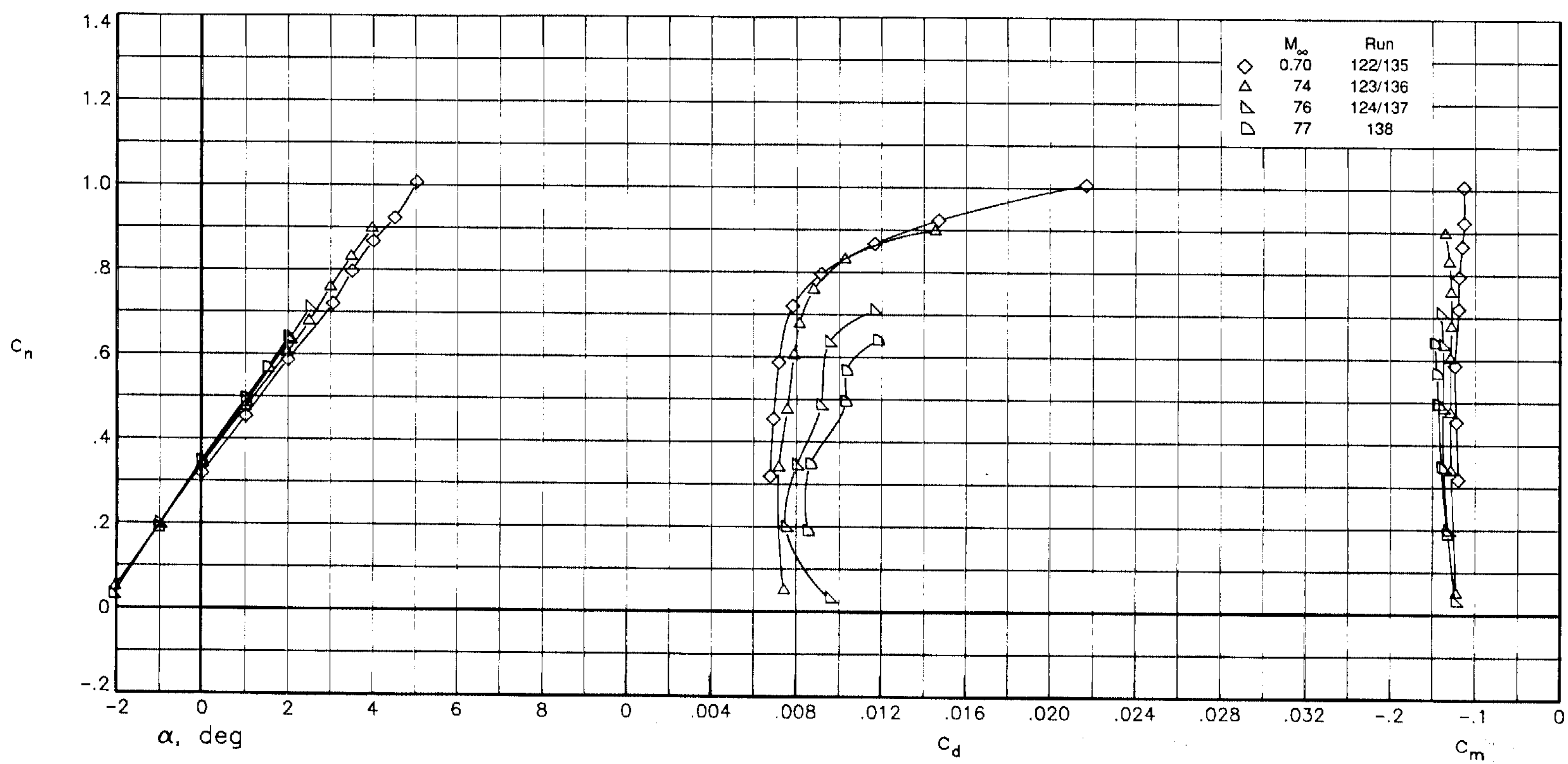

(f) $R_c = 42.0 \times 10^6$.

Figure 19. Concluded.

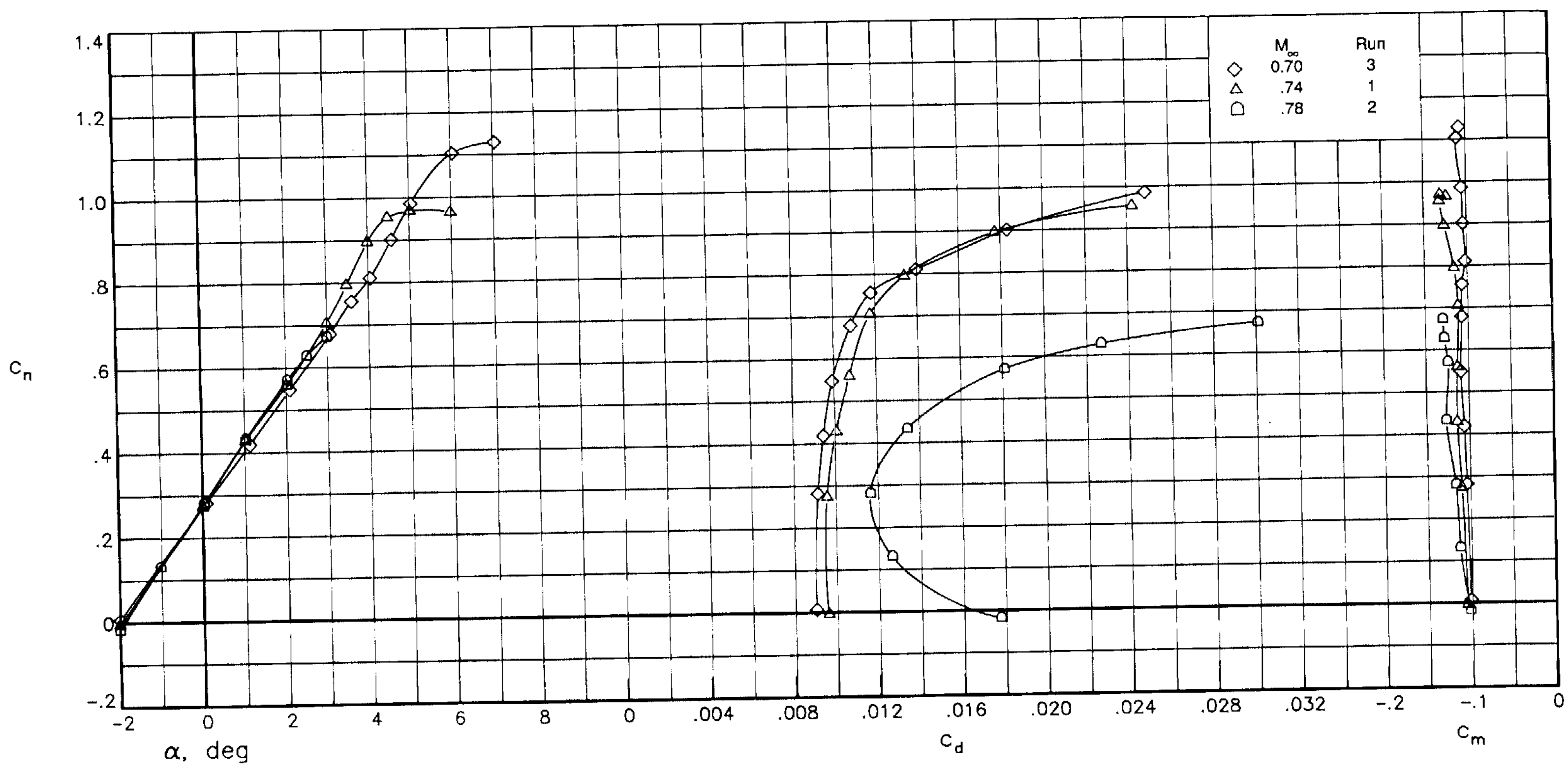

(a) $R_c = 4.4 \times 10^6$.

Figure 20. Effect of Mach number on airfoil aerodynamic characteristics with fixed transition.

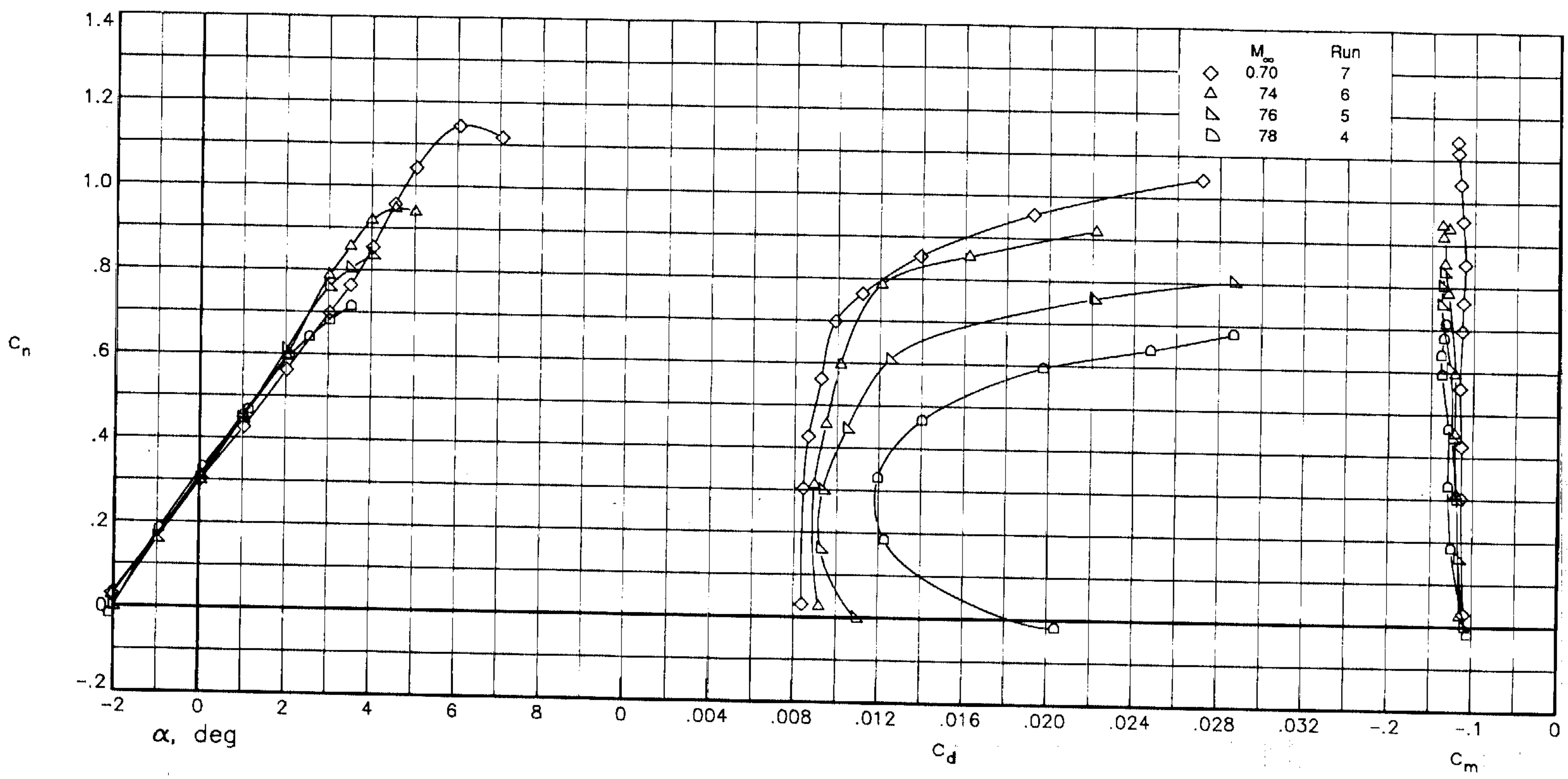

(b) $R_c = 7.7 \times 10^6$.

Figure 20. Continued.

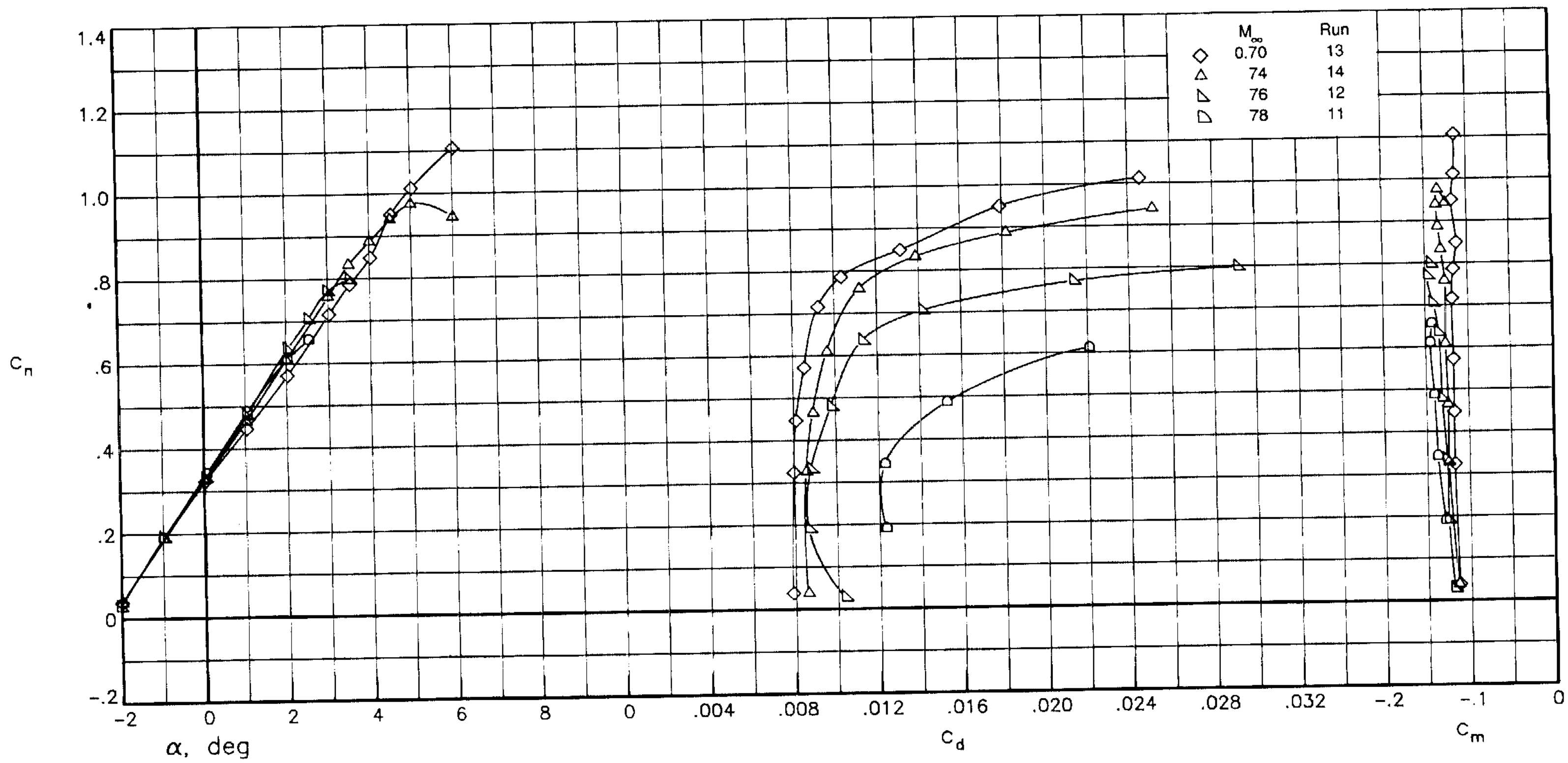

(c) $R_c = 14.0 \times 10^6$.

Figure 20. Concluded.

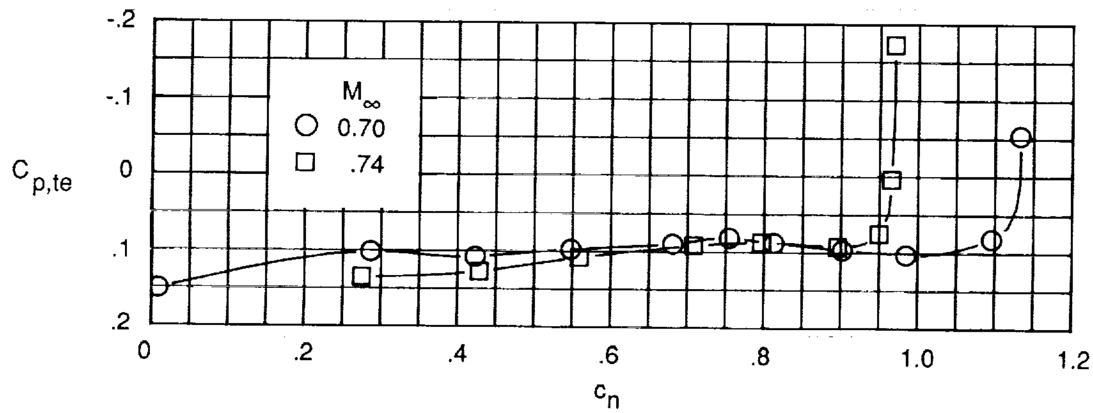

(a) $R_c = 4.4 \times 10^6$.

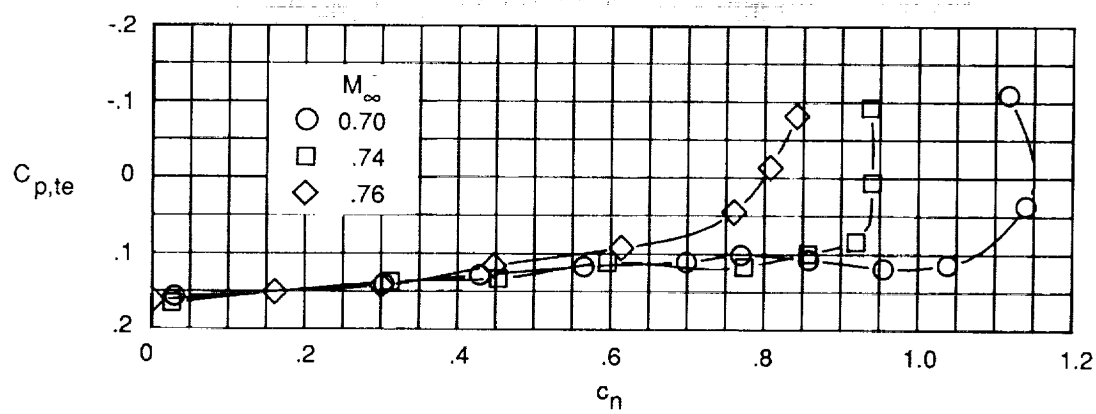

(b) $R_c = 7.7 \times 10^6$.

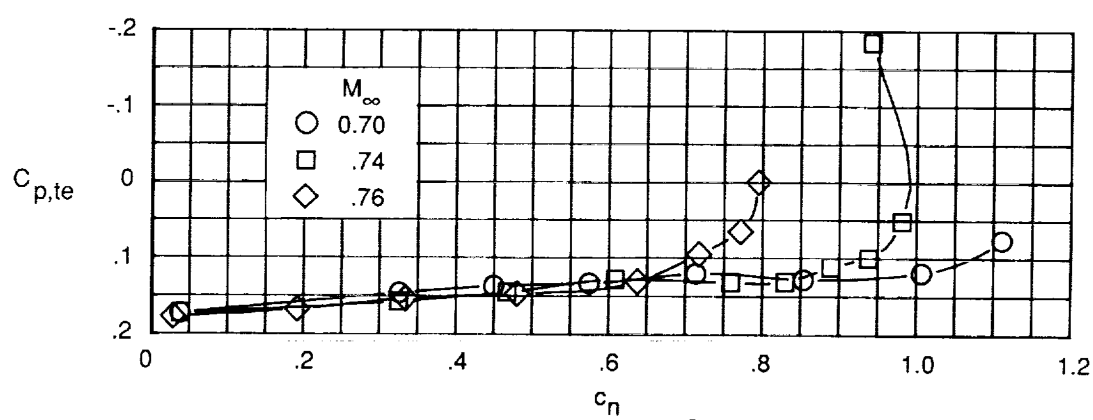

(c) $R_c = 14.0 \times 10^6$.

Figure 21. Effect of Mach number on variation of trailing-edge pressure coefficient with normal-force coefficients. Fixed transition.

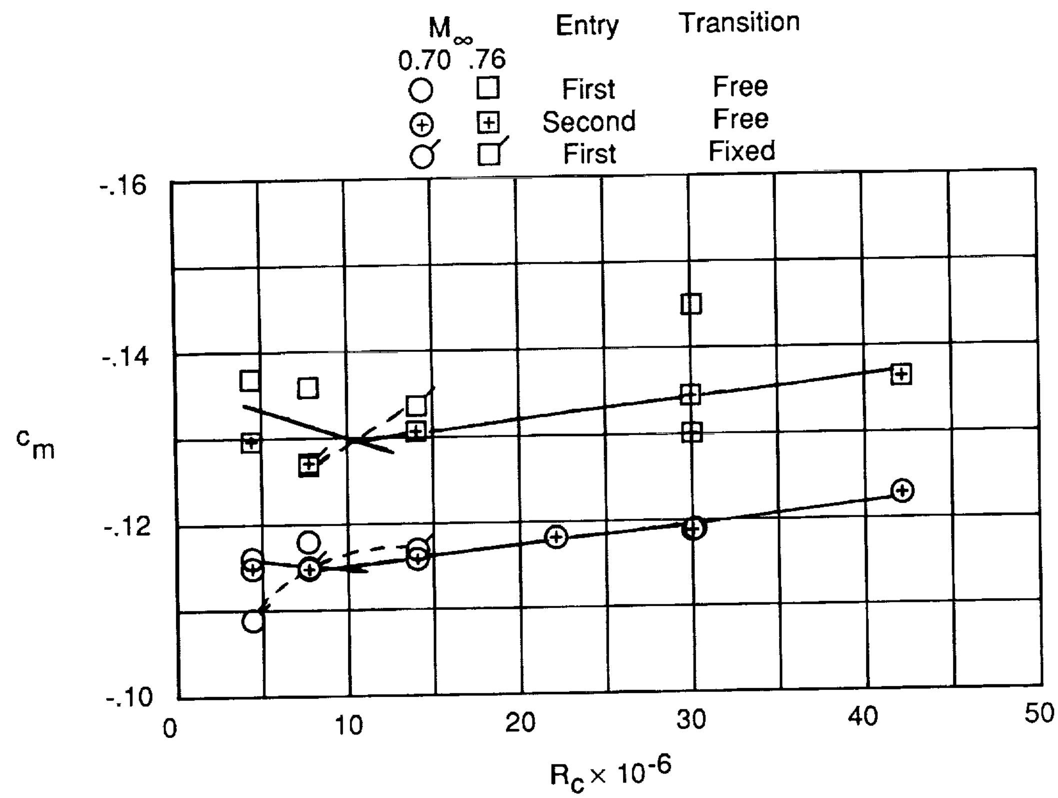

(a) c_m versus R_c.

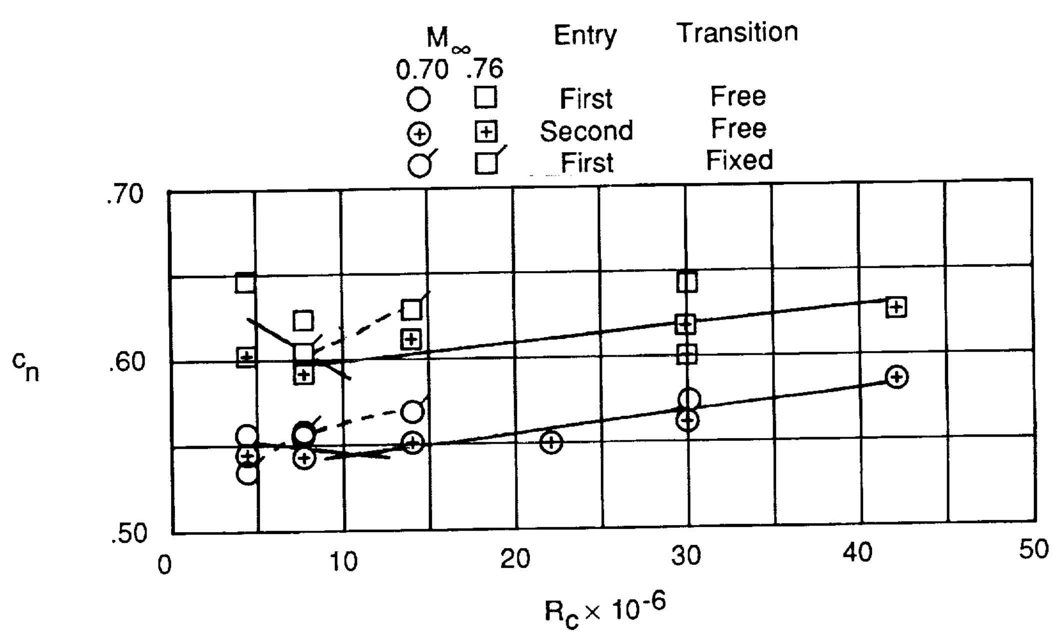

(b) c_n versus R_c.

Figure 22. Effect of transition and Mach number on variation of pitching-moment and normal-force coefficient with Reynolds number. $\alpha = 2°$.

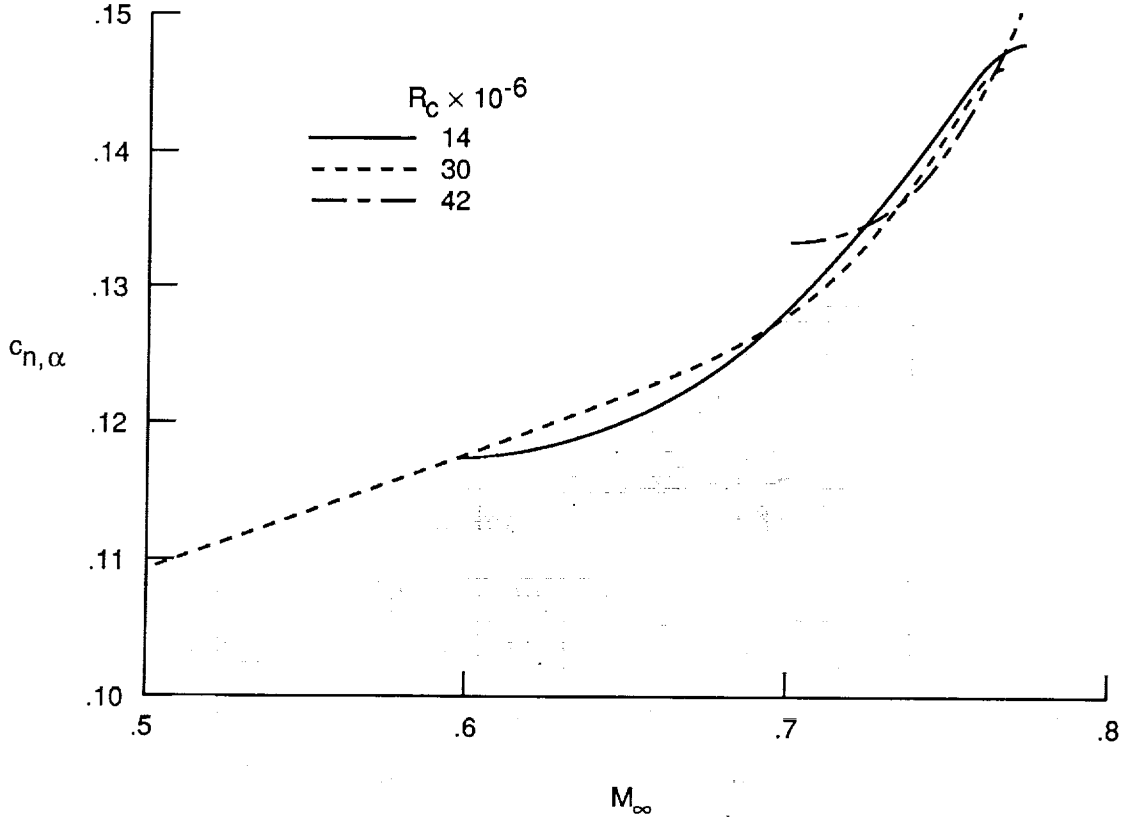

Figure 23. Effect of Reynolds number on variation of normal-force curve with Mach number. $-2^\circ < \alpha < 2^\circ$; free transition.

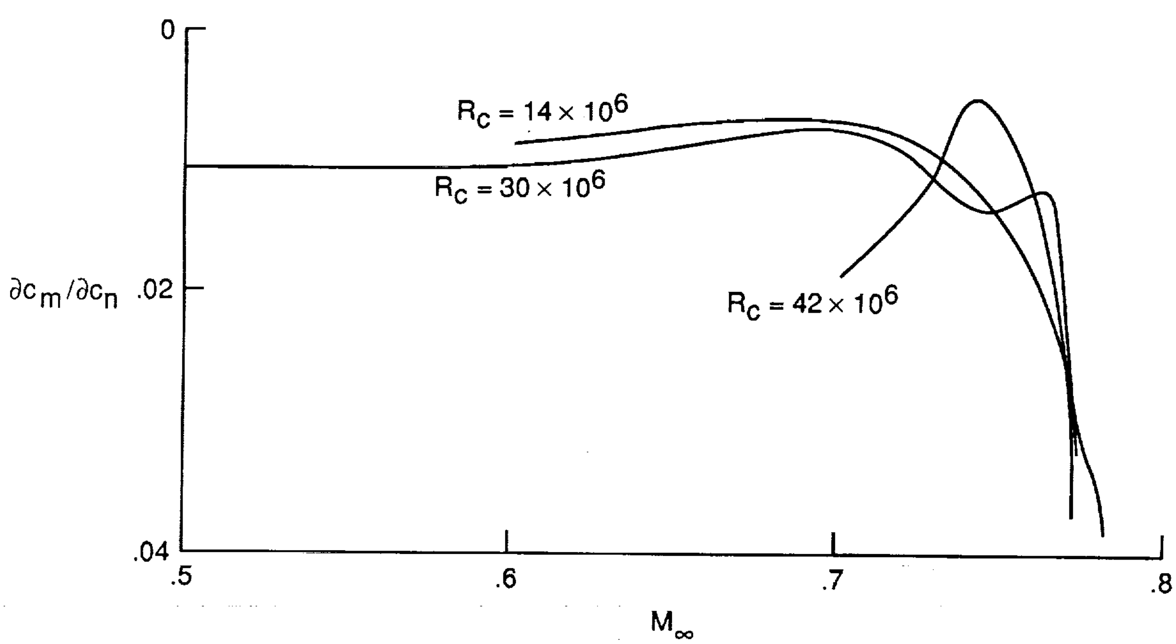

Figure 24. Effect of Reynolds number on variation of stability parameter with Mach number. $c_n = 0.40$; fixed transition.

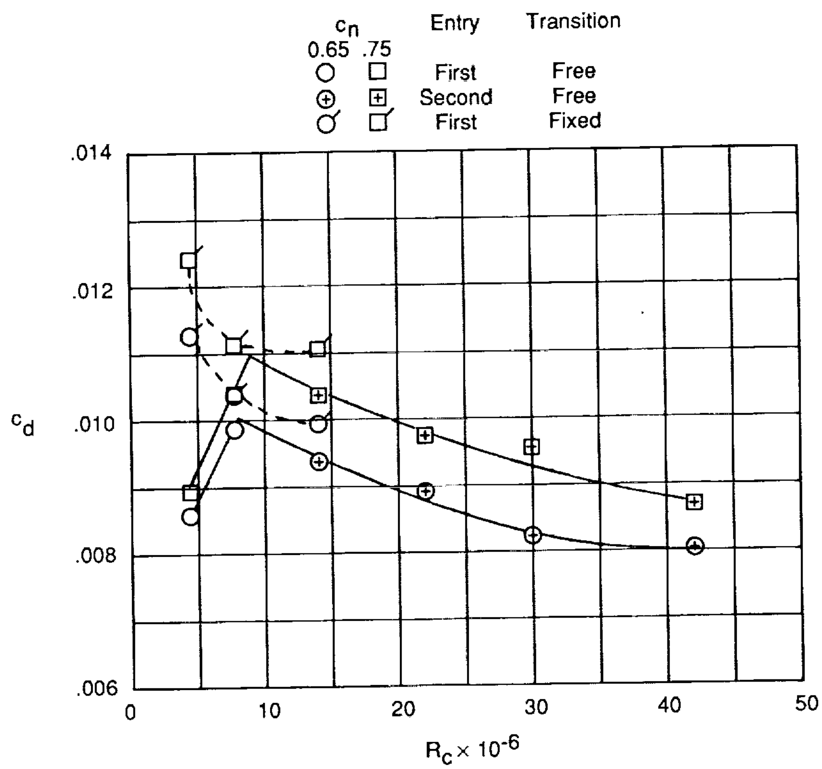

(a) $M_\infty = 0.74$.

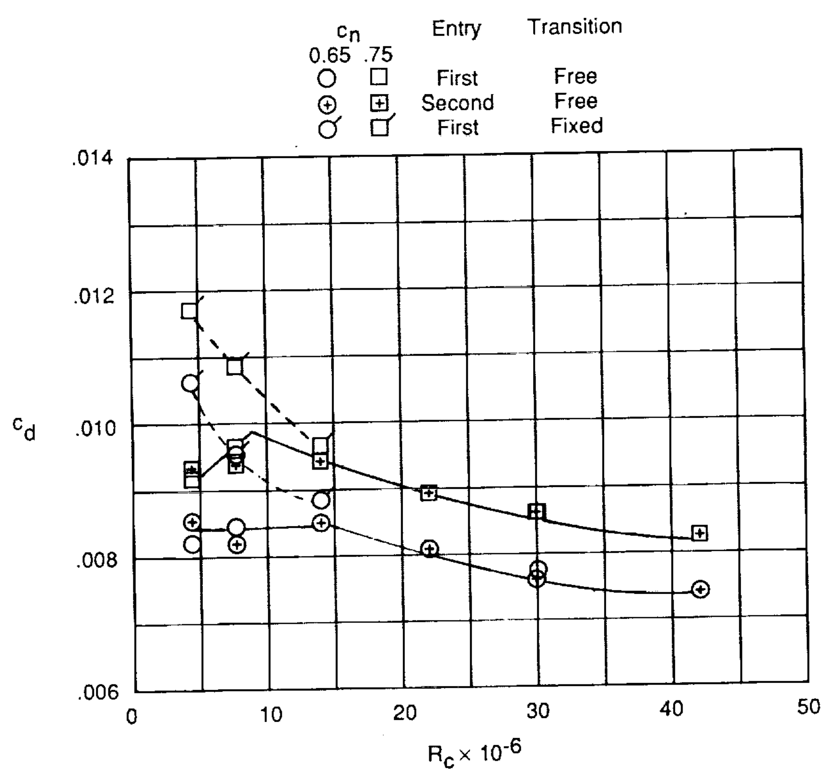

(b) $M_\infty = 0.70$.

Figure 25. Variation of drag coefficient with Reynolds number for two constant normal-force coefficients.

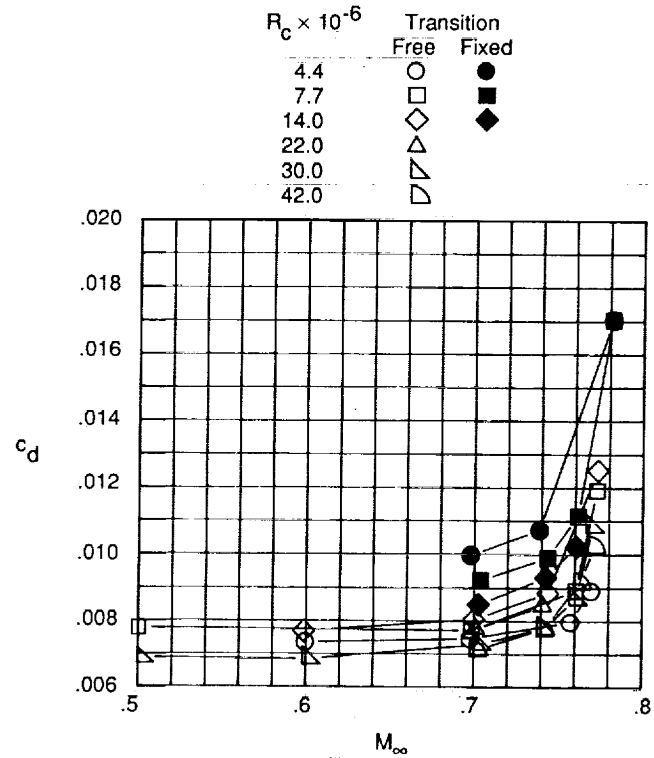

(a) $c_n = 0.55$.

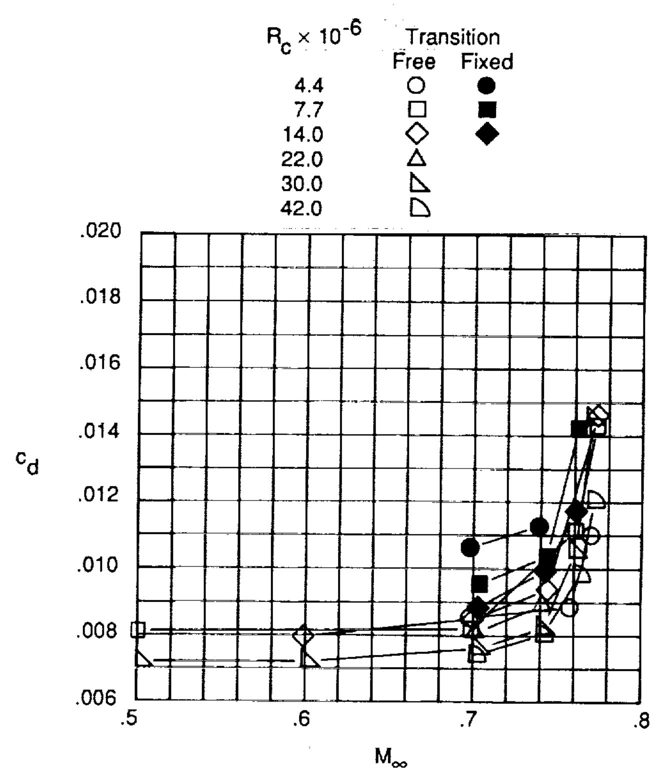

(b) $c_n = 0.65$.

Figure 26. Effect of Reynolds number on variation of drag coefficient with Mach number.

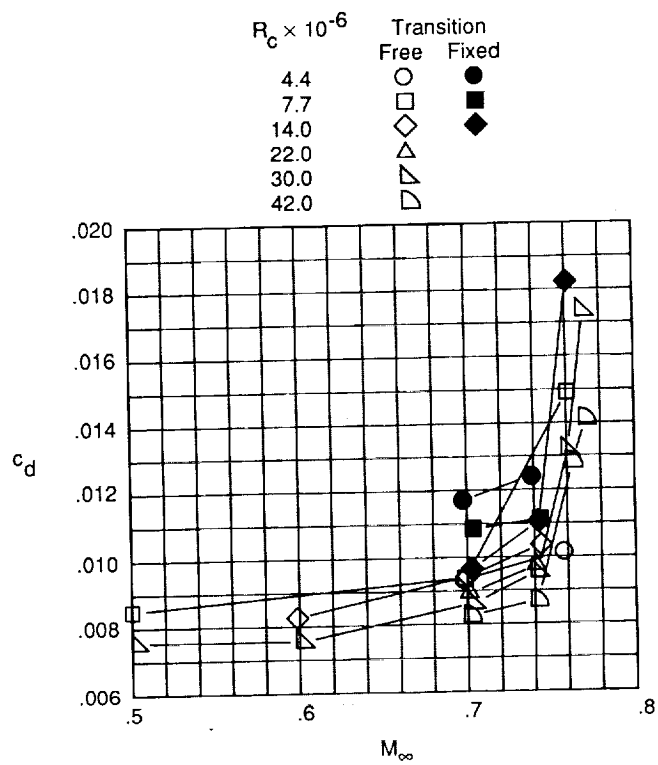

(c) $c_n = 0.75$.

Figure 26. Concluded.

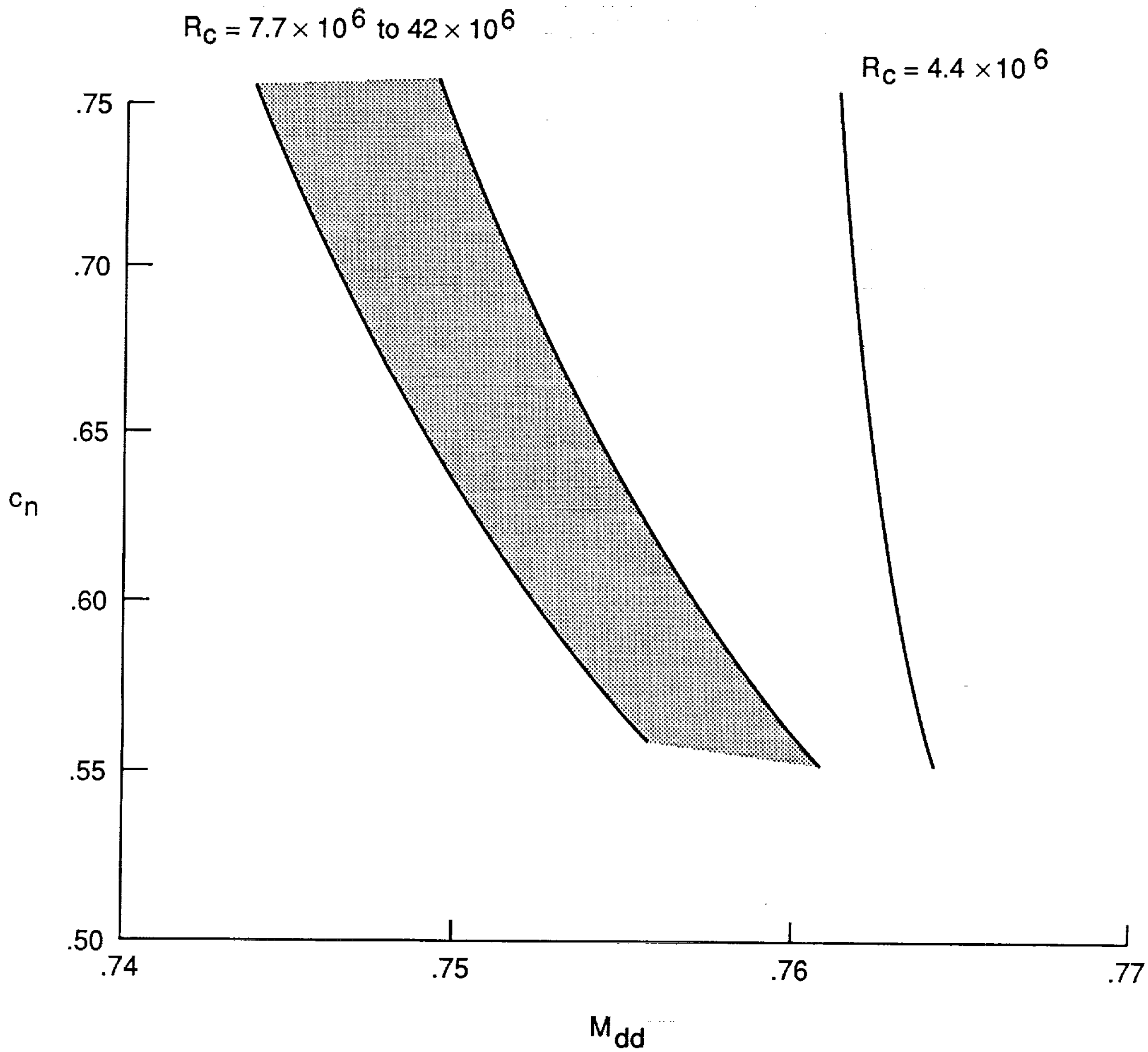

Figure 27. Effect of Reynolds number on drag-divergence Mach number characteristics. Free transition.

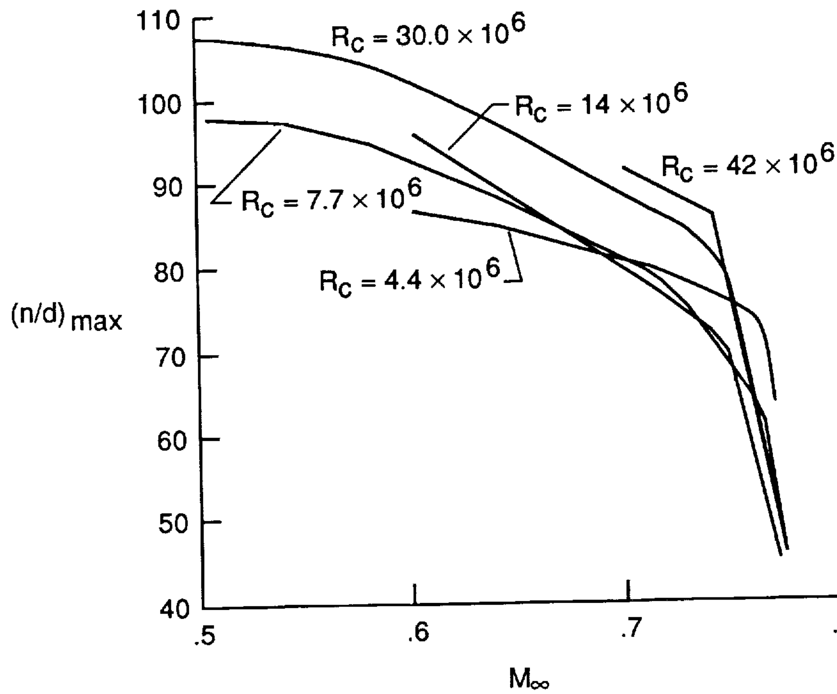

Figure 28. Effect of Reynolds number on variation of ratio of normal force to drag with Mach number. Free transition.

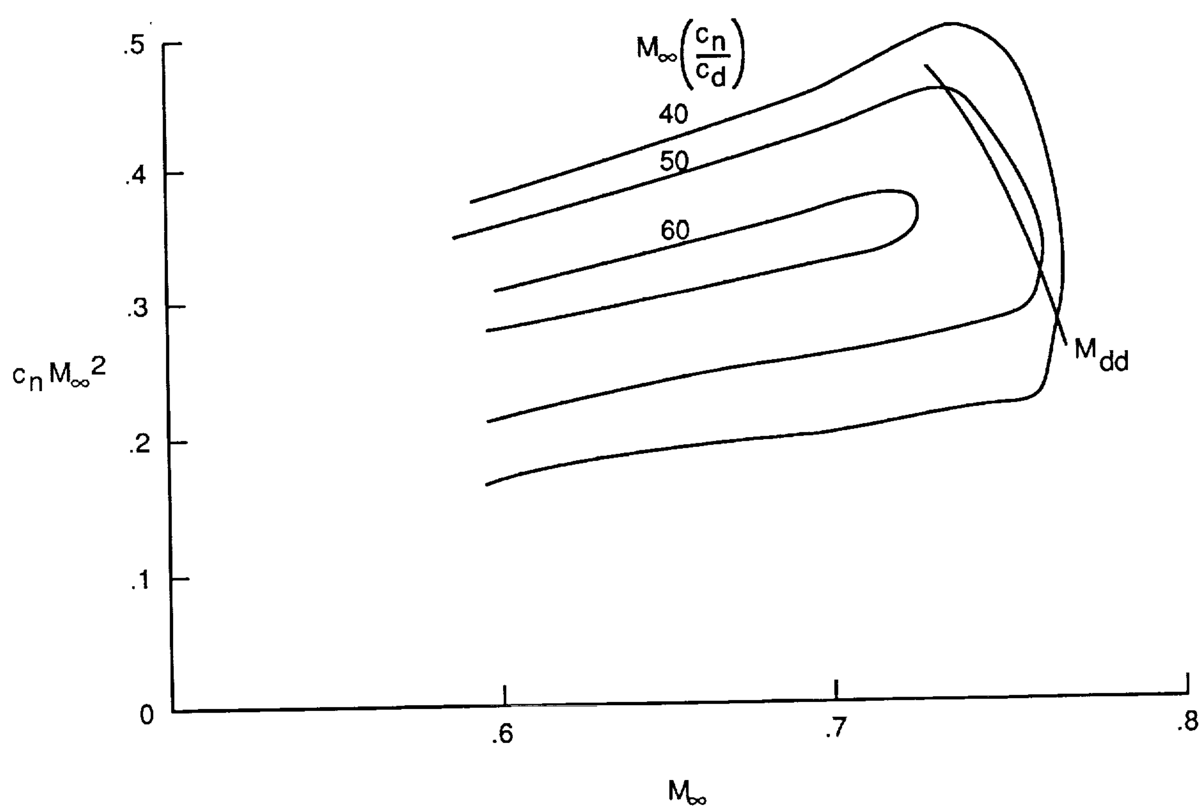

Figure 29. Performance map for TR77 airfoil model. Free transition; $R_c = 30.0 \times 10^6$; second-entry data.

NASA
National Aeronautics and Space Administration

Report Documentation Page

1. Report No.	2. Government Accession No.	3. Recipient's Catalog No.
NASA TM-4189		

4. Title and Subtitle
High Reynolds Number Test of the Boeing TR77 Airfoil in the Langley 0.3-Meter Transonic Cryogenic Tunnel

5. Report Date
July 1990

6. Performing Organization Code

7. Author(s)
Julio Chu, Stuart G. Flechner, Acquilla S. Hill, and Roger A. Rozendaal

8. Performing Organization Report No.
L-16724

9. Performing Organization Name and Address
NASA Langley Research Center
Hampton, VA 23665-5225

10. Work Unit No.
505-61-01-01

11. Contract or Grant No.

12. Sponsoring Agency Name and Address
National Aeronautics and Space Administration
Washington, DC 20546-0001

13. Type of Report and Period Covered
Technical Memorandum

14. Sponsoring Agency Code

15. Supplementary Notes
Julio Chu, Stuart G. Flechner, and Acquilla S. Hill: Langley Research Center, Hampton, Virginia.
Roger A. Rozendaal: Boeing Commercial Airplanes, Seattle, Washington.

16. Abstract
A Boeing TR77 airfoil associated with the Advanced Technology Airfoil Tests (ATAT) program has been tested in the Langley 0.3-Meter Transonic Cryogenic Tunnel. Limited analysis of the data indicated that increasing Reynolds number for a fixed Mach number resulted in increased normal-force and nose-down pitching moment and decreased drag coefficient. Increasing Mach number while keeping the Reynolds number constant yielded the expected increase in normal-force slopes and nose-down pitching-moment coefficients, and a decrease in angle of attack associated with maximum normal-force coefficient. Turbulent boundary-layer flow was achieved over the airfoil with aluminum disks at low Reynolds numbers for the test Mach number range.

17. Key Words (Suggested by Authors(s))
Cryogenic wind-tunnel test
High Reynolds number test
Two-dimensional airfoil

18. Distribution Statement
[redacted]
REVIEW for general release
July 31, 1992

Subject Category 02

19. Security Classif. (of this report)	20. Security Classif. (of this page)	21. No. of Pages	22. Price
Unclassified	Unclassified	76	

[redacted]

[redacted]

[redacted]